Advances in clinical neurophysiology

Lascano, Agustina Maria

Section de médecine clinique
Département des neurosciences cliniques
Service de Neurologie

"Advances in clinical neurophysiology"

Thèse
présentée à la Faculté de Médecine
de l'Université de Genève
pour accéder à la fonction de privat-docent
par

Agustina Maria LASCANO

Genève
2020

Publications

The present thesis was based on the following manuscripts:

I. Brodbeck V, Spinelli L, **Lascano AM**, Wissmeier M, Vargas MI, Vulliemoz S, Pollo C, Schaller K, Michel CM, Seeck M. EEG Source Imaging: a prospective study of 152 operated epileptic patients. Brain 2011; 134: 2887-2897.

II. **Lascano AM**, Pernegger T, Vulliemoz S, Spinelli L, Garibotto V, C. Korff, Vargas MI, Michel CM, Seeck M. Yield of MRI, high-density source imaging (HD-ESI), SPECT and PET in epilepsy surgery candidates. Clin Neurophysiology 2016; 127: 5-7.

III. **Lascano AM**, Grouiller F, Genetti M, Spinelli L, Seeck M, Schaller K, Michel CM. Surgically relevant localization of the central sulcus with high-density SEP compared to fMRI. Neurosurgery 2014; 74: 517-26.

IV. **Lascano AM**, Hummel T, Lacroix JS, Landis B, Michel CM. Spatio-temporal dynamics of olfactory processing in the human brain : an event-related source imaging study. Neuroscience 2010; 167: 700-708.

V. **Lascano AM**, Brodbeck V, Lalive P, Chofflon M, Seeck M, Michel CM. Increasing the diagnostic value of evoked potentials in multiple sclerosis by quantitative topographic analysis of multichannel recordings. J Clin Neurophysiol 2009; 26: 316325.

Acknowledgements

I would like to express my deepest gratitude to my supervisors Professor Andreas Kleinschmidt, Professor Christoph Michel, and Professor Margitta Seeck for their active guidance and precious mentoring in this research project. Without their support, I would not have made headway in this dissertation. I especially would like to thank Professor Theodor Landis for his academic support.

I extend my sincere gratitude to Professor Patrice Lalive and Professor Serge Vulliémoz for their enthusiastic encouragement and constructive comments on this work. Special thanks should be given to my former colleagues who participated in the development of this research: Dr. Verena Brodbeck, Dr. Dennis Brunet, Dr. Mélanie Genetti, Dr. Fréderic Grouiller and Dr. Laurent Spinelli. I would also like to thank Dr. Markus Gschwind, Dr. Pierre Mégevand, Dr. Tonia Rihs and the members of the jury for their willingness to give their time so generously and provide their acute comments on this dissertation.

I also take this opportunity to express a deep sense of gratitude to all researchers and collaborators from other Departments of the University Hospitals of Geneva (Ear, Nose and Throat Clinics, Neurosurgery, Radiology, Neuropediatrics) and the technicians of the electroencephalography laboratory of the Department of Neurology for their help with the recordings and data acquisition. I would like to pay my special regards to Professor Philippe Eigenmann, representative of the Faculty of Medicine for his mentoring on this dissertation.

I also acknowledge with a deep sense of reverence, my gratefulness towards my husband Pablo, my son Camilo, my family and friends back in Argentina for their moral support and encouragement throughout my study.

Summary

Recent developments in neurophysiological methods have broadened our understanding of the human brain and improved management of neurological disorders. Electric source imaging (ESI) is a non-invasive technique which applies mathematical algorithms to localize the source of a given electroencephalogram (EEG) or evoked potential (EP) pattern in real time. This technique allows reconstructing brain activity measured from scalp electrodes and can be applied in the individual patient to fit different clinical purposes. ESI based on high-density EEG recordings significantly improved non-invasive preoperative evaluation of epilepsy surgery and helped to include patients previously not considered surgical candidates. In experimental settings, ESI is performed to localize areas involved in sensory processing. Brain source imaging of somatosensory evoked potentials (SEP) are employed during presurgical planning to localize the functional cortex and to avoid this region during lesion resection. Research laboratories apply ESI to chemosensory event-related potentials (CSERP) to elucidate the spatial and temporal dynamics of the olfactory pathway. Nowadays, ESI is used for either clinical or research purposes, since it provides objective measurements of brain mapping that cannot be achieved by conventional analysis which are restricted to the scalp surface.

Table of contents

Glossary

EEG	Electroencephalography
EP	Evoked Potential
ESI	Electric Source Imaging
CSERP	Chemosensory Event-related Potential
SEP	Somatosensory Evoked Potential
VEP	Visual Evoked Potential
OEP	Olfactory Evoked Potential
LEP	Laser Evoked Potential
MRI	Magnetic Resonance Imaging
fMRI	Functional Magnetic Resonance Imaging
MEG	Magnetoencephalography
DCES	Direct Cortical Electrical Stimulation
PET	Positron Emission Tomography
SPECT	Single-photon Emission Computed Tomography
MS	Multiple Sclerosis
CIS	Clinically Isolated Syndrome
EDSS	Expanded Disability Status Score
NMOSD	Neuromyelitis Optica Spectrum Disorders
AD	Alzheimer’s disease
PD	Parkinson’s disease
CNS	Central Nervous System

Introduction

> I see the sun, and if I don't see the sun, I know it's there. And there's a whole life in that, in knowing that the sun is there.
>
> Fyodor Dostoyevsky. The Brothers Karamazov (Chapter 4).

Like *Helios*, the Titan god of the sun, the brain has been an element of fascination since ancient Greek times. Studies from the 17th century were mainly focused on the field of neuroanatomy and clinical neurology. However, it was not until the end of the 19th century that prominent neurophysiologists Richard Caton and Adolf Beck measured neural activity in rabbits and dogs by means of electrophysiological recordings[1]. In 1929 Hans Berger reported his results on the first human electroencephalogram (EEG)[2].

Since that moment, tremendous progress has been made in terms of EEG recording and analysis, hence, redefining its use as a functional imaging technique. This was made possible by improving the spatial resolution in terms of sampling (i.e. increasing the number of sensors) and applying more sophisticated signal processing techniques (i.e. source imaging) to examine the electrical activity of the brain[3, 4]. This breakthrough led to a change of paradigm: from EEG waveform description to topographical analysis and functional maps of electrical activity (i.e. electromagnetic source imaging or ESI).

Source imaging based on multichannel EEG and evoked potentials (EP) helps to understand the brain generators of an activity observed on the scalp surface and can be applied to solve different clinical and research questions.

During the past 20 years, ESI has thrived in the field of presurgical evaluation of patients with medically refractory epilepsy[5, 6]. It allows localizing the irritative zone and abnormal non-epileptiform interictal activity[7], irrespective of the lesion size[8, 9] and patient age[10, 11]. The main advantage of ESI over conventional imaging methods (e.g. magnetic resonance imaging or MRI) is its high temporal resolution, in the range of milliseconds, which permits to determine the onset and the propagation of the epileptic activity across time (i.e. network involved). Candidates for epilepsy surgery must undergo pre-operative

evaluation to decide if the surgical procedure can help to control seizures. For this purpose, definition of the epileptogenic zone is essential[12]. Multimodal presurgical workup includes high-resolution MRI imaging, video scalp EEG, neuropsychological evaluation and, if results are inconclusive, the following investigations can be applied: interictal positron emission tomography (PET), ictal single-photon emission computed tomography (SPECT), magnetoencephalography (MEG), and electromagnetic source imaging techniques (ESI)[5].

Source imaging of EP can be used to identify the eloquent cortex, which is the area controlling a specific brain function (e.g. motor, sensory or language). Mapping the eloquent cortex is useful for multiple purposes: i) to understand and locate brain function[13], ii) to tailor surgical resections and provide good post-operative outcome in patients with epilepsy and/or brain tumours, while limiting possible cognitive or sensorimotor deficits[14]. EP has the main advantage of being non-invasive and is less time-consuming than direct cortical electrical stimulation (DCES) which is the current gold standard for mapping brain function. As a matter of fact, Papanicolaou and colleagues have recently suggested that it is more reasonable to apply invasive techniques only if results obtained with non-invasive methods are inconclusive or ambigous[15].

This dissertation aims at bridging the gap between traditional EEG/EP recordings and modern improvements in neurophysiological data analysis. In the first part, basic principles of EEG/EP analysis and acquisition will be described (section 1 and 2). Secondly, contemporary ways of measuring scalp EEG/EP will be detailed (section 3). Finally, suggested clinical use of modern EEG/EP analysis will be tackled (section 4), and experimental studies will be included (section 5). A comprehensive review on current clinical use of EP was included as supplementary material (appendix).

1. Principles of conventional electroencephalography

Electroencephalography (EEG) is a non-invasive neurophysiological method which monitors, records, and displays spontaneous electrical activity of the brain. It is used for diagnosis of brain pathology, specially epilepsy, encephalopathy and sleeping disorders. In some countries it is applied as an adjunct test to confirm brain death.

1.1. Generation of cortical field potentials

For neuronal electric fields to be recorded at a distance, it is necessary that a population of neurons work together as a functional entity. This is the case of apical dendrites of cortical pyramidal cells that are oriented perpendicular to the cortical surface and parallel to each other in the form of a palisade. When these neurons are synchronously activated, extracellular currents will flow, the longitudinal components will summate, and transversal components will cancel-out behaving as a current dipole layer[16]. The electric field potentials generated by a given neuronal population can be recorded at a distance by means of electrodes[17].

Equipment for EEG recording consists of scalp/needle electrodes (see section 1.2.), lead wires, jack boxes, cables coupled to high-input impedance amplifiers, voltage dividers, filters, selector switches and a digital data acquisition system (see section 1.3.)[18].

1.2. Fundamental of EEG measurement

EEG can be recorded from human brain by the placement of electrodes on the scalp. Surface electrodes coated with gold, platinum, or silver (chloride) are the most frequently used. Needle electrodes can also be applied.

Standard electrode placement include the 10-20 international system or its extension to a 10-10 system[19, 20]. According to the guidelines established in 2016 by the American Clinical Neurophysiology Society, 10-20 system is largely enough in a clinical setting and the use of a 10-10 system is recommended in presurgical evaluation for epilepsy units[21]. Using anatomical landmarks on the skull in the nasion, preauricular points and inion, the head is divided into proportional positions (10% or 20%) to ensure equal inter-electrode spacing and to provide full coverage of the head sphere. Electrode naming is based on a numbering system (i.e. odd = left; even = right hemisphere; Z = midline) and letter-based system (e.g. F = frontal, T= temporal lobe).

Routine EEG uses between 21 and 32 active electrode sites. It has been acknowledged that spatial sampling provided by these systems is not enough in research, resulting in an approximation of averaged-reference data and inaccurate source localization[7].

1.3. Digital EEG and data analysis

Digital EEG refers to the recording, storage, and analysis of the data on the computer. Analog conditioning of EEG data is achieved by using a high-gain and low-noise amplifier and filtering devices. Digital conditioning of EEG is made through the analog-digital converter. The advent of digital EEG allowed data to be reviewed off-line while manually applying frequency filters (i.e. high and low pass) and spatial filters (i.e. bipolar versus referential montage). These post-hoc changes allow for noise reduction and, thus, more accurate interpretation of the EEG.

Traditional EEG analysis relies on visual inspection of traces and, therefore, on the clinician's expertise. For this reason, EEG appraisal remains somewhat subjective. It is true that experienced neurologists can distinguish the type of epilepsy only by "eyeballing". However, in epilepsy surgery, precise identification of epileptogenic zone is far more complex, and the implication is much more important. One way to solve this conundrum is by applying sophisticated EEG analysis (for more details see section 3.3.).

2. Principles of evoked potentials

Evoked potentials (EP) are defined as electric responses of the nervous system to externally induced stimulation and recorded from the scalp using a standard EEG electrode setting. The main role of EP is to evaluate the functional integrity of the sensory and motor systems. EP can detect abnormality whenever imaging techniques are not feasible or the results are equivocal.

Conversely to EEG, which reflects the brain's spontaneous electrical activity, EP are time-locked to a given stimulus. Since a single EP response has a rather small amplitude, stimulus averaging allows response summation and background noise to be cancelled, thus, increasing the signal-to-noise ratio.

The response is characterized by a succession of negative and positive peaks called components whose shape and latency vary according to the stimulus applied. For instance, somatosensory EP (SEP) occur within 20ms after stimulation, whereas, visual EP (VEP) are long latency potentials occurring at 100ms. Peaks are named according to their polarity (P = positive; N= negative) and latency or as number in a sequence. Traditional EP analysis is based on waveform description in terms of absolute latency

(ms), amplitude (uV), intercomponent latency, amplitude ratio between two waveforms and left-to-right asymmetry.

Since results are affected by technical factors and interindividual variability (sex, age, body size, etc.), a control population of healthy subjects (n>20), with no family or personal history of neurological disease, should be studied to establish the normative data set for each laboratory[22]. Individuals of the same age range than the group of studied patients should be included. A result is considered abnormal whenever it varies 2.5-3.0 standard deviations (SD) above the mean of the control group.

EP are named according to the stimulated neural pathway. Routine EP testing includes visual, somatosensory, motor and (brainstem) auditory. The type of stimulation and parameters (intensity, duration, stimulation rate and repetitions) depends on the tested EP modality. International recommended standards for clinical practice, recording and interpretation were elaborated for some EP modalities[23-26].

As this dissertation is based on a series of publications in the field of EP, only a few techniques are summarized below. Technological aspects of EP acquisition, interpretation, description, and clinical uses of visual, somatosensory, and olfactory (CSERP = chemosensory event-related potentials) will be detailed. However, this essay will not include an explanation on other EP modalities: auditory, nociceptive (laser) and motor EP. A review of the clinical use of the different EP modalities is included in this dissertation (see appendix)[27].

2.1. Visual evoked potentials

Visual evoked potentials (VEP) quantify the integrity of the visual pathway from the retina to the occipital cortex. VEP measures an electrical signal that is recorded at the scalp in response to a light signal.

2.1.1. Technical aspects

The most common luminous stimulus is a checkerboard pattern-reversal given its low inter-subject reliability. Black and white check sizes and field types are adapted according to the clinical question. For instance, smaller checks (15'') are more sensitive to foveal disorders, whereas larger check (30 or 60'') stimulate the peripheral vision and, instead, minimize problems related to amblyopia. Concerning field type, full pattern

stimulation is routinely used, and hemi-field stimulation is applied when evaluating chiasmatic or retro-chiasmatic lesions. Given its high inter-individual variance, un-patterned stimulation (flash instead of black and white checks) is reserved to patients who cannot fixate, namely infants, unconscious/sedated and those with severely impaired visual acuity.

Electrodes are placed over the occipital region (Oz, O1 and O2), referenced to a frontal electrode[25]. Main components include a succession of negative-positive-negative peaks labelled as N1 peaking at 75ms, P1 peaking at 100ms and N2 peaking at 145ms. Changes in latency, amplitude and waveform topography are reported. However, difference in P1 (P100) latency and inter-ocular variance of this component is the most reliable measurement in clinical practice.

2.1.2. Clinical correlates

VEP and its multifocal variant (mf-VEP; stimulating up to 60 simultaneous sectors of the visual field), are used to assess optic nerve damage[28]. Since VEP latency reflects the "myelin status" of the optic nerve, it is helpful in assessing demyelinating disorders of the central nervous system (CNS), for example multiple sclerosis (MS) and neuromyelitis optica spectrum disorder (NMOSD)[29, 30].

MS is a chronic autoimmune condition, which affects young adults, and is characterized by axonal loss, demyelination, and astrocytic gliosis. Disease diagnosis requires objective evidence of CNS lesions disseminated in time and space, typical clinical presentation, and exclusion of an alternative diagnosis. The McDonald criteria for diagnosing MS were revised in 2017 and allowed shortening the time to diagnosis[31].

NMOSD is distinct from MS in that is associated with serum aquaporin-4 immunoglobulin G antibodies (AQP4). Clinical features, imaging findings and treatment response also differs from MS. The core clinical characteristics required for patients with NMOSD with AQP4 antibodies include damage in the optic nerve (more than half of the optic nerve length or including optic chiasm), spinal cord (extensive transverse myelitis), area postrema, brainstem, cerebral parenchyma, or diencephalon[32].

Historically, VEP were used to support MS *diagnosis* but they were swiftly replaced by MRI[31, 33]. Curiously, a recent observational real-life study showed that MS misdiagnosis is not unusual (up to 24%), and it mainly occurs due to misinterpretation of nonspecific

MRI findings (e.g. non-specific white matter abnormalities). Authors suggested that a normal VEP exam can help to differentiate from other MS mimics with a negative predictive value of 92.5%[34]. In addition, several trials used EP to *monitor disease progression* under disease modifying treatments[35] and to *predict future disability* for up to 20 years[36]. Finally, the advent of neuroprotective agents repurposed the use of VEP as a *biomarker* for remyelination and treatment response in MS trials[37-39].

Although EP measurements are frequently used in MS, few data are available on its clinical value in NMOSD. A recent longitudinal study showed increased VEP abnormalities in a cohort of 167 patients with NMOSD despite the absence of acute visual symptoms (i.e. optic neuritis)[40]. In addition, a comparative study with optical coherence tomography showed superiority of VEP in assessing asymptomatic visual impairment in NMOSD[41]. To sum up, these findings support the diagnostic (i.e. ruling-out MS mimics), prognostic and monitoring value of VEP in demyelinating CNS disorders and optic neuropathies.

Pathologies which alters conduction in the retino-striate pathway will result in VEP abnormalities. This includes optic nerve damage of tumoral (e.g. glioma), toxic (e.g. alcohol, medication such as tacrolimus or ethambutol), ischemic, nutritional (including vitamin B12 deficiency), genetic (e.g. Friedreich's ataxia, mitochondrial disorders, albinism) or compressive origin (e.g. sarcoidosis) (for a review see Holder, 2004[42]). VEP are frequently delayed in different eye conditions, namely glaucoma and amblyopia[43]. It is also extremely helpful in the assessment of functional visual loss and detection of malingering[44]. This list is indicative only and non-exhaustive.

2.2. Somatosensory evoked potentials

Somatosensory EP (SEP) assess the entire sensory system, from the peripheral nerve to the somatosensory cortex via the dorsal column pathways. They are used in a variety of clinical settings (see section 2.2.2.).

2.2.1. Technical aspects

The most frequently stimulated sites include median nerve at the wrist for the upper limb and tibial nerve at the ankle for lower limb evaluation. Cranial nerves (trigeminal), ulnar nerve and peroneal nerve can also be assessed.

Transcutaneous electrical stimulation is applied to a mixed nerve using a constant current/voltage stimulator. Stimulus intensity is adjusted to elicit a painless thumb/toe twitch, probably leading to simultaneous activation of cutaneous, muscle and joint afferents, as well as efferent fibers (muscle)[45]. Unfortunately, this is considered a drawback of the technique, which is sought to stimulate both sensory and motor cortices. Other stimulation techniques such as thermal, laser (pain pathway) and vibrotactile (skin mechanoreceptors) stimulation were developed to specifically activate the spino-thalamic and the lemniscal pathyway, respectively[46-48]. Nevertheless, these are not used in routine clinical practice.

Electrodes are placed along the neuraxis at a peripheral (Erb's point or popliteal fossa), medullar (cervical, lumbar), and scalp level (centroparietal ipsilateral and contralateral to the stimulated side, centroparietal midline)[23]. Several components are recorded at these sites: 1) the first waveform constitutes a peripheral response arising at 9ms for the upper limb (N9) and 8ms for the lower limb (N8), 2) followed by a negative potential ascending from the spinal cord (upper limb: N13; lower limb: N22), 3) then a negative peak originating from multiple generating sources from the brainstem and the thalamus (upper limb: N18; lower limb: N34) and, 4) finally, a main component originating from the primary somatosensory cortex (upper limb: N20; lower limb: P37). Criteria for abnormality include prolonged absolute latency and interpeak latencies, as well as the absence of the abovementioned components determined by visual inspection.

2.2.2. Clinical correlates

Sensory function is difficult to assess and is based on subjective observations that are verbally expressed by the patient. SEP provides an objective and functional assessment of the somatosensory pathway and can help on patients with diagnostic uncertainty. Until the advent of imaging methods, SEP were used to depict subclinical lesions or to validate sensory complaints[49]. Currently, SEP is considered complementary to structural exams (MRI) and clinical examination.

The role of EP was largely studied in MS. Initially, they were performed as a decision *diagnostic* support[50, 51]. Nevertheless, with the establishment of the 2010 McDonald revised diagnostic MS criteria, clinical and radiological features prevailed and EP were disregarded[52]. With time, SEP were reappraised as a *monitoring* and *prognostic* tool in

combination with other EP modalities (i.e. establishing EP scores)[53]. In an early study, combined abnormal SEP and motor EP performed at disease onset, were highly predictive of clinical disability (Expanded Disability Status Scale or EDSS) at five years (OR 11.0)[54]. Further retrospective studies showed similar results[53, 55-57], suggesting that SEP may be useful to identify MS patients at high risk of long-term disease progression and guide on the decision-making process regarding disease modifying therapies[35].

The role of SEP in non-traumatic comatose patients has been largely established[58, 59]. Bilateral absence of cortical median nerve SEP predicts poor outcome in hypoxic/ischemic brain damage and, thus, can help to decide on withdrawal of life sustaining therapies. Despite a low pooled sensitivity (around 46%), SEP is highly specificity with a 0.7% false positive rate for poor outcome, as described on a systematic review including eight studies[59]. However, to avoid overinterpretation of SEP results, this decision must be based in a multimodal approach by means of neurological examination, auditory EP mismatch negativity, EEG and brain imaging[60, 61]. Modern EEG recording by means of ESI was applied in research studies to detect transition into different brain states[62]. To our knowledge, no study has been reported so far on SEP source imaging and coma prognostication. It would be interesting to know if this technique provides additional information to conventional SEP (i.e. gain in sensitivity).

SEP are used in a preoperative and intraoperative setting to guide surgical resections of lesions which are lying in functional areas. The main aim is to avoid permanent postoperative neurological damage. Intraoperative SEP monitoring is performed to obtain a “real time” picture of the entire sensory system all through surgery. Clinical uses for intraoperative SEP monitoring include intracranial and spinal surgery, as well as cerebrovascular interventions (for a review see MacDonald et al. 2019[63]). Some limitations of the technique are mainly related to anaesthesia and other physiological variables (i.e. hemodynamic, temperature, etc.). These variables can modify the EP response[64]. International recommendations were established for intraoperative monitoring with SEP[63]. Preoperative assessment in patients with drug resistant epilepsy and in neuro-oncology will be detailed in section 3.2.

Optimal recording conditions, criteria of abnormality and clinical use has not yet been well established in other EP modalities. Non-routine examination comprises pain-related

laser evoked potential (LEP), chemosensory event-related potentials (CSERP), vestibular myogenic (VEMP), multimodal assessment (mmEP) (for a review see Lascano et al., 2017)[27].

2.3. Chemosensory event-related potentials

Olfactory dysfunction is a frequent complaint encountered by the ear and nose specialist. It is observed in neurodegenerative disorders or as a complication of head trauma or post-viral infection. Chemosensory testing should be considered to determine the severity of the complaint, provide safety counselling, start olfactory training (i.e. sniffing a set of odorants) and propose therapies (intranasal vitamin A and oral omega-3)[65].

Chemosensory examination includes i) psychophysical assessment, including tests of odour threshold, identification or discrimination by means of sniffing sticks, and ii) electrophysiological tests: electro-olfactogram (i.e. potentials measured at the level of the olfactory epithelium) and CSERP (for a review on olfactory assessment see Doty 2015)[66]. As opposed to psychophysical tests, which depend on the subject's ability to cooperate, CSERP provide an objective and reliable measure of the entire olfactory pathway.

2.3.1. Technical aspects

Odour stimuli is delivered into the nostril by means of a computer-controlled olfactometer. This device allows precise administration of a rectangular-shaped stimulus into an odorless and constant airstream, trying to reproduce a "physiological" setting and avoiding irritation of the olfactory mucosa. Different odour types, scent concentrations, stimulus duration, flow rate and interstimulus interval are applied to suit the clinician's needs (see section 2.3.2).

Electrodes are placed in the midline (Fz, Cz and Pz) and in centro-parietal locations (C3, C4), referenced to linked earlobes. A minimum of 10-30 consecutive artefact-free trials, separated by an interstimulus interval of > 1 second, are required to measure reliable responses and avoid habituation. Typical CSERP response includes a negative-positive complex (N1-P2) peaking between 200-700 ms. Earlier (P1) and later components (P2-

P3) are inconstant and depend on the stimulus property. CSERP response also varies according to demographic factors, for example gender and age[67].

2.3.2. Clinical correlates

CSERP have received increasing attention in the past 20 years. Ear, nose and throat clinics propose the use of CSERP as a complementary tool in the assessment of olfactory dysfunction, especially if the nature of the problem is unclear[68].

Post-viral anosmia, following an infection of the upper respiratory tract, is one of the main causes of olfactory dysfunction in adults. Smell loss is a common complaint in patients with coronavirus disease 19 (COVID-19) given the probable neurotropic properties of the virus[69]. Although the exact mechanism underlying olfactory dysfunction in COVID-19 is poorly understood, viral infection can be responsible of damage of the olfactory mucosa and the olfactory receptor neuron. In this sense, CSERP can help to establish prognosis of the olfactory disorder[70]. A study by Rombaux and collaborators performed in 27 patients with post-infectious olfactory loss showed that persistence of CSERP predicts a favourable outcome with an 83% specificity[71].

Several CSERP studies were performed to better understand olfactory function in neuropsychiatric disorders[72], neurodevelopmental delay[73], neurodegenerative diseases (Alzheimer's and Parkinson's[74]), MS[75], temporal lobe epilepsy[76] and sino-nasal diseases. Although CSERP showed its ability to detect olfactory dysfunction in these group of patients, how the results apply to an individual subject and to solve a unique question is currently unknown. In addition, the lack of clinical practice guidelines and the high machinery cost, make CSERP difficult to apply in routine. For more information concerning future perspectives of the technique see section 4.3.

3. Electroencephalography as a functional neuroimaging method

The use of specialized techniques to examine brain function is referred to as *functional neuroimaging* and has revolutionized the way we study neuroscience in humans. Functional neuroimaging is used to explore how human brain works and the way it is connected. For this to occur, the technique should provide an optimal spatial and temporal resolution as well as complete spatial coverage. Unfortunately, most imaging

methods do not possess all these properties and a trade-off must often be made between spatial and temporal accuracy.

3.1. Brain functional imaging techniques

Modern functional neuroimaging methods can be divided into two groups: i) electromagnetic-based devices, by means of EEG and MEG, and ii) hemodynamic techniques, namely functional magnetic resonance imaging (fMRI) and PET. All these methods have their advantages and disadvantages.

There is a clear trade-off between metabolic-based and electromagnetic-based methods. While the first provide an excellent spatial resolution, in the order of mm^3, the second offers measurements with a superior temporal resolution, in the millisecond range[77, 78]. The temporal resolution with: i) fMRI is limited by the slow hemodynamic response time (in seconds), and with ii) PET is constrained by the measurement of the radiotracer activity and imaging reconstruction (in seconds or minutes). In a nutshell, EEG and MEG capture ongoing human brain physiological changes much better than other brain imaging techniques (such as fMRI or PET scanners), while providing good quality resolution in the space domain.

Although EEG and MEG are very similar methods, the former records brain electrical fields, while the latter measures brain magnetic fields. Several studies suggest that localization precision with EEG can be superior to that of MEG, provided they present the same number of sensors[79]. This is partly because EEG is sensitive to both radial and tangential dipoles, whereas MEG signals are mainly generated by intra-neuron currents derived from tangentially oriented sources to the surface of the scalp[80, 81]. The advantage of one technique over the other is still a constant matter of debate[79, 82, 83]; nonetheless, EEG has the benefit of being more affordable and readily available on a clinical setting.

Recent engineering approaches have been developed to improve the spatial resolution of these modalities, called (electrophysiological) *source imaging*. Typically, these approaches require a large spatial coverage by means of electrodes in case of EEG and sensors with MEG recordings.

3.2. High-density electroencephalography

Standard electrode placement provides an incomplete coverage of the human skull (for more details see section 1.2.). In order to obtain good spatial resolution, the International Federation of Clinical Neurophysiology (IFCN) recommend the use of at least 75-256 scalp electrodes to record EEG in a research setting, especially in non-invasive epileptic source localization[84]. This is referred to as "*high density EEG*". These recommendations are based on several studies showing epilepsy focus misplacement whenever conventional EEG setup was applied (i.e. < 32 electrodes). Conversely, more accurate localization was obtained while using a larger number of sensors and individual head template models[3, 85, 86].

Moreover, powerful multi-channel EEG recording systems with high sampling rates and complex software were manufactured to keep up with the increasing number of electrodes[87, 88]. With the advent of commercially available multichannel EEG systems, mapping of the scalp electric field became possible. However, the cost of the equipment and the required computational expertise could be considered a downfall.

3.3. Mapping and electric source imaging

In electrophysiological terms EEG/EP *mapping* is sought to be a precursor to *electric source imaging* (ESI) since correct analysis of these scalp field maps provide valuable information on the underlying sources in the brain. Scalp EEG can be portrayed as a constantly changing map constituted of shifting electric currents originated from the underlying post-synaptic potentials. Since each electrode represents a current sample point; an increasing number of electrodes will improve the "map's resolution".

The aim of ESI is to study a specific brain function and relate it to its architectonic structure[89, 90]. However, there are several constraints that need to be solved: the EEG forward problem (calculate the potentials at the electrode position from an intracranial source) and inverse problem (find the underlying brain generators which are generated by a measured EEG).

To reach the scalp, pyramidal cell post-synaptic potentials must pass through several layers of brain tissue, cerebrospinal fluid, skull, and skin, with different conductivities, thus attenuating the electric fields. This current flow attenuation needs to be properly modelled to determine the scalp field map recorded by a set of electrodes and

generated by a given source, this is known as the EEG forward problem[91]. The use of realistic three-dimensional head models based on accurate co-registration of scalp electrodes' position with the MRI volumes, allow to solve the forward problem. Local skull thickness on the individual head and exact electrode position are applied to determine how that electrical activity relates to the different sources in the brain. It is highly recommended to use the individual MRI of the patient to build the head model. Amongst the different head models, boundary-element and the volume element methods are the most frequently applied (for a review see Michel and He)[92].

An understanding of the so-called forward problem is necessary to approach the inverse problem. The EEG inverse problem tries to find the electrical intracranial source which better explains the result observed on a surface EEG (source reconstruction). The main limitation of the inverse problem is that there is no single solution[93]. The only way to get around this conundrum is to assume that neural sources are better described by a given model (i.e. equivalent dipoles, distributed solutions) and, subsequently, reduce the number and spatial configuration of possible solutions. The choice of a model depends on the type of dataset and the number of neuronal generators. Some inverse solutions restrict the number of sources (e.g. equivalent dipoles)[94], while others represent the brain activity with several points distributed across the entire space (e.g. distributed solution)[95]. The latter has the advantage that it considers the brain as a "network", which can be particularly useful while analysing epileptic activity. To this day, no consensus has been established with respect to the choice of head modelling and the inverse solution algorithm. Several academic and commercial software packages for EEG/MEG source localization are available. For a recent review on the technical and methodological aspects of ESI see Michel & Brunet 2019[96].

4. Clinical yield of high-density electric source imaging

4.1. Presurgical localization of the epileptic focus

About a third of people with epilepsy are drug-resistant and many of them are potential surgical candidates (50% will be candidates and 2/3 seizure free)[97, 98]. However, accurate localization of the cerebral abnormality that might cause epilepsy can be quite challenging. The main aim of surgery is to achieve seizure freedom, although this is not always achieved.

Characterization of the epileptogenic zone has evolved across time. Luders and colleagues defined it as “the area of cortex that is necessary and sufficient for initiating seizures and whose removal is necessary for complete abolition of seizures”[99]. However, there are other areas interacting with the epileptogenic zone which are also responsible for epileptic seizures: the irritative zone (interictal epileptic spikes generator), the seizure onset zone (seizure generator), the symptomatogenic zone (area producing ictal symptoms), the epileptogenic lesion and the functional deficit zone (malfunctioning area during the interictal period). Unfortunately, the epileptogenic lesion is not always visible in brain MRI. Around 16% of patients with drug resistant epilepsy presented with normal MRI and only 38% became seizure free after surgery (versus 66% in the MRI positive group)[100]. Proper identification of the epileptogenic zone and potential overlap with the other areas, particularly in MRI negative patients, may lead to surgery and, ideally, increase the likelihood of seizure freedom.

At present, there is no standalone technique which can reliably detect the epileptogenic zone. Presurgical evaluation of the epileptic candidate includes a multimodal approach[12] by means of semiology, neuropsychological exams, PET, high-quality structural MRI, video-EEG telemetry, ictal single-photon emission computed tomography (SPECT), MEG. When these techniques are concordant, epilepsy surgery can be proposed, provided that the epileptogenic zone is not lying in areas of the cortex that are vital for language, sensorimotor or other cognitive functions (for further information on mapping the eloquent cortex see section 4.2.). This highlights the importance of a multimodal approach in the presurgical assessment of epilepsy.

Current technological advances in terms of EEG/MEG recording and analysis, motivated the use of EEG and/or MEG source imaging to estimate the underlying brain activity using an electric conduction model constructed from the individual patient’s MRI (for further information see section 3.3.). ESI has proven its worth in identifying interictal and ictal epileptic activity, and, thus, assist clinicians to determine the epileptogenic zone. A recent study showed that interictal ESI maximum correlated with the seizure onset zone recorded with intracranial EEG in 38 patients with focal epilepsy. The resection of the depicted area was associated with a favourable surgical outcome[101]. Moreover, resection of the seizure onset zone without including areas presenting with interictal epileptiform abnormalities resulted in poor surgical outcome in 6/13 patients with lateral-

temporal and extra-temporal epilepsy[102]. However, these results cannot be generalized, since accurate localization of the irritative zone does not always imply that lesion resection will lead to seizure control.

Despite the advantages of the technique a survey on the clinical use of ESI across Europe showed that only 9/25 centres applied this technique as part of their multimodal diagnostic workup[103]. This might be due to technical and financial reasons. ESI requires expertise in analysing the EEG and advanced computer skills to process the data (e.g. spike selection, co-registration of patient's MRI, source localization). Recent efforts have focused in developing a semi-automated spike detection method and source localization from long-term EEG recordings. Results were compared to seizure-free outcome at one year, showing a 78% of diagnostic accuracy[104]. Automated detection of interictal activity is an interesting alternative, to improve analysis procedure.

4.2. Preoperative mapping of the eloquent cortex

4.2.1. Non-invasive localisation of the somatosensory cortex

Localizing and delineating the eloquent areas prior to surgery is extremely important if planned resection occur near these areas. This is particularly relevant during preoperative assessment for epilepsy surgery (see section 4.1.) or brain tumours. Since certain lesions can distort visual inspection of anatomical structures in the MRI, accurate preoperative delineation of the central sulcus by means of SEP and/or motor mapping is crucial to ensure successful outcome in intracranial surgery. Sensory and motor mapping can be combined to optimize localization results.

As opposed to fMRI, SEP has the advantage of evaluating "real-time" changes of the sensorimotor systems for a relatively low cost and, due to its good safety profile, it can be repeated several times on the same patient. However, fMRI provides a more accurate spatial resolution. Combination of both techniques could allow for more accurate identification of the eloquent cortex, providing better surgical outcomes.

Preoperative SEP is nowadays possible by means of ESI and can be used to: i) predict post-operative outcome, ii) for medical-legal reasons and, iii) to identify and avoid functional sensory cortex surrounding the unhealthy brain tissue. Although very few centers perform source imaging based SEP recordings, it can be used as part of a multimodal evaluation in association with other neurophysiological techniques (i.e.

electrocortical stimulation, motor EP, MEG) and imaging methods (i.e. functional MRI) to minimise the risk of causing long-lasting deficits.

Besides electrical stimulation of the median and tibial nerves, other methods were developed to specifically activate the somatosensory cortex, while avoiding participation of the motor cortex: pneumatical, vibrotactile, nociceptive (laser EP or LEP), etc[48, 105]. However, these methods are not part of the routine evaluation of a patient with sensory complaints in a presurgical setting.

In this essay, we present a method for presurgical evaluation of the somatosensory cortex by means of a painless pneumatical tactile stimulation combined with modern analysis of EP (i.e. ESI). Localization accuracy will be assessed in comparison with invasive procedures and fMRI in a group of pharmacoresistant epilepsy patients and in healthy subjects.

4.2.2. Neuroanatomical correlates of olfactory function

Unlike other sensory modalities, olfaction bypasses the thalamus, sending projections directly to the piriform cortex and, later, to other brain regions. Even though the anatomical circuitry has been largely established in animal models[106] and imaging studies[107], little is known about the spatio-temporal dynamics of olfactory processing in the human brain.

Initial neuroimaging investigations of the human olfactory system were conducted in the early 90's, using PET and fMRI, and provided important information on the structures involved in smell[108, 109]. As stated above, these techniques render a high spatial resolution with a low temporal precision (see section 3.1.). For this purpose, electrophysiological measurement of olfactory function by means of CSERP were developed. CSERP responses vary in terms of amplitude and latency according to the stimulated nostril, age, sex, odour characteristic (hedonistic versus aversive compounds) and concentration[67].

While hemispheric specialization of cognitive domains such as language and computation are well established, lateralization of olfactory processing is currently unknown. Several studies proposed a right hemispheric dominance in the treatment of olfactory information, relationship with the hand-dominance and the olfactory bulb volume was suggested[108, 110].

This dissertation presents the first CSERP study recorded with EEG source imaging in healthy volunteers. It provides additional information on the spatio-temporal neural dynamics in processing of olfactory sensory stimuli.

4.3. Olfactory assessment in neurological disorders

4.3.1. Presymptomatic detection of neurodegenerative diseases

Olfactory dysfunction is one of the earliest pre-clinical signs of Parkinson's disease (PD), Alzheimer's disease (AD) and subjects with mild cognitive impairment (MCI)[111]. Even though the mechanisms underlying olfactory loss are different between AD and PD, it is known to correlate with disease stage[112] and is independent of normal-aging smell loss[113]. A recent meta-analysis including almost 80 scientific publications, suggested that PD's olfactory dysfunction is partly explained by a peripheral olfactory process impairment (i.e. abnormal sniffing pattern) rather than a disturbance in higher-order cognitive skills. The opposite seems to be true for AD[113]. However, in terms of electrophysiological findings, there is no such distinction, since both disorders are associated with prolonged latency but normal amplitude of CSERP components[74].

CSERP latencies of late components (P3) were significantly prolonged in asymptomatic individuals carrying the E4 allele of the apolipoprotein E gene (APOE4)[114, 115]. These individuals are sought to be at risk of AD, cognitive decline and vascular diseases as compared with those carrying the E3 allele. The identification and validation of markers for diagnosis and follow-up of AD and other forms of dementia is extremely important. Accurate diagnosis of AD can be difficult in elderly patients presenting with combined cognitive, behavioural, and affective complaints. CSERP could be used as a screening tool for dementia in patients with early cognitive complaints and to differentiate from late-life onset depression[116]. Early disease detection and staging, together with cerebrospinal and plasma biomarkers, can be useful to select candidates for treatment trials in AD. Given that these therapies aim at reducing the neurodegenerative burden of the disease, CSERP can serve as a follow-up tool, with a satisfying test-retest reliability, for degenerative olfactory changes in AD.

Although PD is generally thought of as a movement disorder, several non-motor symptoms, including loss of the sense of smell and sleep disorders, occur at early stages of the disease. Conversely, cognitive decline does not emerge until late in the

progression of PD. Abnormal smell function assessed by CSERP predicted early cognitive decline (i.e. Montreal cognitive assessment score) in recently diagnosed patients[117]. In this study, CSERP was capable to predict cognitive impairment in PD.

In addition, odour assessment can help to distinguish between PD and tauopathies associated with parkinsonism: corticobasal degeneration and progressive supranuclear palsy[118]. However, olfactory ability should not be used to distinguish multiple system atrophy and dementia with Lewy bodies from PD. Olfactory function is also affected in these diseases and even predicted conversion to dementia with Lewy body in a group of 9/34 (26.5%) patients with REM sleep behaviour disorder at 2.5 years[119].

It becomes evident that olfaction provides a window for understanding neurodegenerative diseases. However, there is a strong need for the application of reliable tools with low inter-rater variability to evaluate the olfactory function. To conclude, CSERP is a reliable method and several studies have proven its worth in the early diagnosis, prediction of cognitive impairment and assessment of treatment response in neurodegenerative diseases.

4.3.2. Prognostic value in neuro-oncology

A recent study showed a strong correlation between olfactory dysfunction and unfavourable outcome in a cohort of 73 patients with gliobastoma multiforme[120]. Interestingly, there is no correlation between olfactory function and MRI findings, since both patients and controls (i.e. subjects with other neurological diseases) showed no radiological abnormalities in the olfactory pathway. Although neurotoxic effects of radiotherapy and chemotherapy cannot be ruled out, it has been hypothesized that malignant stem-like cells might infiltrate the olfactory bulb, thus, causing olfactory impairment. We can postulate that olfactory testing including CSERP could help to predict patients at risk of developing a more severe disease course.

4.4. Prognostic marker in multiple sclerosis

MS is a disease with an heterogenous presentation and different disease subtypes (progressive versus relapsing-remitting forms). The treatment of MS is evolving rapidly with an increasing number of therapies. Current treatment target is to achieve “no-evidence of disease activity” (NEDA): absence of inflammatory activity on MRI, clinical

relapses, and disease worsening (EDSS score). Patients achieving NEDA at two years had a positive predictive value of 78% for lack of progression at 7 years[121]. Specialized MS centres are also including brain atrophy and neurofilament light chain concentration into the equation (NEDA-5). It makes sense to adopt a composite score using different clinical and paraclinical studies. EP has many advantages over other paraclinical studies: it can be repeated numerous times and at different stages of the disease, it is relatively cheap, and it is very easy to perform.

Although several studies have proven the use of multimodal EP in predicting clinical evolution in MS (see section 2.1.2. and 2.2.2.), some evidence exists concerning the added value of ESI as a prognostic marker. Microstate analysis of high-density EEG performed in 53 relapsing-remitting MS patients showed a correlation between altered temporal fluctuation of scalp topographies, decreased cognitive performance and an increased two year annualized relapse rate[122]. We can hypothesize that electrophysiological tools could be use in MS disease prognosis and treatment monitoring, together with imaging and biological biomarkers. However, further studies are required to validate this finding.

5. Experimental studies

This dissertation is based upon five studies which were published in peer-reviewed journals:

I. Brodbeck V, Spinelli L, **Lascano AM**, Wissmeier M, Vargas MI, Vulliemoz S, Pollo C, Schaller K, Michel CM, Seeck M. EEG Source Imaging: a prospective study of 152 operated epileptic patients. Brain 2011; 134: 2887-2897.

II. **Lascano AM**, Pernegger T, Vulliemoz S, Spinelli L, Garibotto V, C. Korff, Vargas MI, Michel CM, Seeck M. Yield of MRI, high-density source imaging (HD-ESI), SPECT and PET in epilepsy surgery candidates. Clin Neurophysiology 2016; 127: 5-7.

III. **Lascano AM**, Grouiller F, Genetti M, Spinelli L, Seeck M, Schaller K, Michel CM. Surgically relevant localization of the central sulcus with high-density SEP compared to fMRI. Neurosurgery 2014; 74: 517-26.

IV. **Lascano AM**, Hummel T, Lacroix JS, Landis B, Michel CM. Spatio-temporal dynamics of olfactory processing in the human brain : an event-related source imaging study. Neuroscience 2010; 167: 700-708.

V. **Lascano AM**, Brodbeck V, Lalive P, Chofflon M, Seeck M, Michel CM. Increasing the diagnostic value of evoked potentials in multiple sclerosis by quantitative topographic analysis of multichannel recordings. J Clin Neurophysiol 2009; 26: 316325.

All studies applied modern techniques for electroencephalography (EEG) and evoked potentials (EP) recording and analysis, by means of electric source imaging (ESI), to solve a given research question in different neurological domains: epilepsy, MS, and olfactory processing.

Even though the hypothesis and type of disease studied differs, the technique applied remains the same. This essay intends to show that ESI is a neurophysiological tool that can be easily applied in clinical practice and provide additional information, while compared to conventional EEG or EP analysis, in terms of diagnosis, prognosis, and disease/treatment monitoring.

While application of ESI in clinical practice is varied, this dissertation assesses its use in three specific domains:

Pre-surgical evaluation of epileptic patients

Accurate pre-operative assessment allowing to define the epileptogenic zone and to avoid the eloquent cortex (see below) is vital to ensure success of surgical treatment in intractable epilepsy. Studies I and II examined the clinical value of source imaging based on high-density EEG recordings (ESI) as a standalone technique (study I) or in association with other imaging methods (study II). Results and success rate were measured in terms of post-operative outcome (i.e. seizure-freedom).

The first study assessed the sensibility and specificity of ESI based on high-density EEG recordings (i.e. 128-256 electrodes) versus standard EEG setup (19 to 32 electrodes) and other imaging techniques in a prospective cohort of 152 epileptic patients. It also compared the use of an individual head model versus a template brain for source localization (see section 3.3.).The second study compared the added value of ESI in association with other imaging techniques in a larger number of patients (n=190).

Mapping brain cortex

Study III and IV assessed the use of high-density EP recording to map brain sensory functions in normal subjects and epileptic patients. Study III demonstrated the capability

of imaging the somatosensory cortex by means of non-invasive electrophysiological measurements as opposed to invasive intracranial EEG findings (DCES) and functional MRI. Study IV investigated large-scale spatio-temporal dynamics of olfactory sensory processing by means of source imaging based high-density EP recordings in a group of twelve healthy volunteers.

Topographic analysis of evoked potentials in multiple sclerosis

Study V compared sensibility and specificity of both conventional and topographic EP analysis, while using multiple sclerosis as a disease model. Traditional EP analysis relies on latency and amplitude measures of the different components. Whereas, modern analysis includes objective detection of EP components and extraction of novel information in terms of electric field potential. Reliability, validity, and clinical utility of ESI analysis of visual and somatosensory EP was evaluated in this study.

Study I

Brodbeck V, Spinelli L, **Lascano AM**, Wissmeier M, Vargas MI, Vulliemoz S, Pollo C, Schaller K, Michel CM, Seeck M. EEG Source Imaging: a prospective study of 152 operated epileptic patients. Brain 2011; 134: 2887-2897. Doi: 10.1093/brain/awr243.

- Impact Factor: 11.814
- 5-year Impact Factor: 11.773
- Average citations per year: 19.2
- Sum of times cited (without self-citations): 192
- Copyright clearance (license number): 4840790546832 (Oxford University Press)

doi:10.1093/brain/awr243 Brain 2011: 134; 2887–2897 | 2887

BRAIN
A JOURNAL OF NEUROLOGY

Electroencephalographic source imaging: a prospective study of 152 operated epileptic patients

Verena Brodbeck,[1] Laurent Spinelli,[2] Agustina M. Lascano,[1] Michael Wissmeier,[3] Maria-Isabel Vargas,[3] Serge Vulliemoz,[2] Claudio Pollo,[4] Karl Schaller,[5] Christoph M. Michel[1] and Margitta Seeck[2]

1 Department of Basic and Clinical Neurosciences, University of Geneva, 1211 Geneva, Switzerland
2 EEG and Epilepsy Unit, Neurology Clinic, University Hospital Geneva, 1211 Geneva, Switzerland
3 Department of Radiology, University Hospital of Geneva, 1211 Geneva, Switzerland
4 Department of Neurosurgery, University Hospital (CHUV), 1011 Lausanne, Switzerland
5 Department of Neurosurgery, University Hospital Geneva, 1211 Geneva, Switzerland

Correspondence to: Prof. Margitta Seeck, MD,
EEG and Epilepsy Unit, Neurology Clinic,
University Hospital (HUG) and University of Geneva,
4, Rue Gabrielle-Perret-Gentil,
CH-1211, Geneva
E-mail: margitta.seeck@hcuge.ch

Electroencephalography is mandatory to determine the epilepsy syndrome. However, for the precise localization of the irritative zone in patients with focal epilepsy, costly and sometimes cumbersome imaging techniques are used. Recent small studies using electric source imaging suggest that electroencephalography itself could be used to localize the focus. However, a large prospective validation study is missing. This study presents a cohort of 152 operated patients where electric source imaging was applied as part of the pre-surgical work-up allowing a comparison with the results from other methods. Patients ($n = 152$) with >1 year postoperative follow-up were studied prospectively. The sensitivity and specificity of each imaging method was defined by comparing the localization of the source maximum with the resected zone and surgical outcome. Electric source imaging had a sensitivity of 84% and a specificity of 88% if the electroencephalogram was recorded with a large number of electrodes (128–256 channels) and the individual magnetic resonance image was used as head model. These values compared favourably with those of structural magnetic resonance imaging (76% sensitivity, 53% specificity), positron emission tomography (69% sensitivity, 44% specificity) and ictal/interictal single-photon emission-computed tomography (58% sensitivity, 47% specificity). The sensitivity and specificity of electric source imaging decreased to 57% and 59%, respectively, with low number of electrodes (<32 channels) and a template head model. This study demonstrated the validity and clinical utility of electric source imaging in a large prospective study. Given the low cost and high flexibility of electroencephalographic systems even with high channel counts, we conclude that electric source imaging is a highly valuable tool in pre-surgical epilepsy evaluation.

Keywords: EEG; electric source imaging; focus localization; temporal lobe epilepsy; epilepsy surgery

Abbreviations: MEG = magnetoencephalography; SPECT = single-photon emission-computed tomography; PET = positron emission tomography; ESI = electric source imaging

Received June 3, 2011. Revised August 15, 2011. Accepted August 16, 2011

Introduction

Surgical resection of the epileptogenic zone is an under-utilized and potentially curative treatment for pharmacoresistant patients with focal epilepsy. Crucial to the success of surgical treatment is a robust pre-surgical evaluation protocol that identifies and localizes the epileptic focus—both to specify the surgical target and to define that target's proximity to indispensable cortical areas. Non-invasive imaging methods are of utmost importance in the pre-surgical evaluation process. In clear cases, they make further invasive investigations—with their inevitable costs and risks—unnecessary. In more difficult cases, they give important *a priori* information that guides and helps validate the results of the invasive procedures.

So what methods should this non-invasive pre-surgical protocol include? Magnetic resonance imaging (MRI), positron emission tomography (PET) and single-photon emission-computerized tomography (SPECT) are the most established non-invasive imaging methods in pre-surgical evaluation and have their undoubted value. They correctly localize the epileptic area in ~50–80% of cases depending on the presence or absence of a structural lesion (Spanaki *et al.*, 1999; Henry and van Heertum, 2003; Knowlton *et al.*, 2008). The conventional 19- to 32-scalp EEG is generally not considered a reliable localization method, even though it is the most essential tool to characterize the epileptic syndrome.

A recent comprehensive review (Plummer *et al.*, 2008) suggests that electric source imaging deserves a place in the routine work-up of patients with localization-related epilepsy. Electric source imaging is a technique that applies inverse source estimation methods to non-invasive scalp EEG recorded with multiple electrodes arrayed across the entire scalp ('whole head'). However, the authors noted that while studies done to date—largely with small patient numbers—were promising, a prospective validation study conducted on a larger patient group was still required. With the present study, we intend to fill that gap. We report the results of a prospective and blinded electric source imaging analysis of 152 patients who were subsequently operated with a follow-up period of >1 year.

One point that deserves special attention relates to the usefulness of the non-invasive methods for surgical guidance. Electric source imaging is the co-registration of the electric source estimations with the brain structure of the individual patient or a template MRI. Many of the source localization studies in epilepsy [particularly those using magnetoencephalography (MEG)] utilize spherical head models and subsequent co-registration of equivalent dipoles with the patient's MRI using simple fiducial-based matching methods (e.g. Sutherling *et al.*, 2008; Knowlton *et al.*, 2009). Others utilize a template MRI to construct a realistic head model based on finite or boundary element meshing methods (Fuchs *et al.*, 2006; Zumsteg *et al.*, 2006; Holmes *et al.*, 2008; Wennberg *et al.*, 2011). From a surgical point of view, it is obvious that such strategies do not necessarily provide correct solutions within the 'individual' patient brain on which the surgeon wants to operate. Particularly, lesions and deformations are not taken into account despite the fact that brain anomalies are often encountered in symptomatic epilepsy.

While the advantages of using the individual brain as head model for source localization are obvious, a study showing the effective benefit as compared with a template brain in a large patient cohort has not yet been performed. Likewise, the benefit of large electrode arrays as compared with the conventional clinical EEG with low number of electrodes has also not been completely settled.

The specific goals of our study were therefore to: (i) determine the sensitivity and specificity of electric source imaging using standard clinical recordings with fewer than 30 electrodes versus a high number of electrodes (128–256 electrodes); (ii) to analyse the benefit of using individual MRI as a head model for accurate source localization; and (iii) to compare electric source imaging with other established imaging tools including MRI, PET and SPECT.

Materials and methods

Patients

For this study, we included patients from our database matching the following inclusion criteria: they (i) suffered from pharmacoresistant focal epilepsy; (ii) underwent pre-surgical evaluation with MRI and long-term video-EEG recording; (iii) underwent surgical resection of the presumed epileptogenic zone; and (iv) had a post-surgical follow-up of at least 12 months.

We included in this series all 152 patients (76 male) who matched the inclusion criteria. The age range at the time of the surgical intervention was 1–60 years (median 26.6; mean 26.8 years). The age range at epilepsy onset was 0 (post-natal) to 54 years (median 8.0; mean 11.2 years). Site of surgery was temporal ($n = 102$) or extratemporal ($n = 50$; Table 1). Outcome was good to excellent (i.e. Classes 1 and 2) in 88% of all the patients (Table 2). Outcome differed between both groups, with better results in the patients with temporal lobe epilepsy, compared with the patients with extratemporal lobe epilepsy ($P < 0.01$; Table 2). Twenty-nine patients had a Phase II investigation with intracranial recordings. Supplementary Table 1 gives the characteristics of each of the 152 patients.

Table 1 Site of surgery ($n = 152$)

Site of surgery	*n*
Temporal lobe surgery	102
Extratemporal lobe surgery	50
Single lobe	
Frontal	18
Parietal	6
Occipital	5
Multiple lobes	
Temporo-parietal	6
Parieto-occipital	4
Fronto-temporal	3
Temporo-occipital	2
Fronto-central	1
Temporo-parieto-occiptal	4
Fronto-parieto-temporal	1

Table 2 Outcome after surgery

Group	Engel Class I (%)	Engel Class II (%)	Engel Class III (%)	Engel Class IV (%)
All ($n = 152$)	117 (77.0)	16 (10.5)	13 (8.6)	6 (4.0)
Temporal ($n = 102$)	87 (85.3)	9 (8.8)	2 (2.0)	4 (3.9)
Extratemporal ($n = 50$)	30 (60.0)	7 (14.0)	11 (22.0)	2 (4.0)

Engel Class I: no more seizures with impaired consciousness; Class II: decrease of seizures of >80%; Class III: decrease of 50–80%; Class IV: decrease <50%. Difference between the outcome of temporal and extratemporal lobe surgery is significant ($P < 0.01$).

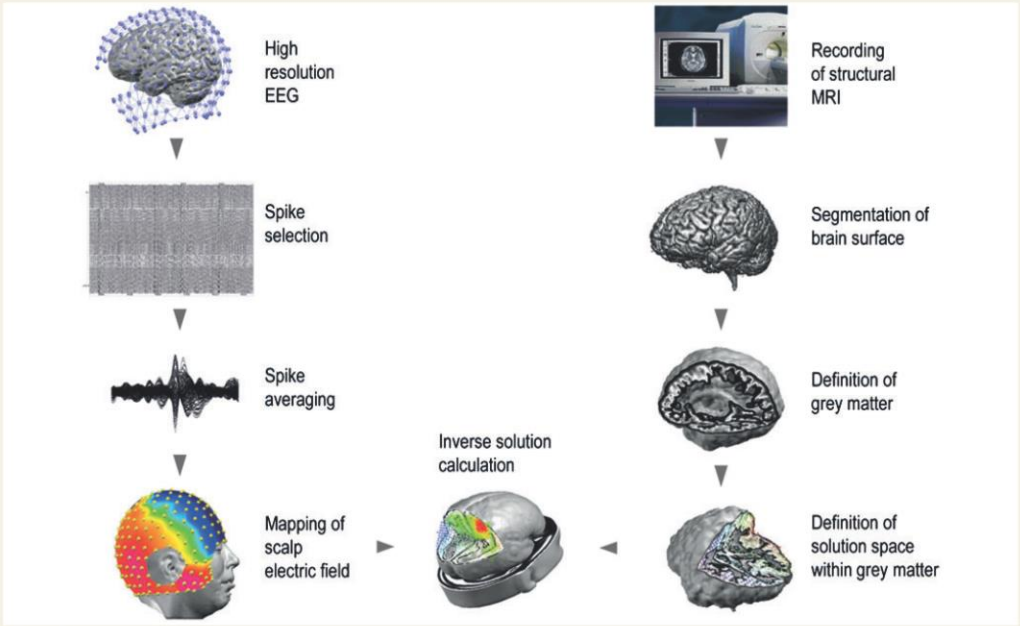

Figure 1 Illustration of the different steps of electric source imaging. (*Left*) Workflow of the EEG analysis. Spikes are manually selected from the EEG (here: 256 channels) and averaged. The potential map at 50% of the rising phase of the averaged spike is used for source analysis. (*Right*) Workflow of the automatic MRI analysis. Segmentation of the brain and grey matter allowed building a simplified realistic head model (SMAC model) with the solution points distributed in the grey matter of the individual brain. This head model is used for the inverse solution calculation, which in this study was based on a distributed linear inverse solution called LAURA.

Electroencephalogram recordings

Conventional long-term video-EEG recording was performed on all patients with standard clinical EEG setups of 19–29 electrodes (10/10 system). Impedances were kept below 10 kΩ, the sampling rate was 256 Hz and band-pass filters were set to 0.1 and 120 Hz, with a vertex contact as the reference electrode.

Ictal scalp recordings were obtained in our laboratory in 146 patients. They were of frontal origin in 12, temporal in 81, parietal in two and occipital in five patients. Seven patients had non-localizing ictal discharges and 35 had bilateral onset.

In 55 patients, a high-resolution EEG was also recorded. Of these patients, 14 had 256 electrode array recordings and 40 had recordings with 128 electrode arrays. For one young patient (2 years old), a 64 electrode array was used. The high-resolution EEG was recorded with the Geodesic Sensor Net® where the electrodes are interconnected by thin rubber bands, containing small sponges soaked with saline water that touch the patient's scalp surface directly (Electrical Geodesics Inc.). The net was adjusted so that Fpz, Cz, Oz and the pre-auricular points were correctly placed according to the international 10/10 system. The tension structure of the net ensured that the electrodes were evenly distributed over the scalp and that they were positioned at approximately the same location across patients. Electrode-skin impedances were kept below 20 kΩ. EEG was continuously recorded for 30 min at a sampling rate of 1 kHz and band-pass filter of 0.1–100 Hz, with the vertex electrode as reference. The EEG was analysed using a semi-automatic procedure, which is illustrated in Fig. 1 and described below.

Electric source imaging method

Selection of interictal epileptogenic discharges and averaging

The offline analysis started with the visual selection of artefact-free interictal epileptogenic discharges by one of the authors (V.B.) experienced in reading clinical EEG and blinded to the patient history. The interictal epileptogenic discharges thus identified were compared with the results of the unblinded review by M.S. or S.V., who were in charge of the patient, and disagreement was resolved through discussion. In only very few patients, there was a discrepancy in the judgement (3/152; 1.9%).

In all patients, the standard EEG (low-resolution EEG) was available first and reviewed in order to determine the epileptogenic contacts with the most prevalent interictal epileptogenic discharges (i.e. >70%). In order to facilitate the recognition of the interictal discharges, the high-resolution EEG was reviewed in a simplified montage, and if interictal epileptogenic discharges were found, marked within the full montage.

Based on a report of the commission of terminology (Chatrian, 1974), the selection criteria were as follows: (i) paroxysmal occurrence; (ii) abrupt change in polarity; (iii) duration <200 ms; and (iv) the interictal discharge has a physiological field. While the Committee on Terminology differs between spikes (<70 ms) and sharp waves (<200 ms), we agree with Walczak and colleagues (2008) that the clinical utility of this differentiation is uncertain, in particular, in the present context. Deep sources may well present 'only' with sharp waves, which is due to the mixture of epileptogenic and overlying physiological electrical currents. Spikes and sharp waves are referred to as interictal epileptogenic discharges.

The interictal epileptogenic discharges were marked at the exact time point of maximal negativity on the electrode trace that showed highest amplitude. Only isolated interictal epileptogenic discharges were included in the analysis (i.e. without any other discharges within ±500 ms) and only the most dominant interictal epileptogenic discharge type was selected. All interictal epileptogenic discharges in a given patient had similar morphology and topography. Interictal epileptogenic discharges were then aligned to the global field power peak and averaged over epochs of ±500 ms around this peak. The EEG map at the 50% rising phase of the averaged interictal epileptogenic discharges was selected and subjected to the source localization procedure because it has been shown that the primary focus is most reliably localized during the rising phase of the interictal epileptogenic discharge, while the interictal epileptogenic discharge peak already involves areas of propagation (Lantz *et al.*, 2003; Ray *et al.*, 2007). All EEG analysis was carried out using the freely available software Cartool (Brunet *et al.*, 2011; https://sites.google.com/site/fbmlab/cartool).

Source localization

Source estimation was performed using the linear distributed inverse solution known as LAURA (local autoregressive average; Grave de Peralta *et al.*, 2004; Michel *et al.*, 2004). This source model is based on the physical law that the strength of a source regularly regresses with distance. Using a regular grid of solution points, the method incorporates this law in terms of a local autoregressive average with coefficients depending on the distance between solution points.

Head model

We used a simplified realistic head model to calculate the forward solution in which the anatomical head shape is taken into account and the solution space is constrained to the grey matter subspace within the volume conductor (SMAC model; Spinelli *et al.*, 2000). More concretely, the brain surface is extracted from the MRI and the best fitting sphere for this surface is calculated. Then the source space is warped according to the ratio of the sphere radius and the real surface radius. Around 3000 solution points are distributed with equal distances in the grey matter of this wrapped space. Because of this slight deformation of the brain to a best-fitting sphere, the lead field matrix could be computed using the known analytical solutions for a three-shell spherical head model (Ary *et al.*, 1981). These lead field matrices were then incorporated in the linear inverse solution algorithm LAURA described above. Finally, the result was back-transformed to the original head shape using the same transformation parameter. In order to evaluate the difference between the individual MRI and an average template MRI (see below), we calculated the SMAC head model for each individual MRI as well as for the averaged template MRI of the Montreal Neurological Institute (MNI) brain. In the case of the individual MRI, the individual anatomy was respected and altered cerebral structures were accounted for. The SMAC head model method has been successfully used in several previous clinical and experimental studies (e.g. Michel *et al.*, 2004; Phillips *et al.*, 2005; Brodbeck *et al.*, 2009, 2010; Groening *et al.*, 2009; Vulliemoz *et al.*, 2009, 2010; Siniatchkin *et al.*, 2010) and produces localization precisions that are comparable with realistic boundary element models (Guggisberg *et al.*, 2011).

Magnetic resonance imaging

All patients had MRI scans as part of the pre-surgical evaluation. They were acquired either with a 1.5 T Eclipse scanner (Picker Inc.) or a 3T Trio scanner (Siemens). The MRI was performed according to a standardized epilepsy protocol: coronal T_2-weighted fast spin-echo; repetition time 3092; echo time 11/100; voxel size 0.9 × 0.9 × 9.6 mm, coronal and axial fluid-attenuated inversion recovery (FLAIR; repetition time 11 000; echo time 140; inversion time 2800; voxel size 0.45 × 0.45 × 6 mm), sagittal 3D gradient echo T_1 (repetition time 12; echo time 4; voxel size 0.98 × 0.98 mm^2; thickness 1 mm) and diffusion sequences.

In 142 patients, the structural MRI showed a pathological result indicating an epileptogenic lesion; the other 10 patients had a normal MRI (five of the latter with temporal lobe epilepsy; Table 3).

Table 3 MRI findings

MRI finding	*n*
Normal	10
Abnormal	142
Hippocampal sclerosis (Hippocampal sclerosis alone/ Hippocampal sclerosis + ipsilateral anterior temporal lobe atrophy or other pathology)	53 (33/20)
Arteriorvenous malformation, cavernoma	13
Gliosis and focal atrophy	21
Neuronal migration disorder	
Dysplasia	18
DNET, ganglioglioma	19
Tuberous sclerosis	8
Lisencephaly/schizencephaly/heterotopia/ Sturge–Weber Syndrome	4
Other	
Porencephalic cysts	6

DNAT = dysembryoplastic neuroepithelial tumour.

In 29 patients, MRI showed multi-focal abnormalities. Both patients with normal MRI and multifocal lesions were considered together as 'non-focal'.

Positron emission tomography and single-photon emission-computed tomography acquisition

Fluorodeoxyglucose PET was carried out using 2-[^{18}F]fluoro-2-deoxy-D-glucose in all but one patient. Areas with focally decreased fluorodeoxyglucose uptake were identified by visual analysis.

For the ictal and interictal SPECT, a single bolus of 740 MBq of ethlenecysteinate dimer labelled with technetium-99 m ([^{99m}Tc] ethlenecysteinate dimer) was injected. SPECT scans were obtained 20–60 min after injection on a three-head Toshiba CGA-9300 camera. Only patients with an ictal exam were considered for analysis, verified by review of video-EEG recording. A total of 127 patients underwent ictal and interictal SPECT. Focus localization was determined by visual analysis and comparison of the ictal and interictal exam. In 70% of the patients, visual analysis was completed by subtraction analysis (SISCOM). From this point on, we will refer to both ictal and interictal SPECT with or without SISCOM analysis as 'ictal SPECT'.

Surgery

Patients underwent temporal or extratemporal surgical intervention considered appropriate for their needs. Each case was discussed in our weekly interdisciplinary case conference. Patients had left ($n = 71$) or right ($n = 81$) hemispheric resections. Temporal lobe surgery included all patients with a resection of temporal structures ($n = 102$), i.e. mesial temporal structures and to a variable degree anterior and/or lateral temporal neocortex. As in the patients with extratemporal lobe epilepsy ($n = 50$), resection was tailored and based on EEG, neuroimaging, analysis of ictal semiology and neuropsychological results. In the whole group, 31 patients had unilobar resections and 19 patients underwent multilobar resections.

All patients were seen postoperatively by the neurosurgeon and neurologist or neuropaediatrician. Mean follow-up was 4 years, 10 months (standard deviation: ± 2 years 10 months, median 5 years 3 months). Surgical outcome was measured at the latest visit.

Sensitivity and specificity evaluation

To evaluate the effect of the underlying brain template, we compared localization precision using the individual MRI and the averaged template MRI of the MNI as SMAC-transformed head model for the forward solution (see above).

In addition, we evaluated the effect of the number of electrodes on localization precision, i.e. comparing electric source imaging based on 64–256 EEG recordings (high-resolution electric source imaging) with those of standard EEG channel number (19–29 channels; low-resolution electric source imaging). This led to four constellations: low-resolution electric source imaging with template MRI, low-resolution electric source imaging with individual MRI, high-resolution electric source imaging with template MRI and high-resolution electric source imaging with individual MRI.

We considered seizure freedom following the operation to be the so-called 'ground truth'—unambiguous proof of correct localization of the epileptogenic focus. Sensitivity was defined as the percentage of patients with focus localization within the resected zone of all patients who were seizure-free ($n = 117$). We also computed this analysis for the Classes I and II patients together ($n = 133$). Specificity is defined as the percentage of patients with focus localization outside the resected zone in those patients who had an Engel Class III or IV outcome after surgery ($n = 19$).

We also determined the positive and negative predictive value. The positive predictive value represents the probability of becoming seizure-free when the source maximum was resected, and the negative predictive value represents the probability of continuing to have seizures if the electric source imaging focus was not resected. Since not all patients underwent high-resolution EEG, we performed a separate statistical analysis with those patients in whom high-resolution electric source imaging recordings were available (Tables 4 and 5). We used chi-square tests to assess the statistical significance of the difference of localization accuracy between the different constellations for the electric source imaging. A $P < 0.05$ was considered significant. In order to better appreciate the yield for temporal and extratemporal lobe epilepsies, we also performed a separate analysis for both patients groups.

Results

Yield of low versus high number of scalp electrodes for electric source imaging

Table 4 summarizes the overall sensitivity, specificity, positive and negative predictive values for all possible constellations of

Table 4 Comparative values of different constellations of low-resolution electric source imaging, high-resolution electric source imaging, individual MRI, template MRI in the whole population and in the 52 patients who received all four electric source imaging variants

Measure	LR-ESI/t-MRI (%)		LR-ESI/i-MRI		HR-ESI/t-MRI		HR-ESI/i-MRI
	$n = 152$	$n = 52$	$n = 98$	$n = 52$	$n = 55$	$n = 52$	$n = 52$
Sensitivity	55.6	59.1	65.9	72.7	76.1	75.0	84.1
Specificity	58.8	62.5	53.8	75.0	55.6	62.5	87.5
PPV	92.6	89.7	91.8	94.1	89.7	91.7	97.4
NPV	15.5	21.7	28.1	33.3	31.3	31.3	50.0

The left column values are based on the total number of patients. The right column values are based on the 52 patients that had received high resolution electric source imaging/individual MRI.
HR-ESI = high resolution electric source imaging based on 128–256 channel EEG recordings; i-MRI = patient's individual MRI; LR-ESI = low resolution electric source imaging based on 19–29 channel EEG recordings; t-MRI = template MRI;. NPV = negative predictive value; PPV = positive predictive value.

Table 5 Sensitivity, specificity, positive predictive value and negative predictive value of structural MRI, PET, SPECT and high resolution electric source imaging/individual MRI

Measure	MRI (%)		PET (%)		SPECT (%)		HR-ESI/i-MRI (%)
	n = 152	*n* = 52	*n* = 147	*n* = 51	*n* = 119	*n* = 43	*n* = 52
Sensitivity	76.3	72.7	68.7	65.1	57.7	54.3	84.1
Specificity	52.9	50.0	43.8	37.5	46.7	62.5	87.5
PPV	94.5	94.1	93.8	93.3	88.2	86.4	97.4
NPV	25.6	33.3	19.6	28.6	13.7	23.8	50.0

The left column values are based on the total number of patients. The right column values are based on the 52 patients that had high-resolution electric source imaging/individual MRI.
HR-ESI/i-MRI = high-resolution electric source imaging/individual MRI based on 128–256 channel EEG recordings and individual MRI; NPV = negative predictive value; PPV = positive predictive value.

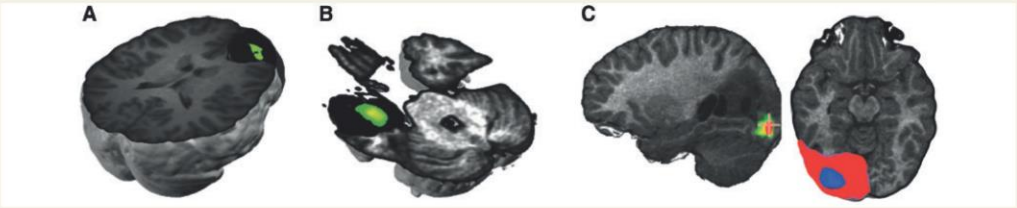

Figure 2 Examples of correct EEG source localization in operated and seizure-free patients. (**A**) Thirty-five-year-old patient with right frontal epilepsy and normal MRI. After subdural recordings, a polar frontal lobectomy was performed, which rendered the patient seizure-free. Histopathology revealed cortical dysplasia and gliosis. The green spot indicates the source maximum, which is superimposed on the postoperative MRI with the resected area marked in black. (**B**) Twenty-two-year-old patient with temporal lobe epilepsy and normal MRI. After depth recordings a left anterior temporal lobectomy was performed. Histopathology showed gliotic changes. The source maximum (green) was found within the resected area indicated in black. (**C**) Six-year-old female with a left occipital cystic lesion due to a ganglioglioma. A partial parieto-occipital lobectomy rendered the patient seizure-free. The source maximum was found in the occipital perilesional space (green) and lay within the resected area (indicated as blue spot in the red area that marks the resected zone).

low- and high-resolution electric source imaging and template and individual MRI for the patients who benefitted from surgery (Engel Classes I and II) versus those who did not (Engel Classes III and IV). The highest sensitivity (84.1%) and specificity (87.5%) were obtained with high-resolution electric source imaging using the patient's individual MRI as the head model (Fig. 4). Lowest values were obtained with low-resolution electric source imaging and template MRI (55.6 and 58.8%, respectively), followed by low-resolution electric source imaging/individual MRI and high-resolution electric source imaging/template MRI.

Considering only the 52 patients who underwent high-resolution electric source imaging and where an individual MRI was available, similar values were obtained (Table 4). If only patients with complete seizure freedom were analysed (Engel I), the sensitivities were as follows: low-resolution electric source imaging/template MRI 59.5%, low-resolution electric source imaging/individual MRI 70.8%, high-resolution electric source imaging/template MRI 81.6% and high-resolution electric source imaging/individual MRI 86.1% (Figs 2 and 3).

The statistical evaluation of the yield of high-resolution EEG and individual MRI was performed with the 43 patients for whom all imaging (i.e. including ictal SPECT) were available. This analysis revealed significant differences between both the high-resolution electric source imaging–individual MRI versus the low-resolution electric source imaging–individual MRI ($P < 0.004$), and the high-resolution electric source imaging–individual MRI versus the high-resolution electric source imaging-template MRI ($P < 0.002$).

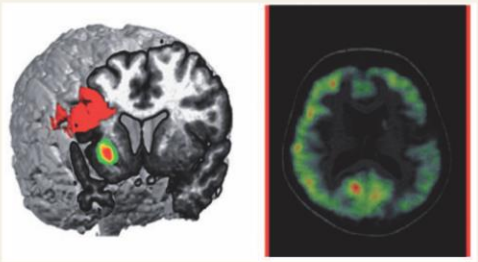

Figure 3 Example of a patient who was not seizure-free after operation; an 18-year-old patient with a surgical intervention in the right frontal posterior area (indicated in red) as suggested by intracranial recordings. The patient continued to have seizures after surgery. The electric source imaging source (green) showed a right insular maximum, which was concordant with a local hypometabolism found in the PET (*right*).

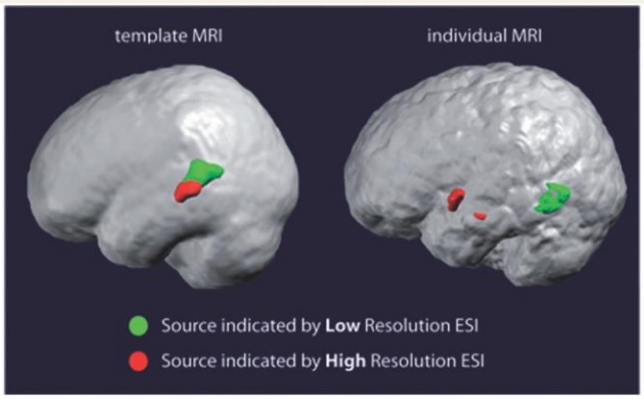

Figure 4 Example of a patient with non-concordant results between high- and low-resolution electric source imaging. Solutions using a template MRI are shown on the *left*, with the individual MRI on the *right*, low-resolution electric source imaging source superposed in green and high-resolution electric source imaging in red. The patient is a 13-year-old male with Engel Class II outcome after resection of the left temporal lobe. Only high-resolution electric source imaging based on the individual MRI correctly indicated a left anterior temporal source. Low- and high-resolution electric source imaging based on the template MRI indicated a parietal source.

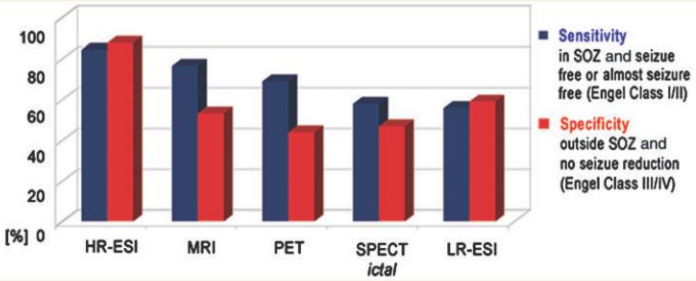

Figure 5 Sensitivity and specificity of the different imaging methods with respect to surgery outcome. High-resolution EEG with 128 or 256 electrodes had highest sensitivity (correct localization in seizure-free or almost seizure-free patients, Engel Classes I and II) and highest specificity (not localized in the resected zone in patients and without major benefit from surgery, Engel Classes III and IV).
HR-ESI = high-resolution electric source imaging; LR-ESI = low-resolution electric source imaging; SOZ = seizure onset zone.

Comparison of high-resolution electric source imaging/individual MRI with the established structural and functional imaging techniques

Almost all patients had a PET exam ($n = 147$). Ictal SPECT was obtained from 119 (79%) patients. Compared with high-resolution electric source imaging (using individual MRI) the structural MRI alone provided slightly lower sensitivity (76.3% versus 84.1%) and markedly lower specificity (52.9% versus 87.5%), followed by PET (sensitivity 68.7%, specificity 43.8%) and ictal SPECT (sensitivity 57.7%, specificity 46.7%; Table 5 and Fig. 5). In the group of 43 patients, who had all imaging exams (35 Engel Classes I + II, eight Engel Classes III + IV), similar sensitivities and specificities were obtained as with the entire patient group (sensitivity: high-resolution electric source imaging/individual MRI 80%, MRI 71.4%, PET 62.9%, ictal SPECT 54.3%, specificity: high-resolution electric source imaging/individual MRI 88%, MRI 50%, PET 37.5%, ictal SPECT 62.5). The details of the results of all 152 patients are given in Supplementary Table 1.

Comparison of patients with temporal versus extratemporal lobe epilepsy

In order to determine the relative yield of electric source imaging for patients with temporal and extratemporal lobe epilepsies, sensitivities and specificities were calculated for all electrical source imaging constellations and imaging exams separately for

Table 6 Comparison of sensitivity of all electric source imaging constellations separately for cases with temporal and extratemporal lobe epilepsy

Group	LR-ESI/t-MRI, *n* (%)	LR-ESI/i-MRI, *n* (%)	HR-ESI/t-MRI, *n* (%)	HR-ESI/i-MRI, *n* (%)
TLE	102 (57.3)	56 (67.3)	*n* = 26 (100)	*n* = 25 (91.7)
ETLE	50 (51.3)	42 (63.6)	29 (76.2)	27 (75.0)

ETLE = extratemporal lobe epilepsy; HR-ESI = high-resolution electric source imaging based on 128–256 channel EEG recordings; LR-ESI = low-resolution electric source imaging based on 19–29 channel EEG recordings; TLE = temporal lobe epilepsy.

Table 7 Comparison of sensitivity of all imaging exams in those patients who underwent high resolution electric source imaging/individual MRI and the other imaging exams

Group	HR-ESI/i-MRI, *n* (%)	MRI, *n* (%)	PET, *n* (%)	Ictal SPECT, *n* (%)
TLE	25 (91.7)	25 (70.8)	24 (69.6)	19 (61.1)
ETLE	27 (75.0)	27 (75.0)	27 (60.0)	24 (47.1)

ETLE = extratemporal lobe epilepsy; HR-ESI = high-resolution electric source imaging based on 128–256 channel EEG recordings; LR-ESI = low-resolution electric source imaging based on 19–29 channel EEG recordings; TLE = temporal lobe epilepsy.
Due to too small numbers of the negative cases, only sensitivity values are given.

both patient groups. Due to the small number of negative cases in the subgroups, the calculation of specificity, positive and negative predictive values was not meaningful. Again, highest sensitivity values were obtained for high-resolution electric source imaging/individual MRI, somewhat higher for temporal than for extratemporal lobe epilepsy. However, the difference was not significant (Table 6). In the group of 25 patients with temporal lobe epilepsy and 27 patients with extratemporal lobe epilepsy, respectively, who had high-resolution electric source imaging/individual MRI, again this imaging technique compares favourably to the other imaging exams, providing the highest sensitivity values (Table 7).

Discussion

Pre-surgical evaluation usually requires a comprehensive—and often costly—battery of brain imaging tools, to obtain precise localizing information regarding the epileptogenic focus. Only after the focus is completely removed, will the patient have a realistic chance of postoperative seizure freedom, which is still difficult to obtain with patients without magnetic resonance lesion and/or extratemporal lobe epilepsy. The current study was undertaken to determine the overall yield of electric source imaging prospectively in a large patient population referred for evaluation of pharmacoresistant epilepsy. Our gold standard was seizure freedom after operation, as used in many electric source imaging, magnetic source imaging and EEG–functional MRI studies (e.g. Thornton *et al.*, 2010; Grouiller *et al.* 2011; Seo *et al.*, 2011). If electric source imaging of interictal discharges were localized within the resected volume, the solution was considered correct. The same criterion was used for the other imaging methods as well. It is the level of precision that is clinically relevant in the presurgical evaluation.

In our series of 152 patients with epilepsy, electric source imaging based on high-resolution EEG (mostly with 128 or 256 electrodes), and with the patient's own MRI as the head model, provided excellent localization precision with a sensitivity of 84% and specificity of 88%. When only standard EEG was available for electric source imaging (low resolution), a sensitivity of 66% was obtained, when ESI was based on the individual MRI. Not unexpectedly, lowest sensitivity and specificity were obtained when using only standard EEG and a template MRI. Thus, if the epileptogenic zone was identified with high-resolution electric source imaging/individual MRI, the chances that the focus was indeed at this site were 84%. We also had a few failure cases and in-depth analysis revealed that in most of them, propagated interictal epileptiform discharges (to the ipsilateral anteromesial temporal lobe) were used for electric source imaging, given that they were the only clearly visible epileptogenic anomalies. The true foci, at distance, of the electric source imaging focus were characterized by low-amplitude rapid rhythms, seen in the intracranial ictal and interictal EEG. The excellent localizing value of high-frequency oscillations (Urrestarazu *et al.*, 2007; Worrell *et al.*, 2008) or high-frequency interictal discharges (McGonigal *et al.*, 2007) is well established. In order to improve the sensitivity of high-resolution electric source imaging even further, the visualization of these β- or γ-rhythms in the scalp EEG would be mandatory, which, however, is difficult in light of the small size of signals and possible muscle artefacts contamination.

The present study confirms previous studies on electric source imaging in epilepsy with smaller numbers of patients. In a group of 32 patients (Michel *et al.*, 2004*b*), correct localization on a lobar level was obtained in 93.7% with electric source imaging based on 128 channel EEG. Sperli and colleagues (2006) analysed the standard clinical EEG with electric source imaging of 30 operated and seizure-free children, using mostly 29 electrodes and the patients' MRI (i.e. low-resolution electric source imaging/individual MRI). They reported correct localization on a lobar level in 90% of the cases. However, correct localization at a lobar level does not necessarily mean that the source maximum was within the resected zone, which was the criterion in the current study. In the study by Michel and colleagues (2004*b*), this criterion was applied in the 24 operated patients. In this case, correct localization was found in 79% using high-resolution electric source imaging/individual MRI, which is comparable with the current result with a larger number of patients.

Electric source imaging is a particularly valuable tool for analysing patients with normal MRI. Brodbeck and colleagues (2010) analysed 10 operated patients in whom modern MRI sequences failed to provide evidence of an epileptogenic (temporal and extratemporal) lesion. Nevertheless, electric source imaging showed correct focus localization in eight of them. Thus, even in this particularly difficult patient group where the MRI provides no relevant information, electric source imaging helped clinicians

to determine the epileptogenic focus in the individual brain with excellent precision.

This study does not include a comparison with MEG recordings because it is not a typical part of the pre-surgical work-up at the University Hospital in Geneva, and thus the issue of whether it can make a cost-effective contribution to the localization of the epileptic focus is not addressed in the present publication. Some key issues that deserve attention in future studies that do look at MEG potential contribution include the ongoing discussion about how deeply EEG and MEG can 'see'. There are concerns that MEG may miss deep sources and that it is insensitive to sources with radial orientation (Ahlfors *et al.*, 2010), which appears to be less of an issue in EEG (Lejten *et al.*, 2003).

Another debate concerns the possibility to localize mesial temporal interictal epileptiform discharges through inverse solutions. Several studies suggest that anterior temporal spikes recorded on the scalp are rather the result of anterior or lateral neocortical temporal activity or common activity of neocortical and mesial temporal sources, and that neither EEG nor MEG can see spikes confined to the mesial temporal structures (Alarcon *et al.*, 1994; Emerson *et al.*, 1995; Huppertz *et al.*, 2001; Gavaret *et al.*, 2004; Wennberg 2011). However, simultaneous surface and intracranial EEG studies indicated that deep mesial temporal sources could be properly localized by electric source imaging if their small volume-conducted signals can be identified in the scalp EEG, or if they are averaged (Lantz *et al.*, 2001; Nayak *et al.*, 2004; Zumsteg *et al.*, 2005; Nahum *et al.*, 2011). It remains to be shown in future studies using simultaneous intracranial EEG if mesial temporal interictal epileptiform discharges could be localized non-invasively with high-density EEG/MEG or with combined EEG–functional MRI (Sperli *et al.*, 2006; Kaiboriboon *et al.*, 2010; Vulliemoz *et al.*, 2010; Grouiller *et al.*, 2011).

Another potential concern regarding the use of electric source imaging for pre-surgical epilepsy evaluation is that it is done using 'interictal discharges' instead of 'ictal recordings', which are supposedly more relevant when deciding where to operate. However, the scalp EEG studies cited earlier, as well as studies from patients with intracranial electrodes, strongly suggest that careful analysis of the localization of interictal epileptiform discharges, or the majority of interictal epileptiform discharges, allow a good-to-excellent estimate of the ictal source (Asano *et al.*, 2003; Ray *et al.*, 2007). It is important to note that electric source imaging is not restricted to interictal activity as is MEG or functional MRI, because EEG can be recorded over a much longer duration and motion does not make the recordings invalid. Recent studies have shown successful localization of the seizure onset zone with electric source imaging, extending its use to ictal long-term recordings with up to 256 electrodes (Holmes *et al.*, 2008; Stern *et al.*, 2009).

The optimal mathematical approach for the analysis of EEG (or MEG) data for source localization has been addressed in numerous publications and it is beyond the scope of the present publication to go into details. While simple equivalent dipole fitting provides good source estimations (Gavaret *et al.*, 2009; Rose and Ebersole, 2009), a crucial step towards achieving a real 3D imaging of the electrical activity in the brain was obtained by distributed inverse solution algorithms that are able to visualize the current density distribution in the entire brain at each moment in time (for reviews see Michel *et al.*, 2004*a*; Plummer *et al.*, 2008). With these 3D algorithms, the electric source can be identified in most of the patients, even in the presence of large, inhomogeneous lesions (Brodbeck *et al.*, 2009).

Our results from this large patient group show that electric source imaging based on large electrode arrays covering the whole skull is an excellent tool to localize the epileptogenic focus, with excellent sensitivity and specificity. However, until recently, the lack of 'adoption' of EEG-based electric source imaging in the clinical world has mainly been because the application of a high number of electrodes (i.e. between 100 and 200 or even more) was too cumbersome to perform routinely. Due to technical progress, electric source imaging using large-array recordings can be obtained in <30 min and does not require highly experienced, well-trained personnel, expensive shielding or other inconveniences. Commercially available high-resolution EEG systems make recordings from a large number of electrodes fast and easy, and they even integrate with MRI data.

Our source analysis was based on a simplified head model that allowed a fast and analytical solution of the forward problem. More realistic head models based on boundary or finite element meshing of the brain are nowadays available in some software packages and will soon be feasible in daily clinical applications (Michel and He, 2011). There is little doubt that these more realistic head models will further increase the accuracy of electric source imaging, particularly if inhomogeneous conductivities of the brain and orientation constraints of the dipoles are incorporated. Most importantly, however, is the use of the individual MRI of the patient instead of a template MRI, as shown in the current study as well as in a recent study by Guggisberg *et al.* (2011). For almost all patients with epilepsy admitted for surgery, high-resolution MRI is usually available and is easily integrated into the analysis.

From a practical clinical perspective, electric source imaging on the basis of high-resolution EEG (i.e. with 128–256 scalp electrodes) is very interesting. The sensitivity and specificity of electric source imaging is as high as (or even higher than) more established brain imaging techniques, and electric source imaging is relatively inexpensive when compared with nuclear medicine techniques or MRI-based approaches. Moreover, the electric source imaging exam does not require sedation, which considerably reduces the workload for working with children or mentally retarded persons, who are unable to remain immobile for 30 min or more. The more precise focus localization of electric source imaging also allows better preparation for intracranial electrode implantations if deemed necessary (Seeck *et al.* 2010).

Acknowledgements

The EEG data were analysed with the Cartool software (http://brainmapping.unige.ch/Cartool.php), which was developed by Denis Brunet, from the Functional Brain Mapping Laboratory, Geneva, supported by the Centre for Biomedical Imaging (CIBM), Geneva, and Lausanne, Switzerland.

Funding

Swiss National Science Foundation by the grants (SPUM 33CM30-124089 to M.S. and No. 320030-122073 to K.S.).

Supplementary material

Supplementary material is available at *Brain* online.

References

Ahlfors SP, Han J, Belliveau JW, Hamalainen MS. Sensitivity of MEG and EEG to source orientation. Brain Topogr 2010; 23: 227–32.

Alarcon G, Guy CN, Binnie CD, Walker SR, Elwes RD, Polkey CE. Intracerebral propagation of interictal activity in partial epilepsy: implications for source localisation. J Neurol Neurosurg Psychiatry 1994; 57: 435–49.

Ary JP, Klein SA, Fender DH. Location of sources of evoked scalp potentials: Corrections for skull and scalp thicknesses. IEEE Trans Biomed Eng 1981; 28: 834–6.

Asano E, Muzik O, Shah A, Juhasz C, Chugani DC, Sood S, et al. Quantitative interictal subdural EEG analyses in children with neocortical epilepsy. Epilepsia 2003; 44: 425–34.

Brodbeck V, Lascano AM, Spinelli L, Seeck M, Michel CM. Accuracy of EEG source imaging of epileptic spikes in patients with large brain lesions. Clin Neurophysiol 2009; 120: 679–85.

Brodbeck V, Spinelli L, Lascano AM, Pollo C, Schaller K, Vargas MI, et al. Electrical source imaging for presurgical focus localization in epilepsy patients with normal MRI. Epilepsia 2010; 51: 583–91.

Brunet D, Murray MM, Michel CM. Spatiotemporal analysis of multichannel EEG: CARTOOL. Comput Intell Neurosci 2011; 2011, doi:10.1155/2011/813870.

Chatrian GE. Report on the Committee on Terminology. Proceedings of the General Assembly. The VIIIth International £Congress of Electroencephalography and Clinical Neurophysiology. Electroencephalogr Clin Neurophysiol 1974; 37: 521–53.

Emerson RG, Turner CA, Pedley TA, Walczak TS, Forgione M. Propagation patterns of temporal spikes. Electroencephalogr Clin Neurophysiol 1995; 94: 338–48.

Fuchs M, Wagner M, Kastner J. Development of volume conductor and source models to localize epileptic foci. J Clin Neurophysiol 2007; 24: 101–19.

Gavaret M, Badier JM, Marquis P, Bartolomei F, Chauvel P. Electric source imaging in temporal lobe epilepsy. J Clin Neurophysiol 2004; 21: 267–82.

Gavaret M, Trebuchon A, Bartolomei F, Marquis P, McGonigal A, Wendling F, et al. Source localization of scalp-EEG interictal spikes in posterior cortex epilepsies investigated by HR-EEG and SEEG. Epilepsia 2009; 50: 276–89.

Grave de Peralta Menendez R, Murray MM, Michel CM, Martuzzi R, Gonzalez Andino SL. Electrical neuroimaging based on biophysical constraints. Neuroimage 2004; 21: 527–39.

Groening K, Brodbeck V, Moeller F, Wolff S, van Baalen A, Michel CM, et al. Combination of EEG-fMRI and EEG source analysis improves interpretation of spike-associated activation networks in paediatric pharmacoresistant focal epilepsies. Neuroimage 2009; 46: 827–33.

Grouiller F, Thornton RC, Groening K, Spinelli L, Duncan JS, Schaller K, et al. With or without spikes: localization of focal epileptic activity by simultaneous electroencephalography and functional magnetic resonance imaging. Brain 2011; 134: 2867–86.

Guggisberg AG, Dalal SS, Zumer JM, Wong DD, Dubovik S, Michel CM, et al. Localization of cortico-peripheral coherence with electroencephalography. Neuroimage 2011; 57: 1348–57.

Huppertz HJ, Hof E, Klisch J, Wagner M, Lücking CH, Kristeva-Feige R. Localization of interictal delta and epileptiform EEG activity associated with focal epileptogenic brain lesions. Neuroimage 2001; 13: 15–28.

Henry TR, Van Heertum RL. Positron emission tomography and single photon emission computed tomography in epilepsy care. Semin Nucl Med 2003; 33: 88–104.

Holmes MD, Tucker DM, Quiring JM, Hakimian S, Miller JW, Ojemann JG. Comparing noninvasive dense array and intracranial electroencephalography for localization of seizures. Neurosurgery 2008; 66: 354–62.

Kaiboriboon K, Nagarajan S, Mantle M, Kirsch HE. Interictal MEG/magnetic source imaging in intractable mesial temporal lobe epilepsy: spike yield and characterization. Clin Neurophysiol 2010; 121: 325–31.

Knowlton RC, Elgavish RA, Bartolucci A, Ojha B, Limdi N, Blount J, et al. Functional imaging: II. Prediction of epilepsy surgery outcome. Ann Neurol 2008; 64: 35–41.

Knowlton RC, Razdan SN, Limdi N, Elgavish RA, Killen J, Blount J, et al. Effect of epilepsy magnetic source imaging on intracranial electrode placement. Ann Neurol 2009; 65: 716–23.

Lantz G, Grave de Peralta Menendez R, Gonzalez Andino S, Michel CM. Noninvasive localization of electromagnetic epileptic activity. II. Demonstration of sublobar accuracy in patients with simultaneous surface and depth recordings. Brain Topogr 2001; 14: 139–47.

Lantz G, Spinelli L, Seeck M, de Peralta Menendez RG, Sottas CC, Michel CM. Propagation of interictal epileptiform activity can lead to erroneous source localizations: a 128-channel EEG mapping study. J Clin Neurophysiol 2003; 20: 311–9.

Leijten FS, Huiskamp GJ, Hilgersom I, Van Huffelen AC. High-resolution source imaging in mesiotemporal lobe epilepsy: a comparison between MEG and simultaneous EEG. J Clin Neurophysiol 2003; 20: 227–38.

Manford M, Fish DR, Shorvon SD. An analysis of clinical seizure patterns and their localizing value in frontal and temporal lobe epilepsies. Brain 1996; 119: 17–40.

McGonigal A, Bartolomei F, Régis J, Guye M, Gavaret M, Trébuchon-Da Fonseca A, et al. Stereoelectroencephalography in presurgical assessment of MRI-negative epilepsy. Brain 2007; 130: 3169–83.

Michel CM, He B. EEG Mapping and source imaging. In: Schomer D, Lopes da Silva F, editors. Niedermeyer's electroencephalography. 6th edn., Chapter 55. Lippincott Williams & Wilkins; 2011. p. 1179–202.

Michel CM, Lantz G, Spinelli L, De Peralta RG, Landis T, Seeck M. 128-channel EEG source imaging in epilepsy: clinical yield and localization precision. J Clin Neurophysiol 2004b; 21: 71–83.

Michel CM, Murray MM, Lantz G, Gonzalez S, Spinelli L, Grave de Peralta R. EEG source imaging. Clin Neurophysiol 2004a; 115: 2195–222.

Nahum L, Gabriel D, Spinelli L, Momjian S, Seeck M, Michel CM, et al. Rapid consolidation and the human hippocampus: Intracranial recordings confirm surface EEG. Hippocampus 2011; 21: 689–93.

Nayak D, Valentín A, Alarcón G, García Seoane JJ, Brunnhuber F, Juler J, et al. Characteristics of scalp electrical fields associated with deep medial temporal epileptiform discharges. Clin Neurophysiol 2004; 115: 1423–35.

Phillips C, Mattout J, Rugg MD, Maquet P, Friston KJ. An empirical Bayesian solution to the source reconstruction problem in EEG. Neuroimage 2005; 24: 997–1011.

Plummer C, Harvey AS, Cook M. EEG source localization in focal epilepsy: where are we now? Epilepsia 2008; 49: 201–18.

Ray A, Tao JX, Hawes-Ebersole SM, Ebersole JS. Localizing value of scalp EEG spikes: a simultaneous scalp and intracranial study. Clin Neurophysiol 2007; 118: 69–79.

Rose S, Ebersole JS. Advances in spike localization with EEG dipole modeling. Clin EEG Neurosci 2009; 40: 281–7.

Seo JH, Holland K, Rose D, Rozhkov L, Fujiwara H, Byars A, et al. Multimodality imaging in the surgical treatment of children with nonlesional epilepsy. Neurology 2011; 76: 41–8.

Seeck M, Schomer DL, Bergey GK, Niedermeyer E. Intracranial monitoring: depth, subdural and foramen ovale electrodes. In: Schomer DL,

Lopes da Silva F, editors. Niedermeyer's textbook of electroencephalography: basic principles, clinical applications, and related fields. VI edn., Chapter 33. Wolters Kluwer and Lippincott; 2010.

Siniatchkin M, Groening K, Moehring J, Moeller F, Boor R, Brodbeck V, et al. Neuronal networks in children with continuous spikes and waves during slow sleep. Brain 2010; 133: 2798–813.

Spanaki MV, Spencer SS, Corsi M, MacMullan J, Seibyl J, Zubal IG. Sensitivity and specificity of quantitative difference SPECT analysis in seizure localization. J Nucl Med 1999; 40: 730–6.

Sperli F, Spinelli L, Seeck M, Kurian M, Michel CM, Lantz G. EEG source imaging in pediatric epilepsy surgery: a new perspective in presurgical workup. Epilepsia 2006; 47: 981–90.

Spinelli L, Andino SG, Lantz G, Seeck M, Michel CM. Electromagnetic inverse solutions in anatomically constrained spherical head models. Brain Topogr 2000; 13: 115–25.

Stern Y, Neufeld MY, Kipervasser S, Zilberstein A, Fried I, Teicher M, et al. Source localization of temporal lobe epilepsy using PCA-LORETA analysis on ictal EEG recordings. J Clin Neurophysiol 2009; 26: 109–16.

Sutherling WW, Mamelak AN, Thyerlei D, Maleeva T, Minazad Y, Philpott L, et al. Influence of magnetic source imaging for planning intracranial EEG in epilepsy. Neurology 2008; 71: 990–6.

Thornton R, Laufs H, Rodionov R, Cannadathu S, Carmichael DW, Vulliemoz S, et al. EEG correlated functional MRI and postoperative outcome in focal epilepsy. J Neurol Neurosurg Psychiatry 2010; 81: 922–7.

Urrestarazu E, Chander R, Dubeau F, Gotman J. Interictal high-frequency oscillations (100-500 Hz) in the intracerebral EEG of epileptic patients. Brain 2007; 130: 2354–66.

Vergult A, De Clercq W, Palmini A, Vanrumste B, Dupont P, Van Huffel S, et al. Improving the interpretation of ictal scalp EEG: BSS-CCA algorithm for muscle artifact removal. Epilepsia 2007; 48: 950–8.

Vulliemoz S, Rodionov R, Carmichael DW, Thornton R, Guye M, Lhatoo SD, et al. Continuous EEG source imaging enhances analysis of EEG-fMRI in focal epilepsy. Neuroimage 2010; 49: 3219–29.

Vulliemoz S, Thornton R, Rodionov R, Carmichael DW, Guye M, Lhatoo S, et al. The spatio-temporal mapping of epileptic networks: combination of EEG-fMRI and EEG source imaging. Neuroimage 2009; 46: 834–43.

Walczak TS, Jayakar P, Mizrahi EM. Interictal encephalography. In: Engel J Jr, Pedley TA, editors. Epilepsy – a comprehensive textbook. 2nd edn. Wolters-Kluwer Lippincott Williams & Wilkins; 2008. p. 809–823.

Wennberg R, Valiante T, Cheyne D. EEG and MEG in mesial temporal lobe epilepsy: where do the spikes really come from? Clin Neurophysiol 2011; 122: 1295–313.

Worrell GA, Gardner AB, Stead SM, Hu S, Goerss S, Cascino GJ, et al. High-frequency oscillations in human temporal lobe: simultaneous microwire and clinical macroelectrode recordings. Brain 2008; 13: 928–37.

Zumsteg D, Friedman A, Wennberg RA, Wieser HG. Source localization of mesial temporal interictal epileptiform discharges: correlation with intracranial foramen ovale electrode recordings. Clin Neurophysiol 2005; 116: 2810–8.

Zumsteg D, Friedman A, Wieser HG, Wennberg RA. Source localization of interictal epileptiform discharges: comparison of three different techniques to improve signal to noise ratio. Clin Neurophysiol 2006; 117: 562–71.

Study II

Lascano AM, Pernegger T, Vulliemoz S, Spinelli L, Garibotto V, C. Korff, Vargas MI, Michel CM, Seeck M. Yield of MRI, high-density source imaging (HD-ESI), SPECT and PET in epilepsy surgery candidates. Clin Neurophysiology 2016; 127: 5-7. Doi: 10.1016/j.clinph.2015.03.025

- Impact Factor: 3.675
- 5-year Impact Factor: 3.743
- Average citations per year: 8.6
- Sum of times cited (without self-citations): 43
- Copyright clearance: Permission is not required

Clinical Neurophysiology 127 (2016) 150–155

Contents lists available at ScienceDirect

Clinical Neurophysiology

journal homepage: www.elsevier.com/locate/clinph

Yield of MRI, high-density electric source imaging (HD-ESI), SPECT and PET in epilepsy surgery candidates

Agustina M. Lascano [a], Thomas Perneger [b], Serge Vulliemoz [a], Laurent Spinelli [a], Valentina Garibotto [c], Christian M. Korff [d], Maria I. Vargas [e], Christoph M. Michel [f], Margitta Seeck [a,*]

[a] Department of Neurology, Geneva University Hospitals, Switzerland
[b] Division of Clinical Epidemiology, Geneva University Hospitals, Switzerland
[c] Department of Nuclear Medicine, Geneva University Hospitals, Switzerland
[d] Child and Adolescent Department, Geneva University Hospitals, Switzerland
[e] Department of Neuroradiology, Geneva University Hospitals, Switzerland
[f] Functional Brain Mapping Laboratory, Department of Fundamental Neurosciences, Campus Biotech, University of Geneva, Switzerland

See Editorial, pages 5–7

ARTICLE INFO

Article history:
Accepted 6 March 2015
Available online 9 May 2015

Keywords:
Presurgical evaluation
Temporal lobe epilepsy
Drug-resistant epilepsy
Seizure-freedom
Non-invasive procedures

HIGHLIGHTS

- High-density electric source imaging (HD-ESI) in combination with MRI are the best predictors of a favorable postoperative outcome, in terms of complete seizure control.
- PET and SPECT are also associated with good postoperative outcome, but their predictive value is not as high as HD-ESI.
- Our study brings in an important contribution to the validation of HD-ESI as a clinically useful first-line tool.

ABSTRACT

Objective: Preoperative workup aims at localizing the epileptogenic focus to achieve postoperative seizure-freedom. We studied the predictive value of non-invasive techniques, i.e. structural magnetic resonance imaging [MRI], high-density electric source imaging [HD-ESI] and metabolic imaging (positron emission tomography [PET]; single-photon emission computed tomography [SPECT]), in surgically treated patients.
Methods: A prospective study of 190 epileptic operated patients, with >12 months follow-up and analyzed with state-of-the-art algorithms. 58 patients underwent all techniques. We computed sensitivity, specificity, predictive value and diagnostic odds ratio (OR) in relation to postoperative outcome.
Results: Of 190 patients, 148 (77.9%) were seizure-free at follow-up. Resection of the epileptogenic focus was associated with favorable postsurgical outcome ($p < 0.05$). Among 58 patients who underwent all tests, only MRI and HD-ESI were favorable outcome predictors (MRI: OR 10.9, $p = 0.004$; HD-ESI: OR 13.1, $p = 0.004$). Patients with concordant structural MRI and HD-ESI results had 92.3% (24/26) probability of favorable outcome. When both results were negative, probability was 0% (0/5); and when they disagreed, it was 63.0% (17/27).
Conclusions: Combination of MRI and HD-ESI offered the highest predictive value for postoperative seizure-freedom.
Significance: This finding highlights the added value of HD-ESI in the presurgical workup, in particular in combination with an informative MRI.

Abbreviations: EEG, electroencephalography; SPECT, single-photon emission-computed tomography; PET, positron emission tomography; MRI, magnetic resonance imaging; ESI, electric source imaging.

* Corresponding author at: EEG and Epilepsy Unit, Department of Neurology, Geneva University Hospitals, Rue Gabrielle-Perret-Gentil 4, 1211 Geneva, Switzerland. Tel./fax: +41 22 372 8476.
E-mail address: Margitta.Seeck@hcuge.ch (M. Seeck).

http://dx.doi.org/10.1016/j.clinph.2015.03.025
1388-2457/

1. Introduction

Evaluation and management of drug-resistant seizures remains a challenging clinical problem in epilepsy. Notwithstanding the advent of new antiepileptic drugs, nearly one-third of patients with recently diagnosed epilepsy will not achieve seizure remission with pharmacological therapy (Kwan and Sander, 2004). On the other hand, epilepsy surgery in suitable candidates can eradicate or markedly reduce the frequency of seizures in about ~60–70% of patients (Engel, 1993; Wiebe et al., 2001; Kwan and Sperling, 2009) and, therefore, should be considered early in the disease.

Epilepsy surgery requires precise estimation of the epileptogenic zone to be removed in order to obtain seizure-freedom, while preserving the eloquent cortex (Rosenow and Luders, 2001). This is achieved by adding different non-invasive exams (e.g.: video-electroencephalogram [EEG], magnetic resonance imaging [MRI], positron emission tomography [PET] and single-photon emission computed tomography [SPECT]) (Knowlton et al., 2008; Schramm and Clusmann, 2008). In some patients, intracranial EEG monitoring is necessary (Rosenow and Luders, 2001; Knowlton et al., 2008; Schramm and Clusmann, 2008; Yuan et al., 2012).

Few studies including large cohorts (i.e. >50–60 patients) have compared the contribution of non-invasive neurophysiologic techniques in the presurgical work-up. A study of 62 patients undergoing intracranial EEG identified a positive predictive value of 78% for preoperative magnetic source imaging based on magnetoencephalography (Knowlton, 2006), with a sensitivity of 55%. A recent prospective study compared electric source imaging (ESI) in a group of 152 operated patients with a follow-up period of >1 year and found highest sensitivity and specificity (>80%) for ESI based on EEG with high-density electrode recordings (HD-ESI) (Brodbeck et al., 2011).

The aim of the present study, which is an extension of the prospective and methodological study performed by Brodbeck et al. (2011), was to determine which procedure *or combination of procedures* is the most predictive of seizure-free outcome in patients undergoing epilepsy surgery. Secondly, we consider only HD-ESI, given that its superiority over ESI with low electrode counts has been already shown (Brodbeck et al., 2011).

2. Methods

2.1. Patient population

This study was based on a prospectively collected database, including 190 patients who underwent surgery for medically intractable epilepsy at the University Hospitals of Geneva, Switzerland, between 1995 and 2012. All patients had a postsurgical follow-up period of at least 12 months. This study was approved by the local Ethics Committee, in agreement with the Declaration of Helsinki.

Presurgical workup included a thorough neurological examination, a neuropsychological assessment, a psychiatric evaluation, a high-resolution MRI, and in most cases PET. Ictal SPECT and ESI was added whenever possible. Forty-three patients underwent additional intracranial EEG recordings prior to surgical resection, if seizure onset zone could not be determined by non-invasive methods and/or to localize eloquent cortex. Out of those patients who underwent all non-invasive imaging exams ($N = 58$), 23 were implanted with intracranial electrodes.

2.2. Surgery

Surgical decision-making was carried out on an individual basis at our weekly epilepsy surgery consensus conference. Resection was based on concordant information provided by EEG, neuroimaging techniques, observation of ictal semiology and neuropsychological tests. No rules were applied in prioritizing a certain modality. Whenever possible, surgery was performed with the aid of imaging guidance.

Surgical treatment included the resection of the temporal lobe ($n = 125$; 66%), the extra-temporal structures ($n = 60$; 31.5%) and, in a single case, a cerebellar lesion ($n = 1$; 0.5%). Transventricular hemispherotomy was applied in four cases (2%). Out of the 125 patients who underwent temporal lobe surgery, $n = 21$ were limited to the medial temporal lobe only, $n = 20$ to the lateral temporal lobe only, and $n = 84$ included both regions. Extra-temporal lobe surgery comprised unilobar ($n = 31$; out of which 52% targeted the frontal lobe) or multilobar ($n = 29$; 48%) resections. MRI was abnormal in 174 patients.

2.3. Study variables

The outcome variable was the postoperative seizure outcome as determined by the neurosurgeon, neurologist or neuropediatrician on the last follow-up, according to Engel's classification (Engel et al., 1993). Table 1 provides information on the operated site and the postoperative outcome in 190 patients. Predictor variables were the results of preoperative imaging procedures described below.

2.4. High density electric source imaging (HD-ESI)

ESI based on EEG with a high number of electrodes was obtained in 85 patients by recording for 2–24 h with 64 ($n = 2$ infants), 128 ($n = 44$) or 256 electrodes ($n = 39$) using HydroCel Geodesic Sensor Net (Electrical Geodesics Inc., Eugene, OR, USA). EEG was continuously recorded (1–2 h sessions) at a sampling rate of 1 kHz and band-pass filtered between 0.1 and 400 Hz. The Vertex (Cz) electrode was used as recording reference and the data were referenced offline to the average reference. EEG was analyzed by means of a semi-automatic procedure composed by several steps described in Brodbeck et al. (2011).

The most dominant and isolated IEDs (i.e. spikes or sharp waves), with similar localization and morphology, were visually detected by a blinded board certified EEG reader [A.M.L.]. Results were compared to those obtained by two unblinded authors in charge of the patients [M.S. and S.V.]. Numbers of averaged spikes in high-density EEG were on average 27 spikes (SD 34.26).

Interictal epileptic discharges (IED) were averaged across epochs of 500 ms using the free academic software Cartool (D. Brunet, Geneva University Medical Center, Center for Biomedical Imaging, Geneva, Switzerland; http://sites.google.com/site/

Table 1
Postoperative outcome of all 190 epileptic patients.

Operated site	Engel Class I	Engel Class II	Engel Class III	Engel Class IV	Total (%)
ETLE	36	7	14	3	60 (31.5)
TLE					
MTLE	16	4	–	1	21 (11)
LTLE	18	1	1	–	20 (10.5)
M/LTLE	73	5	4	2	84 (44.2)
Subcortical	1	–	–	–	1 (0.5)
Hemispherotomy	4	–	–	–	4 (2.1)
All patients (%)	148 (77.9)	17 (8.9)	19 (10)	6 (3.2)	190

Engel Class I: seizure-free; II: decrease > 80%; III: decrease 50–80%; IV: decrease < 50%; ETLE = extratemporal lobe epilepsy; TLE = temporal lobe epilepsy; MTLE = mesiotemporal lobe epilepsy; LTLE = latero-temporal lobe epilepsy.

fbmlab/cartool). A band-pass filter of 0.1–30 Hz was applied to the on-going EEG. The EEG map at the 50% rising phase of the averaged IED was selected for further source localization.

A local autoregressive average (LAURA) distributed linear inverse solution (Grave de Peralta Menendez et al., 2001; Michel et al., 2004) was applied to estimate the intracranial 3D current density distribution of the averaged IED. We applied a simplified realistic head model based on the individual MRI which constraints the solution space to the gray matter (for methodological details see (Michel et al., 2004; Spinelli et al., 2000).

2.5. Magnetic resonance imaging

MRI was acquired either with a 1.5*T* Achieva (Phillips Healthcare, Netherlands) or a 3*T* Trio scanner (Siemens AG, Germany) and performed according to a standardized state-of-the-art epilepsy protocol (Vargas et al., 2013) using a 32-channel brain coil: (a) coronal T_2-weighted fast spin-echo repetition time (TR) 7520 ms; echo time (TE) 114 ms; voxel size $0.5 \times 0.4 \times 3$ mm (slice thickness); (b) sagittal 3D FLAIR (fluid-attenuated inversion recovery) TR5000; TE419; inversion time (TI) 1800; isotropic voxel size $0.9 \times 0.9 \times 0.9$ mm); (c) sagittal 3D gradient echo T_1TR1750 ms; TE2.29 ms; isotropic voxel size $0.7 \times 0.7 \times 0.7$ mm; (d) diffusion-weighted imaging (DWI) TR 8000 ms; TE 84 ms; 30 directions; (e) and arterial spin labeling (ASL) TR 4000 ms; TE 12 ms; voxel size $3.4 \times 3.4 \times 4$ mm (slice thickness). MRIs were described by a board-certified neuroradiologist with long experience in epilepsy imaging [MIV]. In those patients who had no visible lesion on the MRI, voxel-based comparison with a healthy control group was carried out, as described elsewhere (Huppertz et al., 2009).

2.6. Positron emission tomography

PET acquisition was performed on a BiographHiRez Sensation 16 (Siemens Healthcare, Erlangen, Germany) using a standard protocol recommended by the manufacturer. PET scans were carried out in 185 patients, during the interictal state, using [^{18}F]-labeled fluorodeoxyglucose (FDG). The administered activity was 250 MBq for adults and was adapted to body weight for children. Images were acquired approximately 30 min after tracer administration.

FDG-PET images of a subgroup of adult patients (58 subjects who underwent all four imaging techniques) were also analyzed by voxel-wise comparison with a normal database using *BRASS*™ automated functional brain analysis software (Hermes *BRASS* software, Nuclear Diagnostics AB, Sweden) (Slomka et al., 2001). Each individual FDG-PET image was warped to the reference template and a threshold of 2 SD was set to identify deviations from normal distribution (Radau et al., 2001).

Areas with minimal-to-low grade FDG uptake were visually identified by a board-certified nuclear medicine specialist [V.G.], who interpreted also the SPECT studies (see below).

2.7. Ictal single-photon emission-computed tomography

Ictal SPECT scans was performed using a single bolus injection of 740 MBq (20 mCi) ethlenecysteinate dimer labeled with [99mTc] during seizure. The administered activity was 740 MBq for adults and adapted to body weight for children. Scans were acquired 20–60 min after the radioisotope injection using a three-head gamma camera (Toshiba CGA-9300, Tokyo, Japan). A total of 137 patients were scanned. Focus localization was determined by visual analysis of the ictal exam. Ictal/Interictal SPECT were analyzed by subtraction ictal SPECT coregistered to MRI (SISCOM).

2.8. Test scoring

After data acquisition and processing of all four modalities (MRI $n = 190$, PET $n = 185$, ictal SPECT $n = 163$, HD-ESI $n = 82$), localization findings were defined at a sublobar level. A visual selection method was equally applied across all four techniques. A score was established to assess the degree of localization of the probable seizure-onset zone (Luders et al., 2006): (1) localized within the resected lobe; (2) localized both within and outside boundaries of the operated lobe; (3) localized outside the resected lobe; (4) normal/no pathology detected; (5) exam not performed. For statistical analysis, patients from group (2), (3) and (4) were considered together and compared to group 1 (Table 2). Consensus was reached by a reviewer who was blinded to the final diagnosis [A.M.L.].

2.9. Statistical analysis

We defined a test as being positive if it placed the epileptogenic focus within the resection zone (i.e.: with no activity outside this area). For each test, we computed the proportion of seizure-free patients (Engel Class I) among those with a positive and a negative result, and obtained sensitivity (Sn), specificity (Sp), positive predictive value (PPV), negative predictive value (NPV), and prognostic odds ratio (OR) with its *p*-value. The prognostic OR can be defined as either $\frac{Sn \cdot Sp}{(1-Sn)\cdot(1-Sp)}$ or $\frac{PPV \cdot NPV}{(1-PPV)\cdot(1-NPV)}$; it provides a summary assessment of the predictive ability of a test. We repeated test comparisons in a subset of 58 patients who had available results for the four imaging methods (HD-ESI, MRI, PET and ictal SPECT). Table 3 details the clinical characteristics on that group of patients.

Regarding EEG recordings in the group of 58 patients: $n = 2$ were recorded with 64 electrodes, $n = 31$ using 128 channels and $n = 25$ with 256 electrodes.

We also examined the performance of different tests combination; where having two positive results was compared to any other combination (e.g., comparison of both positive HD-ESI and MRI versus 1/2 or both tests negative). Finally, we used multiple logistic regressions to identify test results that best predicted a seizure-free outcome. The analyses were conducted using IBM SPSS software version 18.

3. Results

3.1. Patients

Of 190 patients, 91 (47.9%) were women. The median age at epilepsy onset was 7.0 ± 10.8 years (range 0–54), and age at surgery

Table 2
Test results and seizure-free outcome in 190 patients.

	Result	*N* (%)	Seizure free, *N* (row %)	*p*-value
MRI	Within resection	132 (69.5)	116 (87.9)	<0.001
	Outside or normal	58 (30.5)	32 (55.2)	
PET	Within resection	120 (63.2)	102 (85.0)	0.006
	Outside or normal	65 (34.2)	42 (64.6)	
	Not done	5 (2.6)	4 (80.0)	
HD-ESI	Within resection	68 (35.8)	57 (83.8)	<0.001
	Outside or normal	14 (7.4)	5 (35.7)	
	Not done	108 (56.8)	86 (79.6)	
SPECT ictal	Within resection	75 (39.5)	60 (80.0)	0.042
	Outside or normal	62 (32.6)	42 (67.7)	
	Not done	53 (27.9)	46 (86.8)	

HD-ESI = electric source imaging high-density; MRI = magnetic resonance imaging; SPECT = single-photon emission computerized tomography; PET = positron emission tomography.

Table 3
Clinical characteristics of the subset of 58 patients.

Sex ratio (M/F)	27/31
Mean age at disease onset	8.95
Mean age at operation	24.76
ETLE/TLE ratio	1:1
Etiology/syndrome	
Hippocampal sclerosis	19
Developmental[§]	6
Tumor[*]	7
Lesional	7
Gliosis	2
Tuberous sclerosis	7
Miscellaneous[^]	2
Non-lesional	8
Mean post-op follow-up period (months)	22.6
Post-operative outcome (Engel Class)	
I	40
II	9
III	7
IV	2
EEG	
Number of electrodes	
64 channels	2
128 channels	31
256 channels	25
Intracranial recordings	23

[§] Transmantle dysplasia, lisencephaly.
[*] DNET, meningioma, meduloblastoma.
[^] Meningitis, head trauma.

was 25.3 ± 15.3 years (range 0.6–60). Fifty-seven (30.0%) patients were <16 years at time of surgery (median age: 8.6 ± 4.6 years).

3.2. Post-surgical outcome

At 12-moths follow-up, seizure outcome was Engel Class I in 148 (77.9%) out of the 190 patients, Engel Class II in 17 (8.9%), Engel Class III in 19 (10.0%) and Engel Class IV in 6(3.2%) (Table 1). Mean follow-up duration was 26.6 ± 27 months. In our sample, patients suffering from extra-temporal lobe epilepsy presented a less favorable postoperative outcome (14/60 were Class III and 3/60 were Class IV), than patients with a temporal lobe intervention ($p = 0.0002$).

3.3. Performance of individual tests

All 190 patients had preoperative EEG recordings and standard MRI data. The number of patients with unavailable results was five for PET scan, 53 for ictal SPECT and 108 for HD-ESI (Table 2). If we detail the test scoring outcome per technique: (a) MRI presented 132/190 results with score 1, 38/190 with score 2 and 20/190 with score 3 + 4; (b) PET had 120/185 results with score 1, 45/185 with score 2 and 20/185 with score 3 + 4; (c) Ictal SPECT presented 75/137 with score 1, 41/137 with score 2 and 21/137 with score 3 + 4; (d) HR-ESI had 68/82 with score 1and 14/82 with score 3.

In the whole sample, all tests performed were associated ($p < 0.05$) with complete seizure control, defined as Engel Class I. The contrast was strongest for MRI, PET and HD-ESI ($p < 0.01$). No imaging technique had both high sensitivity and high specificity.

We then compared test performance indicators among the group of 58 patients who had all tests available (Table 4, upper half). Among these patients, 35 (67.3%) were seizure-free. Only MRI and HD-ESI had prognostic OR greater than 5, and both were statistically significant even in this subsample ($p = 0.016$ and $p = 0.011$, respectively).

Table 4
Test performance in 58 patients in whom all methods were performed, for single tests and for pairs of positive results.

Test	Sensitivity (%)	Specificity (%)	PPV (%)	NPV (%)	OR
MRI	70.7	70.6	85.3	50	5.8
PET	65.9	58.8	79.4	41.7	2.8
SPECT	53.7	70.6	81.5	38.7	2.8
HD-ESI	87.8	47.1	80	61.5	6.4
HD-ESI + MRI[*]	58.5	88.2	92.3	46.9	10.6
HD-ESI + PET[*]	58.5	70.6	82.8	41.4	3.4
HD-ESI + SPECT[*]	43.9	82.4	85.7	37.8	3.7
MRI + PET[*]	56.1	76.5	85.2	41.9	4.2
MRI + SPECT[*]	48.8	88.2	90.9	41.7	7.1
PET + SPECT[*]	46.3	88.2	90.5	40.5	6.5

HD-ESI = electric source imaging high-density; MRI = magnetic resonance imaging; SPECT = single-photon emission computerized tomography; PET = positron emission tomography; PPV = positive predictive value; NPV = negative predictive value; OR = odds ratio.
[*] BOTH tests positive versus any other result.

3.4. Performance of test combinations

As expected, the combination of two positive tests identified fewer seizure-free patients than each positive test alone. Therefore, this resulted in lower values of sensitivity and negative predictive value, and higher values of specificity and positive predictive value (Table 4, lower half). The highest prognostic OR was obtained for the combination of positive results on the HD-ESI and the MRI.

Logistic regression modeling among the 58 patients with all tests confirmed that only MRI and HD-ESI were independent predictors of favorable outcome. Once these two predictors were included in the model, none of the other tests were statistically significant. The adjusted prognostic OR was 13.1 for HD-ESI and 10.9 for MRI (both $p = 0.004$).

The combination of MRI and HD-ESI provided clinically useful results in more than half of the patients (Table 5). In a minority of patients (5/58), both tests were negative, and none of them experienced a favorable clinical outcome (i.e. NPV of 100%). In about half of the patients (26/58), both tests were positive, and 92.3% (24/26) were seizure-free at follow-up. If only one of them was positive and the other negative (27/58), the proportion of seizure-free was 63.0% (17/27).

We attempted to identify additional predictors of excellent outcome among the 27 patients with contradictory results on the MRI and HD-ESI. None of the nuclear imaging modalities (PET, SPECT) were associated with a favorable postoperative outcome ($p > 0.4$).

4. Discussion

In this study, all preoperative imaging exams were associated with favorable postoperative outcome, but the strongest independent indicators were MRI and HD-ESI (independently or in combination; Fig. 1).

Table 5
HD-ESI and MRI in patients with all tests.

Test results	Patients with all tests performed	
	N (%)	Seizure free (row %)
Both negative	5 (8.6)	0 (0.0)
Only MRI positive	8 (13.8)	5 (62.5)
Only HD-ESI positive	19 (32.7)	12 (63.2)
Both positive	26 (44.8)	24 (92.3)
Total	58 (100)	41 (69.5)

HD-ESI = high density electric source imaging; MRI = magnetic resonance imaging.

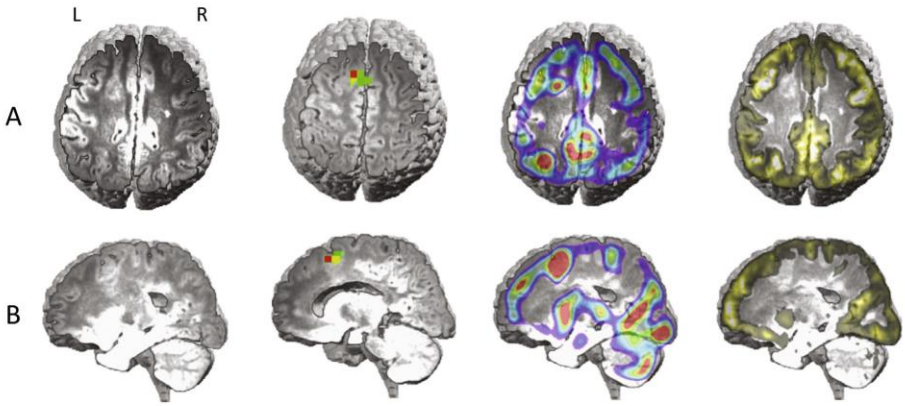

Fig. 1. Localization of non-lesional frontal epilepsy in a child. From left to right: magnetic resonance imaging (MRI), high-resolution electric source imaging (HD-ESI), positron-emission tomography (PET) and single-photon emission computed tomography (SPECT) localizing an anterior left frontal lesion. Dysplasia was confirmed by histopathological analysis. HD-ESI, PET and SPECT's results are projected on the individual anatomic brain. Sagittal (a) and longitudinal (b) slices are presented. This patient who had all concordant examinations was seizure free (Engel Class I) postoperatively after 3 years.

MRI is capable of providing very high spatial resolution, and it is well known that the presence of a lesion is related to better outcome compared to non-lesional epilepsy. The definition of "non-lesional" varies across studies, and may refer either to imaging or histopathological results (Tellez-Zenteno et al., 2010), or may even include patients with hippocampal sclerosis (Lowe et al., 2010). In the present study, we adopted the very conservative and clinically practical definition of "non-lesional"; referring to the absence of a lesion in a high-resolution MRI obtained with an established "epilepsy protocol" including negative findings in a voxel-based comparison with a data set of >300 healthy subjects (Huppertz et al., 2005). Using this definition, MRI rendered a 70% sensitivity and specificity in the subset of 58 patients in whom all tests were performed. This may appear low, but in our population, many patients had multifocal, bilateral or no MRI lesion. Furthermore, even when MRI depicts a unifocal abnormality, the true epileptogenic zone may be more complex. A recent study on 158 patients with frontal lobe epilepsy, of which 76% were lesional cases, only 44% were postoperatively seizure-free (Simasathien et al., 2013). While incomplete resection is foreseeable when the lesion/focus is too close to eloquent cortex; in many cases, like in dysplastic lesions, the epileptogenic focus may not necessarily overlap with the visible structural anomaly. Interestingly, in all 158 patients, intracranial exploration was carried out indicating once more that the use of intracranial EEG is no guarantee of success.

Concerning the remaining techniques, sensitivity values for PET of 60–100% and ictal SPECT (with or without statistical analysis) of 66–97% were reported (Knowlton, 2006; la Fougere et al., 2009). In the present study we obtained different results with ictal SPECT portraying the lowest sensitivity among all tests (48.6%), followed by PET (62.9%), maybe due to a higher percentage of patients with extratemporal foci as opposed to other studies. In MRI-negative temporal lobe epilepsy, a clear unilateral anterior temporal hypometabolism on PET has a similar high rate of postoperative seizure-freedom than hippocampal sclerosis (Carne et al., 2004).

HD-ESI represents focus localization in the 3-dimensional space within the individual patient's MRI. The combination of HD-ESI and MRI achieved a remarkable predictive capacity (i.e. seizure-free) in more than 90% of the patients (24/26, 92.3%) for whom results were concordant; but remained inconclusive for the remainder (17/32, 53%). When neither test was able to locate the epileptogenic zone within the resected area, the results were uniformly unfavorable (100% NPV).

Spatial precision of HD-ESI is in the cm-range. It has been shown that localization precision, to a sub-lobar level, can be obtained by using an electrode setup of more than 63 channels. Further increase from 64 to 128 electrodes showed very little improvement (Lantz et al., 2003). In addition, according to an earlier study from our group on 38 patients undergoing intracranial EEG monitoring, the median distance from the ESI maximum to the nearest electrode involved in the seizure onset was 15 mm, which in most patients co-localized with the intracranial ictal focus (Megevand et al., 2014). This is relatively high, given that intracranial EEG alone is probably an imperfect "gold standard" due to potential spatial undersampling and an interelectrode distance of already 10 mm. These results as well of studies with simultaneous intra- and extracranial EEG recordings also suggest that ESI is capable to detect deeper sources (Koessler et al., 2015; Ramantani et al., 2014).

In patients with discrepant MRI and HD-ESI results, nuclear imaging techniques did not add additional outcome predictors. Further research should focus on this group of patients, perhaps by including HR ictal recordings or research on other epilepsy markers like high frequency oscillations (Jacobs et al., 2010) or imaging changes of ictal rhythmic discharges (Yang et al., 2011). As opposed to interictal discharges, ictal activity is supposed to correspond with the underlying seizure onset area, although our and others' studies (Noe et al., 2013) point to an important role of correct and precise localization of interictal discharges. Systems allowing overnight long-term recordings with 128 or 256 channels maybe able to add HR-ictal recordings. Ictal or interictal, electromagnetic imaging offers a unique non-invasive opportunity to visualize neuronal discharges with both a high temporal and spatial resolution and thus, seems to be the most adequate technique in localizing the epileptogenic focus.

5. Conclusions

Our findings indicate that the use of MRI and ESI in the presurgical workup is associated with optimal seizure control, provided that both techniques concord and that the resection procedure takes the results into consideration. ESI together with MRI, predict the postoperative outcome.

Acknowledgements

This work was supported by the Swiss National Science Foundation, Switzerland [Grants No. 33CM30-140332 to M.S. and C.K. and No. 141165 to S.V.]. Cartool software is developed by Denis Brunet, from the Functional Brain Mapping Laboratory, Geneva, supported by the Center for Biomedical Imaging (CIBM), Geneva and Lausanne, Switzerland. We would like to thank Dr. Verena Brodbeck, Dr. Shahan Momjian and Prof. Karl Schaller for their profound contribution in this research study.

Conflict of interest: M.S. received speaker's fees from UCB, EISAI, EGI and GSK; S.V. from UCB and EGI. C.K. received research fees from UCB. All authors have directly participated in the planning, execution or analysis of the manuscript.

References

Brodbeck V, Spinelli L, Lascano AM, Wissmeier M, Vargas MI, Vulliemoz S, et al. Electroencephalographic source imaging: a prospective study of 152 operated epileptic patients. Brain 2011;134:2887–97.

Carne RP, O'Brien TJ, Kilpatrick CJ, MacGregor LR, Hicks RJ, Murphy MA, et al. MRI-negative PET-positive temporal lobe epilepsy: a distinct surgically remediable syndrome. Brain 2004;127:2276–85.

Engel Jr J. Clinical neurophysiology, neuroimaging, and the surgical treatment of epilepsy. Curr Opin Neurol Neurosurg 1993;6:240–9.

Engel Jr J, Van Ness P, Rasmussen TB, Ojemann LM. Outcome with respect to epileptic seizures. In: Engel Jr J, editor. Surgical treatment of the epilepsies. New York: Raven Press; 1993. p. 609–21.

Grave de Peralta Menendez R, Gonzalez Andino S, Lantz G, Michel CM, Landis T. Noninvasive localization of electromagnetic epileptic activity. I. Method descriptions and simulations. Brain Topogr 2001;14:131–7.

Huppertz HJ, Grimm C, Fauser S, Kassubek J, Mader I, Hochmuth A, et al. Enhanced visualization of blurred gray–white matter junctions in focal cortical dysplasia by voxel-based 3D MRI analysis. Epilepsy Res 2005;67:35–50.

Huppertz HJ, Kurthen M, Kassubek J. Voxel-based 3D MRI analysis for the detection of epileptogenic lesions at single subject level. Epilepsia 2009;50:155–6.

Jacobs J, Zijlmans M, Zelmann R, Chatillon CE, Hall J, Olivier A, et al. High-frequency electroencephalographic oscillations correlate with outcome of epilepsy surgery. Ann Neurol 2010;67:209–20.

Knowlton RC, Elgavish RA, Bartolucci A, Ojha B, Limdi N, Blount J, et al. Functional imaging: II. Prediction of epilepsy surgery outcome. Ann Neurol 2008;64:35–41.

Knowlton RC. The role of FDG-PET, ictal SPECT, and MEG in the epilepsy surgery evaluation. Epilepsy Behav 2006;8:91–101.

Koessler L, Cecchin T, Colnat-Coulbois S, Vignal JP, Jonas J, Vespignani H, et al. Catching the invisible: mesial temporal source contribution to simultaneous EEG and sEEG recordings. Brain Topogr 2015;28:5–20.

Kwan P, Sander JW. The natural history of epilepsy: an epidemiological view. J Neurol Neurosurg Psychiatry 2004;75:1376–81.

Kwan P, Sperling MR. Refractory seizures: try additional antiepileptic drugs (after two have failed) or go directly to early surgery evaluation? Epilepsia 2009;50:57–62.

la Fougere C, Rominger A, Forster S, Geisler J, Bartenstein P. PET and SPECT in epilepsy: a critical review. Epilepsy Behav 2009;15:50–5.

Lantz G, Grave de Peralta R, Spinelli L, Seeck M, Michel CM. Epileptic source localization with high density EEG: how many electrodes are needed? Clin Neurophysiol 2003;114:63–9.

Lowe NM, Eldridge P, Varma T, Wieshmann UC. The duration of temporal lobe epilepsy and seizure outcome after epilepsy surgery. Seizure 2010;19:261–3.

Luders HO, Najm I, Nair D, Widdess-Walsh P, Bingman W. The epileptogenic zone: general principles. Epileptic Disord 2006;8:1–9.

Megevand P, Spinelli L, Genetti M, Brodbeck V, Momjian S, Schaller K, et al. Electric source imaging of interictal activity accurately localises the seizure onset zone. J Neurol Neurosurg Psychiatry 2014;85:38–43.

Michel CM, Murray MM, Lantz G, Gonzalez S, Spinelli L, Grave de Peralta R. EEG source imaging. Clin Neurophysiol 2004;115:2195–222.

Noe K, Sulc V, Wong-Kisiel L, Wirrell E, Van Gompel JJ, Wetjen N, et al. Long-term outcomes after nonlesional extratemporal lobe epilepsy surgery. JAMA Neurol 2013;70:1003–8.

Radau PE, Slomka PJ, Julin P, Svensson L, Wahlund LO. Evaluation of linear registration algorithms for brain SPECT and the errors due to hypoperfusion lesions. Med Phys 2001;28:1660–8.

Ramantani G, Dümpelmann M, Koessler L, Brandt A, Cosandier-Rimélé D, Zentner J, et al. Simultaneous subdural and scalp EEG correlates of frontal lobe epileptic sources. Epilepsia 2014;55:278–88.

Rosenow F, Luders H. Presurgical evaluation of epilepsy. Brain 2001;124:1683–700.

Schramm J, Clusmann H. The surgery of epilepsy. Neurosurgery 2008;62:463–81.

Simasathien T, Vadera S, Najm I, Gupta A, Bingaman W, Jehi L. Improved outcomes with earlier surgery for intractable frontal lobe epilepsy. Ann Neurol 2013;73:646–54.

Slomka PJ, Radau P, Hurwitz GA, Dey D. Automated three-dimensional quantification of myocardial perfusion and brain SPECT. Comput Med Imaging Graph 2001;25:153–64.

Spinelli L, Andino SG, Lantz G, Seeck M, Michel CM. Electromagnetic inverse solutions in anatomically constrained spherical head models. Brain Topogr 2000;13:115–25.

Tellez-Zenteno JF, Hernandez Ronquillo L, Moien-Afshari F, Wiebe S. Surgical outcomes in lesional and non-lesional epilepsy: a systematic review and meta-analysis. Epilepsy Res 2010;89:310–8.

Vargas MI, Becker M, Garibotto V, Heinzer S, Loubeyre P, Gariani J, et al. Approaches for the optimization of MR protocols in clinical hybrid PET/MRI studies. MAGMA 2013;26:57–69.

Wiebe S, Blume WT, Girvin JP, Eliasziw M. A randomized, controlled trial of surgery for temporal-lobe epilepsy. N Engl J Med 2001;345:311–8.

Yang L, Wilke C, Brinkmann B, Worrell GA, He B. Dynamic imaging of ictal oscillations using non-invasive high-resolution EEG. Neuroimage 2011;56:1908–17.

Yuan J, Chen Y, Hirsch E. Intracranial electrodes in the presurgical evaluation of epilepsy. Neurol Sci 2012;33:723–9.

Study III

Lascano AM, Grouiller F, Genetti M, Spinelli L, Seeck M, Schaller K, Michel CM. Surgically relevant localization of the central sulcus with high-density SEP compared to fMRI. Neurosurgery 2014; 74: 517-26. Doi: 10.1227/NEU.0000000000000298.

- Impact Factor: 4.605
- Average citations per year: 17
- Sum of times cited (without self-citations): 2.43
- Copyright clearance (license number): 4840811164343 (Oxford University Press)

Surgically Relevant Localization of the Central Sulcus With High-Density Somatosensory-Evoked Potentials Compared With Functional Magnetic Resonance Imaging

Agustina M. Lascano, MD, PhD*
Frédéric Grouiller, PhD‡§
Mélanie Genetti, PhD*‡
Laurent Spinelli, PhD*
Margitta Seeck, MD*
Karl Schaller, MD¶
Christoph M. Michel, PhD*‡

*Department of Neurology, University Hospital of Geneva, Geneva, Switzerland; ‡Functional Brain Mapping Laboratory, Department of Neurology, University Hospital of Geneva and University Medical Centre, Geneva, Switzerland; §Department of Radiology and Medical Informatics, University Hospital of Geneva, Geneva, Switzerland; ¶Department of Neurosurgery, University Hospitals of Geneva, Geneva, Switzerland

Correspondence:
Christoph M. Michel, PhD,
Rue Michel-Servet 1, CP 1211,
Geneva, Switzerland.
E-mail: Christoph.Michel@unige.ch

Received, September 13, 2013.
Accepted, January 7, 2014.
Published Online, January 23, 2014.

BACKGROUND: Resection of abnormal brain tissue lying near the sensorimotor cortex entails precise localization of the central sulcus. Mapping of this area is achieved by applying invasive direct cortical electrical stimulation. However, noninvasive methods, particularly functional magnetic resonance imaging (fMRI), are also used. As a supplement to fMRI, localization of somatosensory-evoked potentials (SEPs) recorded with an electroencephalogram (EEG) has been proposed, but has not found its place in clinical practice.

OBJECTIVE: To assess localization accuracy of the hand somatosensory cortex with SEP source imaging.

METHODS: We applied electrical source imaging in 49 subjects, recorded with high-density EEG (256 channels). We compared it with fMRI in 18 participants and with direct cortical electrical stimulation in 6 epileptic patients.

RESULTS: Comparison of SEP source imaging with fMRI indicated differences of 3 to 8 mm, with the exception of the mesial-distal orientation, where variances of up to 20 mm were found. This discrepancy is explained by the fact that the source maximum of the first SEP peak is localized deep in the central sulcus (area 3b), where information initially arrives. Conversely, fMRI showed maximal signal change on the lateral surface of the postcentral gyrus (area 1), where sensory information is integrated later in time. Electrical source imaging and fMRI showed mean Euclidean distances of 13 and 14 mm, respectively, from the contacts where electrocorticography elicited sensory phenomena of the contralateral upper limb.

CONCLUSION: SEP source imaging, based on high-density EEG, reliably identifies the depth of the central sulcus. Moreover, it is a simple, flexible, and relatively inexpensive alternative to fMRI.

KEY WORDS: Electrical source imaging, Electroencephalography, Eloquent cortex, Functional imaging, Presurgical evaluation, Primary somatosensory cortex

Neurosurgery 74:517–526, 2014 DOI: 10.1227/NEU.0000000000000298 www.neurosurgery-online.com

CME

SANS LifeLong Learning and NEUROSURGERY offer CME for subscribers that complete questions about featured articles. Questions are located on the SANS website (http://sans.cns.org/). Please read the featured article and then log into SANS for this educational offering.

Noninvasive functional techniques, allowing accurate mapping of the somatosensory cortex in the individual subject, are of interest in planning the resection of intracranial lesions or epileptogenic foci.[1,2] Accurate localization of the central sulcus reduces the risk of postoperative functional deficits in cases where the lesion is close to the sensorimotor region.[3]

Identification of the central sulcus is still done by visual search for anatomical landmarks from images on computer tomography (CT) or magnetic resonance imaging (MRI).[4-6] However, this approach has proven to be unreliable because of the large variability between observers.[1] Moreover, brain anatomy can be severely distorted in

ABBREVIATIONS: DCES, direct cortical electrical stimulation; **EEG,** electroencephalography; **ESI,** electric source imaging; **fMRI,** functional magnetic resonance imaging; **GFP,** global field power; **HD,** high density; **MEG,** magnetoencephalogram; **MNI,** Montreal Neurological Institute; **SEP,** somatosensory evoked potential; **SI,** primary somatosensory cortex

patients with large brain lesions.[7] For this reason, intra- or extraoperative functional mapping through direct cortical electrical stimulation (DCES), performed in combination with electrocorticography, is considered to be the gold standard.[8] However, this procedure is time consuming and/or necessitates preoperative electrode implantation, being, therefore, associated with potential risks.[9,10] Also, if DCES is applied only during surgery, these results are not available for presurgical evaluation.

In the quest for noninvasive methods with added localization yield during presurgical planning, several studies investigated the use of functional magnetic resonance imaging (fMRI).[11-13] fMRI localization accuracy is considered to be very high, providing a topographical layout of the individual digital representation in the primary somatosensory cortex (SI).[14-16] On the other hand, given that fMRI is based on the hemodynamic response, it is thought to be less powerful in lesions that lead to changes in the vascular autoregulation, such as gliomas[17,18] or cerebral ischemia.[19] Moreover, fMRI is not always feasible, particularly in pediatric patients or in those with claustrophobia or carrying ferromagnetic material.

In cases where fMRI is not possible or not useful due to vascular abnormalities, electrophysiological methods based on source localization of stimulus-evoked activity can be considered as an option. Source localization techniques can be based either on magnetoencephalogram (MEG)[20,21] or electroencephalogram (EEG) recordings.[22,23]

MEG-based source localization has demonstrated its usefulness in presurgical assessment[24]; whereas source localization based on EEG has rarely been promoted as a clinical tool.[25] This is rather surprising given that EEG is readily available in clinics and that previous studies have already demonstrated accurate localization of SI with EEG-based source localization methods.[26-30] These studies, however, were performed on few subjects and were targeted at validation of new source localization methods and head models. The stability of SEP source localization across a larger cohort of subjects and direct comparison with fMRI and intracranial recordings in the same subjects has not been systematically evaluated.

In the present study, we intended to evaluate the accuracy of high-density (256-channel) EEG source imaging (HD-ESI) in localizing the SI in individual subjects. We also directly compared the localization of the somatosensory cortex between HD-ESI and fMRI in a group of healthy subjects, and between these 2 noninvasive methods and DCES in a group of patients.

The present study is structured in 3 parts:

1. To determine the variability of the localization of HD-ESI SEPs, healthy subjects underwent mechanical air-puff stimulation. Three-dimensional source localization was determined in the average template MRI of the Montreal Neurological Institute (MNI brain).
2. For the purpose of directly comparing the individual SEP source with the conventionally used cortical stimulation, we proposed HD-ESI to 6 patients who afterward underwent intracranial evaluation with subdural electrodes covering the sensorimotor cortex. We then compared the HD-ESI source localization with the localization of the electrodes that evoked sensory responses during DCES.
3. A second group of healthy volunteers underwent HD-ESI and fMRI under identical stimulation conditions, allowing comparison of both noninvasive techniques in the individual subject.

METHODS

Participants

Healthy Controls

Two groups of healthy controls were studied: (1) 31 subjects (mean age, 29 years; 16 females; 1 left-handed) in whom we recorded high-density scalp SEP (ie, HD-ESI) without MRI; (2) 18 subjects (mean age, 23 years; 7 females; all right-handed) who participated in both high-density scalp SEP and fMRI acquisitions and in whom the individual structural MRI was available. The first group was used to evaluate the correctness of the mean source localization with respect to the known location of the somatosensory cortex in a template brain and to evaluate the variability of this location across healthy subjects, while the second group was used for direct interindividual comparison with fMRI results. None of the subjects presented any previous or current neurological or psychiatric diseases. Before participation, subjects provided written informed consent to procedures that had been approved by the Ethics Committee of the University Hospital of Geneva, Switzerland, in agreement with the Declaration of Helsinki.

Patients

We studied 6 patients with medically refractory epilepsy (median age, 12 years; range, 7-35; 3 females and 3 males; all right-handed) during their noninvasive and, subsequently, their presurgical evaluation in which we performed HD-ESI, DCES, and fMRI (in 4/6). Both HD-ESI and fMRI were performed during the presurgical noninvasive evaluation phase.

We selected patients who satisfied the following criteria: (1) implanted electrodes exploring the precentral and/or the postcentral gyrus; (2) lack of paroxysmal interictal activity or early dissemination of spontaneous ictal discharges toward the peri-rolandic region. Table 1 provides clinical information about the patients who were selected for this study.

Stimulation Parameters

Experiments were conducted in an electromagnetically shielded, sound-attenuated and darkened room. Finger clips with balloon diaphragms (0.8 cm^2 surface) produced nonpainful stimuli (stimulus duration, 50 ms) driven by bursts of compressed air. Stimuli were delivered to the distal phalanx of the thumb at a repetition rate of 2.14 Hz (system built by Christian Wienbruch and Victor Candia; see Wienbruch et al[31] for further details). Air pressure was adjusted to produce a well-defined tactile sensation (2.5 bar). A total of 1000 stimuli per thumb were applied in 1 single block. Identical stimulation parameters were used in all participants. We adapted this protocol for fMRI in which a 24-second block of alternative right and left stimulations separated by a pause of 8 seconds was executed.

TABLE 1. Clinical Information of the 6 Epileptic Patients[a]

Patient	Sex	Age, y	DD, y	Syndrome	Semiology	Structural MRI	Interictal EEG	Intracranial Electrode Placement	Intracranial Seizure Onset zone	Histology
1	M	7	7.7	LFE	R facial clonus, right head deviation, speech arrest	LFPTO abscess resection	LFC	LF (20), interhemispheric (8) LPO (40), LT (14), RT (15)	None recorded	Gliosis
2	F	13	12.3	LFE	R lower and upper limb dystonia, speech arrest	Multiple tubers: LC with transmantle component	LFC	LTP (48), depth to the lesion (24)	LF (clinical), LC (subclinical)	TS
3	M	35	20	LTE	Manual and oral automatisms, behavioral arrest	Normal	LT	LFP (64), LO (12), depth to L hippocampus (8), LT (26)	L hippocampus, (clinical), L angular gyrus (subclinical)	LT: lymphocytic infiltration of the meninges
4	F	26	22	LTOE	R arm sensory Sz, R manual and oral automatisms	LPO gliosis	LPO	LFP (64), LF (12), LT (30), depth to L hippocampus (8), interhemispheric (8)	LTO (clinical) LPO (subclinical)	Gliosis
5	M	11	7	RFPE	L hemibody sensory Sz	Normal	RFC	RFPT (64), RF (16), RT (6), depth to R insula (16), interhemispheric (12)	RP	Normal
6	F	11	8.6	LFE	Perioral sensory Sz, oral automatisms, dysarthria	Normal	LFC	LFPT (64), RFPT (24), L insula (8), LF (8)	LFC	FCD type 2

[a]DD, disease duration; MRI, magnetic resonance imaging; EEG, electroencephalogram; M, male; F, female; R, right; L, left; E, Epilepsy; F, frontal; T, temporal; P, parietal; O, occipital; C, central; Sz, seizure; TS, tuberous sclerosis; FCD, focal cortical dysplasia.

EEG Data Collection

EEG was collected from 256 silver-chloride-plated carbon-fiber electrodes by using a HydroCel Geodesic Sensor Net (Electrical Geodesics Inc, Eugene, Oregon). One pediatric patient was recorded with a 128-channel net (patient 1). Electrodes are interconnected by thin rubber bands and each contained a small sponge that directly touched the scalp's surface.[32] The nets were soaked in saline water before placement. The whole net was applied at once, and no skin abrasion was required. The net was adjusted so that Fpz, Cz, Oz, and the preauricular points were correctly placed according to the international 10/10 system. The geodesic tension structure of the net ensured that the electrodes were evenly distributed across the head and at similar locations across subjects. Electrode-skin impedances were kept below 20 kΩ. EEG was continuously recorded at a sampling rate of 1 kHz and bandpass filtered between 0.1 and 400 Hz. The Vertex (Cz) electrode was used as recording reference, and the data were referenced offline to the average one.

SEP Analysis

SEP Preprocessing

Evoked potentials were computed for each healthy control and each patient, using the free academic software Cartool (D. Brunet, Geneva University Hospital and Medical School, Center for Biomedical Imaging, Geneva, Switzerland; http://sites.google.com/site/fbmlab/cartool). Epochs were selected ranging from 50 ms before to 120 ms after stimulus onset. A high-pass filter of 10 Hz was applied to the ongoing EEG. Epochs with ocular-motor artifacts were determined by voltage thresholds (50 μV) and were excluded after visual inspection.

Spherical spline interpolation was applied on scalp EEG data to interpolate any artifact-contaminated electrode.[33] In addition, the electrodes on the cheek area were excluded and a standard electrode array of 204 channels was used (109 channels in the 1 patient with 128-channel net).

Source Localization of Scalp SEP

Each participant's average SEP map corresponding to the global field power (GFP) peak of the most stable early response, appearing at 40 to 60 ms poststimulus onset,[34,35] was subjected to source localization. GFP corresponds to a parametric assessment of map strength computed as standard deviation of the potential value.[36]

A local autoregressive average distributed linear inverse solution[37-39] was applied with the purpose of estimating the intracranial 3-D current density distribution of the SEP response without any a priori restriction on the location, number, or orientation of the sources. Noise regularization was based on the L-curve method[40] applied to the grand mean SEP and was kept constant for the analysis of the individual subjects. Several simulation studies and application to real data have demonstrated excellent localization performance of this source localization method.[39,41]

A simplified realistic head model called SMAC[39,42] was used for the source localization that restrains the solution space to the grey matter without constraining source orientation. The method extracts the brain surface from the MRI and calculates the best-fitting sphere for this surface. The ratio of the sphere radius and the real surface radius is then determined and the source space is warped accordingly. The source space is then constrained to the gray matter of this warped space and around 5000 solution points are equally distributed within this space. Standard spatial electrode positions were used in all subjects, coregistered to the MRI by adjusting the position of the nasion, inion, Cz, and preauricular landmarks. In the 31 subjects corresponding to group 1, in whom no individual MRI was recorded, the electrodes were coregistered on the scalp surface of the MNI brain (not in the brain or the skull), whereas the individual brain was used for source localization in the 18 subjects of group 2 and in the patients.

An analytical solution was used for the lead field calculation based on a 3-shell spherical head model. The skull relative conductivity was set to 0.05 and adjusted by the estimated skull thickness under each electrode.[43] The results of the inverse solution are back-transformed to the original head shape using the same transformation parameter. It has been shown that this simplified realistic head model produces high localization reliability[39,41,44] and that it is comparable to boundary element models.[45]

In the first group of healthy controls, in whom we evaluated location and stability of HD-ESI, MNI coordinates of the source maximum was determined for each subject. In the second group of healthy participants and the epileptic patients, we compared HD-ESI with the other mapping methods by using the x-y-z coordinates of the individual MRI scans for all modalities.

Electrocorticography and DCES

All patients had extensive coverage of the brain surface with subdural grids, strips, and, occasionally, depth electrodes over the region(s) suspected to be involved in seizure onset and early propagation (Table 1). The platinum electrodes (Ad-Tech; Ad-Tech, Racine, Wisconsin) possessed a diameter of 2.3 mm (subdural grids and strips) or 1.1 mm (depth electrodes) and were arranged at an intercontact distance of 10 mm. The anatomical targeting of electrodes was established in each patient, according to available noninvasive information (interictal and ictal scalp EEG, anatomical MRI, nuclear medicine procedures, and seizure semiology). The exact location of depth electrode contacts in the different cortical and subcortical regions was ascertained by post-implantation high-resolution CT scans rigidly coregistered to pre-operative 3-D T1-weighted MRI by maximizing the normalized mutual information between these 2 images.

DCES was delivered between 2 adjacent intracranial electrodes (Astro-Med Inc, Grass Technologies, Rockland, Massachusetts) with biphasic currents (frequency = 50 Hz; pulse length = 300 μs; pulse duration = 2 s; intensity = 1-10 mA). We calculated the mean x-y-z coordinates of the electrodes in which a sensory response of the upper limb was elicited.

MRI Acquisition

Structural and functional MRI acquisitions were made with a 3T whole-body MRI scanner (Siemens Magnetom Trio, Erlangen, Germany). Two hundred fifty-six functional images were acquired using a single-shot T_2*-weighted gradient-echo Echo-Planar Imaging sequence (repetition time = 1980 ms, echo time = 30 ms, flip angle = 90°, voxel size = 3 × 3 × 3.75 mm^3, 32 slices). A magnetization prepared rapid acquisition gradient-echo 3-D high-resolution T_1-weighted structural image was acquired for individual anatomical localization (repetition time = 1900 ms, echo time = 2.27 ms, TI = 900 ms, flip angle = 9°, voxel size = 1 × 1 × 1 mm^3 acquisition matrix: 256 × 256).

fMRI Processing

Preprocessing of functional images using SPM8 software (Wellcome Department of Imaging Neuroscience, UCL, London, UK) included the

following: (1) realignment of the fMRI time series; (2) rigid-body coregistration of the realigned functional images on the 3-D T1 structural image by maximizing its normalized mutual information with the mean functional image[46]; (3) spatial smoothing of functional images with an isotropic Gaussian kernel (6 mm full width at the half-maximum).

Finally, fMRI time series were whitened and serial correlations were modeled by using an autoregressive filter of order 1. Low-frequency noise and signal drift were removed by using a discrete cosine transform basis set with a filter cutoff period of 128 s. For each of the 2 conditions (ie, left and right thumb stimulation), regressors of interest were created by convolving each block with a canonical hemodynamic response function. Motion-related parameters derived from the realignment of functional images were also included in the model as covariates. Statistical analyses of fMRI data were performed for each subject individually by using a mass-univariate approach based on the General Linear Model.[47]

We contrasted the results using a 1-sample *t* test. The significance level of the resulting SPM[t] maps was set to a threshold of $P < .05$ corrected for multiple comparisons across the whole brain by using family-wise error, except in 2 patients in whom we modified the threshold to $P < .001$ uncorrected for multiple comparisons. In these 2 young children, despite the inclusion of the 6 motion parameters in the model, the sensitivity of fMRI was decreased because of moderate motion (<1.5 mm). However, in these 2 cases, we carefully checked that the fMRI maximum was located in the postcentral gyrus, and that no spurious activation suggestive of motion was visible at this threshold.

In order to have group fMRI activation, we also normalized each individual fMRI of our 18 healthy subjects into the MNI space, and we performed a random-effects group analysis on the individual contrast images by using a 1-sample *t* test ($P < .05$, family-wise error-corrected).

Comparison Between HD-ESI With fMRI and DCES

Comparison was performed on the basis of visual analysis as well as through x-y-z coordinates of maximum activation of each method. For each subject and pair of techniques (HD-ESI vs DCES, HD-ESI vs fMRI, fMRI vs DCES), the distance between the maxima of activation was computed for each of the axis as well as the mean Euclidean distance between the different methods. Parametric independent paired-sample *t* tests were performed for each axis in the group of healthy subjects comparing SEP source localization and fMRI.

RESULTS

Consistency of SEP Source Location (HD-ESI)

Figure 1 shows the grand mean averaged SEP of the 31 healthy controls, the map at the peak latency, and the average source localization in the template MNI brain that was used as head model for the source localization. Across subjects, the GFP peak of the first stable SEP component appeared at a mean latency of 47 ± 5 ms for the left and 47 ± 6 ms for the right thumb stimulation. The mean MNI coordinates on the x-y-z axis were as follows: 39 (±5), −22 (±5), 55 (±4) for the left and −32 (±4), −30 (±5), 60 (±2) for the right thumb SEP. These locations correspond within a 5-mm radius to Brodmann areas 3 and 4, ie, the pre- and postcentral gyrus (Talairach Client from http://www.talairach.org/client.html). In order to illustrate the spread of the source localization across subjects, Figure 2 shows the location of the maximum of the source for each individual subject coregistered to the MNI template. Because the source maximum is overlapped across subjects, we color-coded the location according to the number of subjects having the maximum in that location.

Comparison Between HD-ESI and DCES in Epileptic Patients

Table 2 summarizes the results of the comparison between HD-ESI and DCES in the 6 epileptic patients. Additional fMRI was done in 4 patients. DCES was performed on all 6 patients through implanted subdural electrodes, and both sensory and motor responses were obtained. The electrodes from which a sensory response was elicited were always adjacent to each other. The median Euclidean distance between HD-ESI and DCES was 13 mm (range: 5-20 mm). Note that the distance in the medial-lateral axis was always negative because of the DCES electrode lying on the brain surface while the ESI location was located deeper in the sulcus (see Discussion). An example of this comparison is shown in Figure 3.

Comparison of HD-ESI and fMRI in Healthy Controls

In the second control group of 18 healthy subjects, HD-ESI and fMRI were obtained in all subjects showing reliable activation of the somatosensory cortex with both techniques. Mean MNI coordinates of the fMRI maximal activation were the following: 56 (±2), −15 (±4), 50 (±5) for the left and −55 (±3), −20 (±4), 49 (±4) for the right thumb. These locations corresponded to Brodmann areas 2 and 3 within a 5-mm radius.

Table 3 gives the mean and standard deviation of the difference between the SEP source maximum and the fMRI maximum and the result of the statistical comparison for each of the axes. There was a significant difference ($P < .001$) between both techniques in the x-axis (medial-lateral orientation). The SEP source maximum was identified on both sides more medially than the blood oxygen level-dependent fMRI maximum (difference 16 mm for the left, and 20 mm for the right thumb stimulation). Differences were not significant ($P > .01$) for the y- and z-axis (ie, anterior-posterior and superior-inferior, respectively). In the 4 implanted patients, who also had preoperative fMRI, the Euclidean distance of the fMRI maximum to DCES was, on average, 14 mm (range, 11-17).

DISCUSSION

The aim of this study was to assess the capability of SEP source analysis to localize the primary somatosensory area in the individual subject and to evaluate its yield compared with fMRI.

In agreement with earlier findings, scalp SEP source analysis was able to localize in the contralateral SI cortex with low variability between subjects.[1,48] The evaluation of 31 subjects by using the MRI template revealed deep central sulcus localization with small variability. In terms of Talairach coordinates, the mean location corresponded to area 3b, with a slight extension to area 4 for the left thumb stimulation. Area 3b and area 4 lie within the central

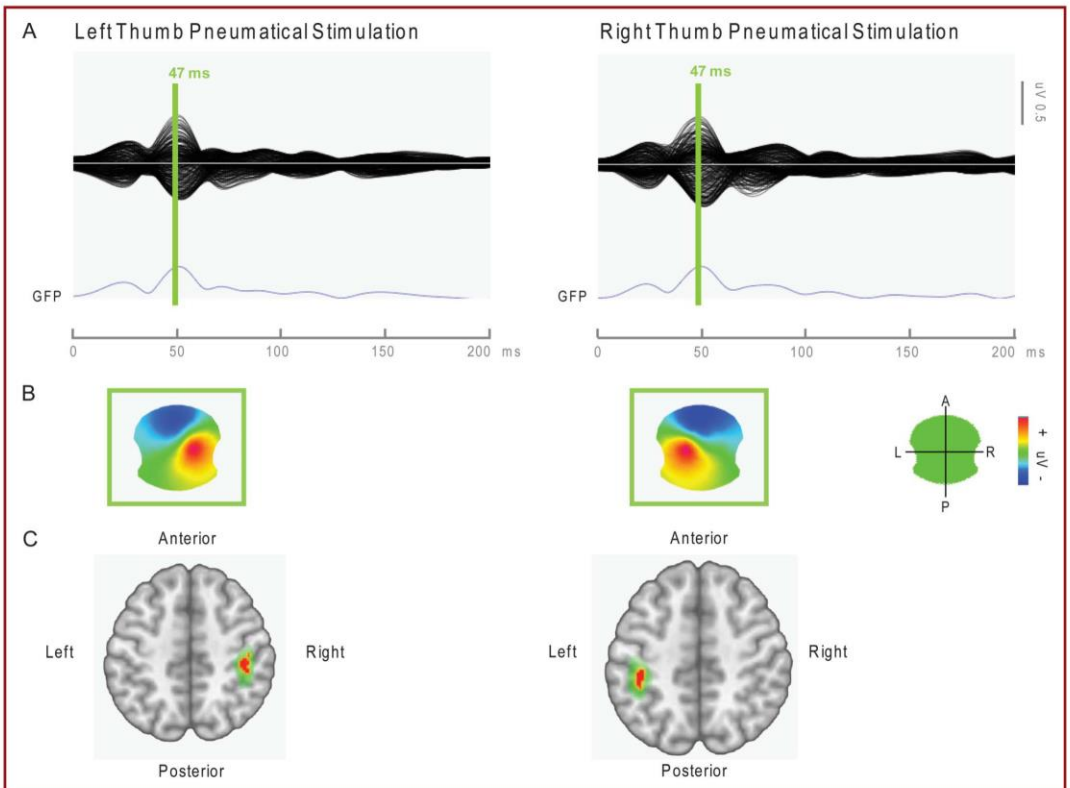

FIGURE 1. *Somatosensory evoked potential (SEP) mapping in response to pneumatical stimulation.* **A**, *pneumatically elicited SEP response, for both left and right upper limb, illustrated as a butterfly plot (overlaid traces) of all 204 electrodes referenced to the average reference. The Global Field Power (GFP) curve is plotted below.* **B**, *the topography of the most significant component at its peak is depicted (map seen from top: red, positive voltage; blue, negative voltage).* **C**, *source localization of the grand mean map displayed on the MNI template brain. Average of 31 healthy controls. MNI, Montreal Neurological Institute.*

sulcus on the posterior (area 3b) and anterior (area 4) wall. Stimulation of mechanoreceptors reaches area 3b through the ventral posterior lateral nucleus of the thalamus and then projects to area 1 for further integration, which is located on the surface of the postcentral gyrus. Given this projection pathway, the correct localization of the first cortical SEP component is expected to be in area 3b. Because of the proximity of area 3b to area 4 (1-2 mm) and the spatial limitation of distributed inverse solution, a discrete spatial blurring within these areas across subjects cannot be avoided. Compared with "DCES" identification of the sensory cortex of the contralateral upper limb, accuracy appeared reasonable with a distance of only 10 to 20 mm. It should be remembered that DCES from subdural electrodes imperfectly maps deep sources, given that it stimulates mainly the gyri on which electrodes are placed, and only indirectly the cortex in the sulci where area 3b is located. Consequently, a difference between ESI and DCES in the medial-lateral orientation has to be expected and it is, thus, physiologically plausible.

Correct identification of the central sulcus was also possible with fMRI in the 18 healthy subjects. The contrast between SEP source localization and fMRI in these subjects provided differences that were comparable with results from other studies using fewer electrodes. They reported Euclidean distances of 16 to 17 mm[1] and even 23.5 mm in a combined EEG-fMRI study.[48] The mean distance between the 2 modalities was also comparable to the distances found by Kober and colleagues,[35] contrasting MEG source imaging and fMRI with the use of a similar stimulation technique. One investigation found a small discrepancy of 5.1 mm and 11.9 mm while measuring high-density EEG and fMRI responses to electric median nerve stimulation, but these values were based on 2 subjects only.[30] Still, it is possible that the air-puff stimulation to the thumb used here leads to less precise

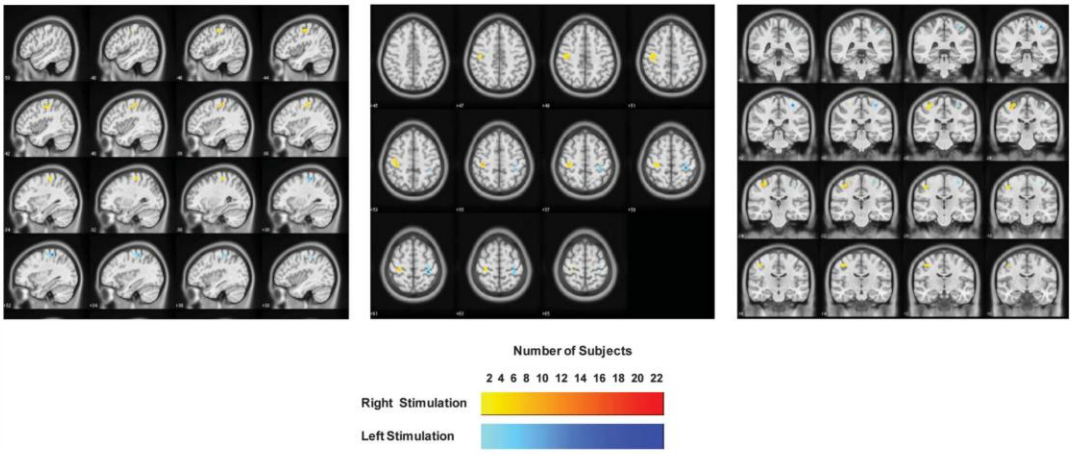

FIGURE 2. *Localization of the SEP source maximum of each individual subject (n = 31) by using the MNI template brain as head model. Because sources overlapped on the same voxel in several subjects, the voxels were color coded according to the number of subjects having the maximum at this voxel (red = right thumb stimulation; blue = left thumb stimulation). The figure illustrates the spread of the localization around the postcentral gyrus. MNI, Montreal Neurological Institute; SEP, somatosensory evoked potential.*

localization than electrical stimulation owing due to a lower signal-to-noise ratio. Also, the simplified realistic head model and the assumed electrode locations might have limited the SEP source localization precision. On the other hand, the air-puff stimulation is much more comfortable and easy to apply (particularly in children). Moreover, the simplified head model and the avoidance of long-lasting precise electrode localization measurements reduce the amount of expert effort and thus reduce costs. Another source of errors that needs to be considered in such studies is the coregistration of the different mapping modalities.[49] We tried to minimize this error by using the same high-resolution individual 3-D T1 structural image as a reference for each modality. The functional images were all coregistered with this individual structural image; the coordinates of each solution point in the grey matter were defined in the T1 space, and the position of DCES electrodes were also defined in the T1 space after coregistration with the CT.

Interestingly, we observed in all participants that the major and most consistent difference between the 2 techniques lied again in the x-axis (medial-lateral orientation). The SEP source maximum

TABLE 2. Distance Comparison Between HD-ESI, fMRI, and DCES in 6 Epileptic Patients Implanted With Subdural Electrodes[a]

	HD-ESI vs fMRI				HD-ESI vs DCES				fMRI vs DCES			
	Coordinates (mm)			Euclidean Distance (mm)	Coordinates (mm)			Euclidean Distance (mm)	Coordinates (mm)			Euclidean Distance (mm)
Patient	dx	dy	dz	sqrt ($dx^2+dy^2+dz^2$)	dx	dy	dz	sqrt ($dx^2+dy^2+dz^2$)	dx	dy	dz	sqrt ($dx^2+dy^2+dz^2$)
1	N/A	N/A	N/A	N/A	−7	5	7	11	N/A	N/A	N/A	N/A
2	−6	12	6	15	−11	8	−3	14	−4	−4	−9	11
3	N/A	N/A	N/A	N/A	−9	14	6	18	N/A	N/A	N/A	N/A
4	−15	10	0	18	−6	5	5	9	9	−6	5	12
5[b]	0	22	−17	28	−11	16	−5	20	11	−6	12	17
6	−21	4	5	22	−3	4	2	5	17	0	−4	17
Mean (abs)	10	12	6	17	8	9	5	13	10	4	8	13

[a]HD-ESI, high-density electric source imaging; fMRI, functional magnetic resonance imaging; DCES, direct cortical electrical stimulation; N/A, not available; dx, distance in the left-right orientation; dy, distance in the anterior-posterior orientation; dz, distance in the superior-inferior orientation; sqrt, square root; abs, absolute values.
[b]Patient 5 was flipped in the left-right axis.

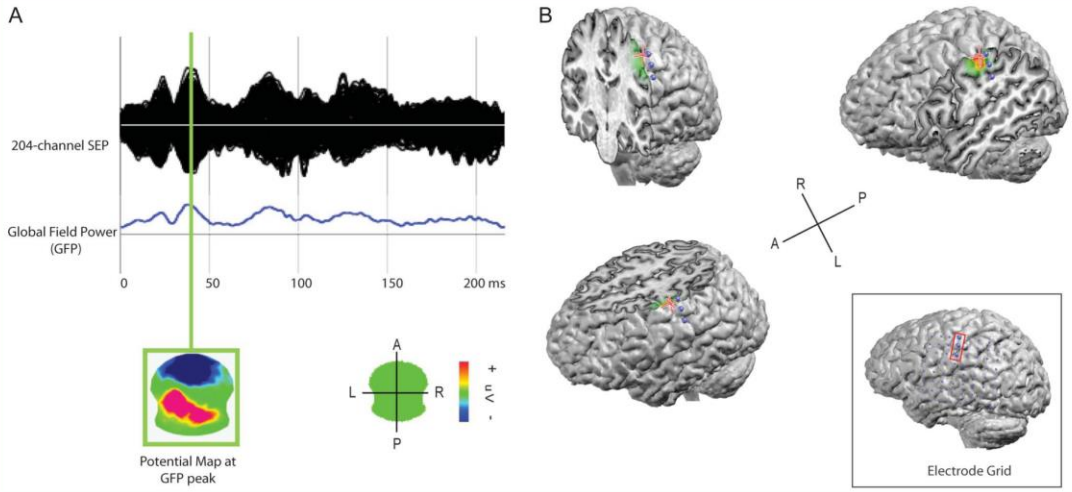

FIGURE 3. *Comparison of electric source imaging (ESI) of the scalp SEP and the location of the electrodes that provoked somatosensory sensation of the upper limb when stimulated with direct cortical electrical stimulation (DCES) in patient 3.* **A**, *pneumatically elicited SEP response, for the right upper limb, illustrated as a butterfly plot (overlaid traces) of all 204 electrodes referenced to the average reference. The topography at the GFP peak at 40 ms is depicted (map color code: red, positive voltage; blue, negative voltage). HD-ESI is calculated and localized by using a linear inverse solution and the patient MRI as head model.* **B**, *the area with maximal source activity is projected on the surface (red cross) of the individual MRI in 3 orthogonal views. The source location is portrayed within the central sulcus and slightly anterior to the 3 electrodes showing a positive DCES result. A general view of the entire grid of patient 3 is displayed over the left hemisphere, and those electrodes with a positive result are enhanced (red rectangle). GFP, Global Field Power; HD, high-density; SEP, somatosensory evoked potential.*

was systematically localized more medial than the fMRI maximum for both stimulation sites. This observation has also been reported in the combined EEG-fMRI study of Christmann and colleagues,[48] and in the MEG-fMRI comparison reported by Kober and colleagues.[35] In the latter study of 34 patients, the MEG dipole was significantly more mesial (average 8 mm) compared with the fMRI maximum. The authors explained this difference by the fact that the early peak of the magnetic evoked field results from the activation of area 3b (comprising the anterior wall of the central sulcus[35]), whereas the fMRI maximum was located in area 1 on the postcentral gyrus. As mentioned above, area 1 is a projection area from area 3b, and is thus activated a few milliseconds later in time.[50] fMRI, lacking of temporal resolution, is dominated by this more integrative processes in SI and the maximum is rather in area 1 than in area 3b.

An alternative explanation for the difference is the fact that fMRI and SEP measure different phenomena: fMRI is based on secondary metabolic and hemodynamic changes that are coupled to neuronal activity, whereas EEG measures directly the post-synaptic neuronal activity. Thus, fMRI activity follows the topology of the draining veins that might not necessarily exactly overlap with the location of the active neurons measured by SEP.[51,52]

TABLE 3. Distance Comparison Between HD-ESI and fMRI in Healthy Controls[a]

	Left Thumb Pneumatical Stimulation				Right Thumb Pneumatical Stimulation			
	Distance HD-ESI vs fMRI, mm				Distance HD-ESI vs fMRI, mm			
	dx	dy	Dz	Euclidean Distance, mm	dx	dy	Dz	Euclidean Distance, mm
Mean	−16	−4	−4	25	21	−8	−4	28
STD	11	16	9	11	12	15	9	13
P value	**.001**	.202	.338	—	**.001**	.036	.311	—

[a]HD-ESI, high-density electric source imaging; fMRI, functional magnetic resonance imaging; STD, standard deviation; dx, distance in the medial-lateral axis; dy, distance in the anterior-posterior orientation; dz, distance in the superior-inferior orientation.

Several studies directly compared noninvasive functional imaging methods with surgical mapping techniques by using either fMRI, MEG/EEG, or both.[1,25,46,52,53] Results were relatively heterogeneous, showing either a slight advantage of fMRI over MEG[1] or vice versa.[54] In the current study of 6 patients with subdural electrodes overlying the sensory cortex, we found similar differences of HD-ESI and fMRI compared with DCES results (13 mm), indicating that both techniques provide similar yield.

Although the distances between the localization methods were similar to those reported in other studies, they are still rather large from a neurosurgical point of view. Although the systematic difference in the medial-lateral axis of the ESI compared with the DCES can be explained, the discrepancies in the other axis as well as the difference of the fMRI maximum to the DCES are not fully understood. It is evident that the methods evaluated here (including the DCES) can only direct the neurosurgeons toward certain anatomical structures and to presumably functionally relevant regions. During surgery of tumors, or during epilepsy surgical procedures in and around eloquent brain regions, intraoperative neuromonitoring and/or mapping still need to be applied.

CONCLUSION

We showed that SEP source localization based on HD-ESI reveals accurate localization in the individual patient/subject. The differences with fMRI were similar to those reported by Kober et al[35] when comparing MEG with fMRI. Several studies have demonstrated similar localization accuracy of EEG and MEG provided that the same numbers of sensors are used.[55-58] EEG systems allowing fast application of >200 electrodes and providing standard EEG localization software are now available.[43,59] Thus, HD-ESI is a reasonable alternative to fMRI or MEG for the delineation of the sensory-motor cortex as part of presurgical planning, particularly in patients with limited cooperation.

Disclosures

The authors have no actual or potential conflicts of interest to report. The authors wish to indicate that they benefitted from equipment that the employing institution purchased with a financial concession. This work was supported by the Swiss National Science Foundation (grant 320030-122073 to K.S., grant 33CM30-140332 to M.S. and C.M.M.). Cartool software (http://sites.google.com/site/fbmlab/cartool) is developed by Denis Brunet, from the Functional Brain Mapping Laboratory, and supported by the Center for Biomedical Imaging (CIBM), Geneva and Lausanne, Switzerland.

REFERENCES

1. Towle VL, Khorasani L, Uftring S, et al. Noninvasive identification of human central sulcus: a comparison of gyral morphology, functional MRI, dipole localization, and direct cortical mapping. *Neuroimage*. 2003;19(3):684-697.
2. Vitikainen AM, Lioumis P, Paetau R, et al. Combined use of non-invasive techniques for improved functional localization for a selected group of epilepsy surgery candidates. *Neuroimage*. 2009;45(2):342-348.
3. Duffau H, Capelle L, Denvil D, et al. Usefulness of intraoperative electrical subcortical mapping during surgery for low-grade gliomas located within eloquent brain regions: functional results in a consecutive series of 103 patients. *J Neurosurg*. 2003;98(4):764-778.
4. Kido DK, LeMay M, Levinson AW, Benson WE. Computed tomographic localization of the precentral gyrus. *Radiology*. 1980;135(2):373-377.
5. Naidich TP, Valavanis AG, Kubik S. Anatomic relationships along the low-middle convexity: part I—normal specimens and magnetic resonance imaging. *Neurosurgery*. 1995;36(3):517-532.
6. Yousry TA, Schmid UD, Alkadhi H, et al. Localization of the motor hand area to a knob on the precentral gyrus. A new landmark. *Brain*. 1997;120(pt 1):141-157.
7. Orrison WW Jr, Rose DF, Hart BL, et al. Noninvasive preoperative cortical localization by magnetic source imaging. *AJNR Am J Neuroradiol*. 1992;13(4):1124-1128.
8. Miller KJ, denNijs M, Shenoy P, Miller JW, Rao RP, Ojemann JG. Real-time functional brain mapping using electrocorticography. *Neuroimage*. 2007;37(2):504-507.
9. Motamedi GK, Okunola O, Kalhorn CG, et al. Afterdischarges during cortical stimulation at different frequencies and intensities. *Epilepsy Res*. 2007;77(1):65-69.
10. Hamer HM, Morris HH, Mascha EJ, et al. Complications of invasive video-EEG monitoring with subdural grid electrodes. *Neurology*. 2002;58(1):97-103.
11. Maldjian JA, Gottschalk A, Patel RS, Pincus D, Detre JA, Alsop DC. Mapping of secondary somatosensory cortex activation induced by vibrational stimulation: an fMRI study. *Brain Res*. 1999;824(2):291-295.
12. Stippich C, Hofmann R, Kapfer D, et al. Somatotopic mapping of the human primary somatosensory cortex by fully automated tactile stimulation using functional magnetic resonance imaging. *Neurosci Lett*. 1999;277(1):25-28.
13. Hammeke TA, Yetkin FZ, Mueller WM, et al. Functional magnetic resonance imaging of somatosensory stimulation. *Neurosurgery*. 1994;35(4):677-681.
14. Schweizer R, Voit D, Frahm J. Finger representations in human primary somatosensory cortex as revealed by high-resolution functional MRI of tactile stimulation. *Neuroimage*. 2008;42(1):28-35.
15. Francis ST, Kelly EF, Bowtell R, Dunseath WJ, Folger SE, McGlone F. fMRI of the responses to vibratory stimulation of digit tips. *Neuroimage*. 2000;11(3):188-202.
16. Gelnar PA, Krauss BR, Szeverenyi NM, Apkarian AV. Fingertip representation in the human somatosensory cortex: an fMRI study. *Neuroimage*. 1998;7(4 pt 1):261-283.
17. Holodny AI, Schulder M, Liu WC, Maldjian JA, Kalnin AJ. Decreased BOLD functional MR activation of the motor and sensory cortices adjacent to a glioblastoma multiforme: implications for image-guided neurosurgery. *AJNR Am J Neuroradiol*. 1999;20(4):609-612.
18. Jiang Z, Krainik A, David O, et al. Impaired fMRI activation in patients with primary brain tumors. *Neuroimage*. 2010;52(2):538-548.
19. Murata Y, Sakatani K, Katayama Y, Fukaya C. Increase in focal concentration of deoxyhaemoglobin during neuronal activity in cerebral ischaemic patients. *J Neurol Neurosurg Psychiatry*. 2002;73(2):182-184.
20. Hari R, Karhu J, Hämäläinen M, et al. Functional organization of the human first and second somatosensory cortices: a neuromagnetic study. *Eur J Neurosci*. 1993;5(6):724-734.
21. Jousmäki V, Hari R. Somatosensory evoked fields to large-area vibrotactile stimuli. *Clin Neurophysiol*. 1999;110(5):905-909.
22. Baumgartner C, Doppelbauer A, Sutherling WW, et al. Somatotopy of human hand somatosensory cortex as studied in scalp EEG. *Electroencephalogr Clin Neurophysiol*. 1993;88(4):271-279.
23. Buchner H, Adams L, Muller A, et al. Somatotopy of human hand somatosensory cortex revealed by dipole source analysis of early somatosensory evoked potentials and 3D-NMR tomography. *Electroencephalogr Clin Neurophysiol*. 1995;96(2):121-134.
24. Ganslandt O, Ulbricht D, Kober H, Vieth J, Strauss C, Fahlbusch R. SEF-MEG localization of somatosensory cortex as a method for presurgical assessment of functional brain area. *Electroencephalogr Clin Neurophysiol Suppl*. 1996;46:209-213.
25. Bast T, Wright T, Boor R, et al. Combined EEG and MEG analysis of early somatosensory evoked activity in children and adolescents with focal epilepsies. *Clin Neurophysiol*. 2007;118(8):1721-1735.
26. Schaefer M, Mühlnickel W, Grüsser SM, Flor H. Reliability and validity of neuroelectric source imaging in primary somatosensory cortex of human upper limb amputees. *Brain Topogr*. 2002;15(2):95-106.
27. Ding L, He B. Sparse source imaging in electroencephalography with accurate field modeling. *Hum Brain Mapp*. 2008;29(9):1053-1067.
28. Finke S, Gulrajani RM, Gotman J, Savard P. Conventional and reciprocal approaches to the inverse dipole localization problem for N(20)-P (20) somatosensory evoked potentials. *Brain Topogr*. 2013;26(1):24-34.

29. Kristeva-Feige R, Grimm C, Huppertz HJ, et al. Reproducibility and validity of electric source localisation with high-resolution electroencephalography. *Electroencephalogr Clin Neurophysiol.* 1997;103(6):652-660.
30. Grimm C, Schreiber A, Kristeva-Feige R, Mergner T, Hennig J, Lücking CH. A comparison between electric source localisation and fMRI during somatosensory stimulation. *Electroencephalogr Clin Neurophysiol.* 1998;106(1):22-29.
31. Wienbruch C, Candia V, Svensson J, Kleiser R, Kollias SS. A portable and low-cost fMRI compatible pneumatic system for the investigation of the somatosensensory system in clinical and research environments. *Neurosci Lett.* 2006;398(3):183-188.
32. Tucker DM. Spatial sampling of head electrical fields: the geodesic sensor net. *Electroencephalogr Clin Neurophysiol.* 1993;873:154-163.
33. Perrin F, Pernier J, Bertrand O, Giard MH, Echallier JF. Mapping of scalp potentials by surface spline interpolation. *Electroencephalogr Clin Neurophysiol.* 1987;66(1):75-81.
34. Mertens M, Lütkenhöner B. Efficient neuromagnetic determination of landmarks in the somatosensory cortex. *Clin Neurophysiol.* 2000;111(8):1478-1487.
35. Kober H, Nimsky C, Moller M, Hastreiter P, Fahlbusch R, Ganslandt O. Correlation of sensorimotor activation with functional magnetic resonance imaging and magnetoencephalography in presurgical functional imaging: a spatial analysis. *Neuroimage*. 2001;14(5):1214-1228.
36. Lehmann D, Skrandies W. Reference-free identification of components of checkerboard-evoked multichannel potential fields. *Electroencephalogr Clin Neurophysiol.* 1980;48(6):609-621.
37. Grave de Peralta Menendez R, Gonzalez Andino S, Lantz G, Michel CM, Landis T. Noninvasive localization of electromagnetic epileptic activity. I. Method descriptions and simulations. *Brain Topogr.* 2001;14(2):131-137.
38. Grave de Peralta RaGAS. Comparison of algorithms for the localization of focal sources: evaluation with simulated data and analysis of experimental data. *Int J Bioelectromagnetism.* 2002;4(1). http://www.electrical-neuroimaging.ch/publications/ijbem_focal.pdf.
39. Michel CM, Murray MM, Lantz G, Gonzalez S, Spinelli L, Grave de Peralta R. EEG source imaging. *Clin Neurophysiol.* 2004;115(10):2195-2222.
40. Hansen C. Analysis of discrete Ill-posed problems by means of the L-curve. *SIAM Rev.* 1992;34:561-580.
41. Brodbeck V, Spinelli L, Lascano AM, et al. Electroencephalographic source imaging: a prospective study of 152 operated epileptic patients. *Brain*. 2011;134(pt 10):2887-2897.
42. Spinelli L, Andino SG, Lantz G, Seeck M, Michel CM. Electromagnetic inverse solutions in anatomically constrained spherical head models. *Brain Topogr.* 2000;13(2):115-125.
43. Brunet D, Murray MM, Michel CM. Spatiotemporal analysis of multichannel EEG: CARTOOL. *Comput Intell Neurosci.* 2011;2011:813870.
44. Brodbeck V, Lascano AM, Spinelli L, Seeck M, Michel CM. Accuracy of EEG source imaging of epileptic spikes in patients with large brain lesions. *Clin Neurophysiol.* 2009;120(4):679-685.
45. Guggisberg AG, Dalal SS, Zumer JM, et al. Localization of cortico-peripheral coherence with electroencephalography. *Neuroimage*. 2011;57(4):1348-1357.
46. Ashburner J, Friston K. Multimodal image coregistration and partitioning—a unified framework. *Neuroimage*. 1997;6(3):209-217.
47. Kiebel SJ, Poline JB, Friston KJ, Holmes AP, Worsley KJ. Robust smoothness estimation in statistical parametric maps using standardized residuals from the general linear model. *Neuroimage*. 1999;10(6):756-766.
48. Christmann C, Ruf M, Braus DF, Flor H. Simultaneous electroencephalography and functional magnetic resonance imaging of primary and secondary somatosensory cortex in humans after electrical stimulation. *Neurosci Lett.* 2002;333(1):69-73.
49. Singh KD, Holliday IE, Furlong PL, Harding GF. Evaluation of MRI-MEG/EEG co-registration strategies using Monte Carlo simulation. *Electroencephalogr Clin Neurophysiol.* 1997;102(2):81-85.
50. Allison T, McCarthy G, Wood CC, Darcey TM, Spencer DD, Williamson PD. Human cortical potentials evoked by stimulation of the median nerve. I. Cytoarchitectonic areas generating short-latency activity. *J Neurophysiol.* 1989;62(3):694-710.
51. Ogawa S, Menon RS, Tank DW, et al. Functional brain mapping by blood oxygenation level-dependent contrast magnetic resonance imaging. A comparison of signal characteristics with a biophysical model. *Biophys J.* 1993;64(3):803-812.
52. Turner R. How much cortex can a vein drain? Downstream dilution of activation-related cerebral blood oxygenation changes. *Neuroimage*. 2002;16(4):1062-1067.
53. Histed MH, Bonin V, Reid RC. Direct activation of sparse, distributed populations of cortical neurons by electrical microstimulation. *Neuron*. 2009;63(4):508-522.
54. Korvenoja A, Kirveskari E, Aronen HJ, et al. Sensorimotor cortex localization: comparison of magnetoencephalography, functional MR imaging, and intraoperative cortical mapping. *Radiology*. 2006;241(1):213-222.
55. Cohen D, Cuffin BN. EEG versus MEG localization accuracy: theory and experiment. *Brain Topogr*. 1991;4(2):95-103.
56. Liu AK, Dale AM, Belliveau JW. Monte Carlo simulation studies of EEG and MEG localization accuracy. *Hum Brain Mapp.* 2002;16(1):47-62.
57. Malmivuo J, Suihko V, Eskola H. Sensitivity distributions of EEG and MEG measurements. *IEEE Trans Bio-med Eng.* 1997;44(3):196-208.
58. Malmivuo J. Comparison of the properties of EEG and MEG in detecting the electric activity of the brain. *Brain Topogr.* 2012;25(1):1-19.
59. Baillet S, Friston K, Oostenveld R. Academic software applications for electromagnetic brain mapping using MEG and EEG. *Comput Intell Neurosci.* 2011;2011:972050.

Acknowledgments

We thank V. Candia and C. Wienbruch for the installation of the mechanical stimulation device.

CME Questions:

1. In localizing the central sulcus, in what orientation is the maximum discrepancy between SEP (somatosensory evoked potential) source imaging and fMRI (functional MRI)?
   A. Anterior-posterior
   B. Medial-lateral
   C. Superficial-deep
   D. Superior-inferior

2. What type of lesion does not affect accuracy of fMRI in localizing the motor cortex?
   A. Large brain tumor with surrounding edema
   B. Ischemic stroke
   C. Vascular tumor
   D. Small and calcified meningiomas

3. In a brain tumor patient who has a ferromagnetic cardiac pacemaker, which non-invasive technique is indicated for precentral gyrus localization?
   A. Functional MRI
   B. Magnetoencephalography
   C. High density somatosensory evoked potential mapping (SEP)
   D. 64-slice CT

Study IV

Lascano AM, Hummel T, Lacroix JS, Landis B, Michel CM. Spatio-temporal dynamics of olfactory processing in the human brain : an event-related source imaging study. Neuroscience 2010; 167: 700-708. Doi: 10.1016/j.neuroscience.2010.02.013

- Impact Factor: 3.244
- 5-year Impact Factor: 3.504
- Average citations per year: 3.0
- Sum of times cited (without self-citations): 33
- Copyright clearance: Permission is not required

Neuroscience 167 (2010) 700–708

SPATIO–TEMPORAL DYNAMICS OF OLFACTORY PROCESSING IN THE HUMAN BRAIN: AN EVENT-RELATED SOURCE IMAGING STUDY

A. M. LASCANO,[a] T. HUMMEL,[b] J.-S. LACROIX,[c] B. N. LANDIS[b,c] AND C. M. MICHEL[a]*

[a]*Functional Brain Mapping Laboratory, Neurology Clinic, University Hospital and Department of Fundamental Neurosciences, University of Geneva Medical School, 1211 Geneva, Switzerland*

[b]*Smell and Taste Clinic, Department of Otolaryngology, University of Dresden Medical School, 01307 Dresden, Germany*

[c]*Department of Otolaryngology, University of Geneva Medical School and Geneva University Hospitals, 1211 Geneva, Switzerland*

Abstract—Although brain structures involved in central nervous olfactory processing in humans have been well identified with functional neuroimaging, little is known about the temporal sequence of their activation. We recorded olfactory event-related potentials (ERP) to H_2S stimuli presented to the left and right nostril in 12 healthy subjects. Topographic and source analysis identified four distinct processing steps between 200 and 1000 ms. Activation started ipsilateral to the stimulated nostril in the mesial and lateral temporal cortex (amygdala, parahippocampal gyrus, superior temporal gyrus, insula). Subsequently, the corresponding structures on the contralateral side became involved, followed by frontal structures at the end of the activation period. Thus, based on EEG-related data, current results suggest that olfactory information in humans is processed first ipsilaterally to the stimulated nostril and then activates the major relays in olfactory information processing in both hemispheres. Most importantly, the currently described techniques allow the investigation of the spatial processing of olfactory information at a high temporal resolution.

Key words: event related potentials, source imaging, olfaction, mesial temporal lobe.

Olfactory perception starts at the level of the olfactory epithelium in the roof of the nasal cavity. Olfactory receptor neurons (ORN) are embedded within the respiratory epithelium and send their axons through the cribriform plate towards the olfactory bulbs (OB). ORN carry olfactory receptors which are key to olfactory information processing (Axel, 1995; Holley et al., 1974). In the OB, axons from ORNs synapse with the mitral cells. Specifically, all ORN carrying the same olfactory receptor converge in the same site within the bulb, called “glomerulus.” Axons from the mitral cells follow the olfactory tract and divide into two bundles. Most fibers directly project to the piriform and entorhinal cortices as well as to the amygdalae, whereas a minority of fibers projects through the thalamus towards the orbito–frontal cortex (OFC) (Gottfried, 2006).

Compared to other sensory modalities the olfactory system has some particularities. First, the majority of the olfactory fibers do not cross but project ipsilaterally into the brain. Second, most olfactory fibers bypass the thalamus and project very early and directly to the piriform cortex, amygdalae and entorhinal cortex which are implicated in emotional and memory processing. This difference in central anatomy has been claimed to be partly responsible for the emotional load that olfactory stimuli are able to evoke (Herz, 2000). Olfaction is not the only chemical sense; the task of decoding our chemical environment is achieved by olfaction, taste and the intranasal and the intraoral trigeminal fibers. These three anatomically distinct sensory systems are rarely excited in an isolated way; in everyday life co-activation often take place. Consequently, at a central nervous level, the information of olfactory, gustatory, tactile or visual afferences converges at the level of the OFC, which is believed to play an important role in forming an odor percept (Rolls, 2008; Rolls and Baylis, 1994; Rolls and Grabenhorst, 2008). All these anatomical structures, including the OB, appear to be connected within a complex network (Haberly, 1998), providing the basis for odor-related changes in behavior. “Top-down” modulation of activation at the various levels of processing is also considered possible through this highly integrated network (Carmichael and Price, 1994). Fig. 1 provides a sketch on a current model about olfactory processing (Gottfried, 2006).

While this suggests that olfactory processing is known in great detail, there are numerous examples indicating that many aspects of human olfactory function are currently unclear. For example, projections between the anterior olfactory nuclei via the anterior commissure have not been documented in humans. In addition, human olfactory tubercles are difficult to find. Furthermore, connections between the OB and structures like the indusium griseum or the nucleus of the horizontal diagonal band have not been found in humans, other than in animals (Carmichael and Price, 1994; Shipley and Geinisman, 1984).

During the last years, functional imaging techniques based on either functional magnetic resonance imaging (fMRI) or positron emission tomography (PET), have significantly contributed to enlarge the anatomical understanding of olfactory processing in humans. For example, individual olfactory functions have been attributed to certain brain structures. Royet et al. (Royet et al., 2001) showed that right OFC is more strongly activated when

*Corresponding author. Tel: +41-22-379-54-57.
E-mail address: christoph.michel@unige.ch (C. M. Michel).
Abbreviations: ERP, event-related potentials; fMRI, functional magnetic resonance imaging; MEG/EEG, magneto- and electro-encephalography; OB, olfactory bulbs; OFC, orbito–frontal cortex; ORN, olfactory receptor neurons; PET, positron emission tomography.

0306-4522/10 $ - see front matter
doi:10.1016/j.neuroscience.2010.02.013

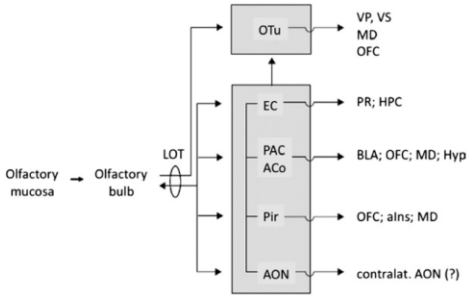

Fig. 1. Schematic diagram of the major olfactory pathways. Regions in gray together represent the primary olfactory cortex. Projections between the olfactory bulb and most areas of the primary olfactory cortex are bidirectional, with the exception of the olfactory tubercle (OTu). Similarly, associational connections between the primary olfactory cortex subregions are reciprocal, apart from OTu. The downstream targets of the primary olfactory cortex represent some of the major projection sites (bottom of Figure), many of which provide feedback to the primary olfactory cortex (not shown), but these connections are not meant to be comprehensive or all-inclusive. While broadly illustrative of the human olfactory system, this diagram is largely based on information obtained from animal models, due to the scarcity of human data. Aco, Anterior cortical nucleus of the amygdala; aINS, agranular insula; BLA, basolateral nucleus of the amygdala; EC, entorhinale cortex; HPC, hippocampus; HYP, hypothalamus; MD, mediodorsal thalamus; PAC, periamygdaloid cortex; PIR, piriform cortex; PR, perirhinal cortex; VP, ventral pallidum; VS, ventral striatum. Adapted from (Gottfried, 2006), modified.

subjects were judging odor familiarity than when they were just trying to detect the odor. In contrast, the left OFC shows enhanced activation when subjects were evaluating odor hedonics. Other work (Plailly et al., 2007) indicated that both the left anterior insula and the left frontopolar gyrus are involved in odor discrimination (see also; Jones-Gotman and Zatorre, 1993). Using fMRI effective connectivity analysis, Plailly et al. (Plailly et al., 2008) showed that the connectivity between the mediodorsal thalamus and the OFC was enhanced when subjects attended to an odor as compared to attending to a simultaneously presented tone, indicating the involvement of the thalamus in conscious smell perception.

Although modern imaging techniques provide unique findings based on high spatial resolution, in order to fully understand olfactory processing there is a need for instruments which provide both, good spatial and temporal resolution (Kettenmann et al., 2001; Miyanari et al., 2006). Such techniques are available in terms of magneto- and electro-encephalography (MEG/EEG) but unfortunately they have not yet been used in a larger scale to explore the sense of smell (e.g., Kettenmann et al., 1996) despite of tremendous achievements that have been made in terms of accuracy of source localization (Babiloni et al., 2000, 2001; Grave de Peralta Menendez et al., 2009; He et al., 1996; Michel et al., 2001, 2004; Pascual-Marqui et al., 2009; Salmelin and Baillet, 2009; Baillet et al., 2001). While it was believed that EEG/MEG obtains only information from the surface of the brain, recent studies with source imaging methods based on high resolution recordings suggests that activity generated in the depth of the brain can be recorded and properly localized (Attal et al., 2007; James et al., 2008, 2009; Lantz et al., 2001; Zumsteg et al., 2005). Thus generators of olfactory activity, even if localized far from the scalp surface, might actually be accessible to EEG/MEG source imaging. Aim of the present investigation was to evaluate the ability of event-related potentials (ERP) source imaging to provide information on the spatio- temporal sequence of information processing in the olfactory pathway.

EXPERIMENTAL PROCEDURES

Participants

Twelve normosmic healthy volunteers (six male; six female; median age: 30 years; age range: 22–46 years) were included in this study. All participants were right handed (Edinburgh Handedness Inventory (Oldfield, 1971)) and non-smokers. Prior to participation, subjects provided written informed consent. The study design had been approved by the Ethics Committee of the University Hospital of Geneva (Geneva, Switzerland) in agreement with the Declaration of Helsinki. Exclusion criteria were presence of current (e.g. allergies) or previous (e.g. anosmia) history of smell disorders and use of medication known to affect chemosensory function (e.g. D2-receptor blocking neuroleptic drugs; Kruger et al., 2008).

Stimulation protocol

Experimental setting. Subjects were instructed to carry out a special breathing technique (velopharyngeal closure; Kobal, 1981), which prevented respiratory airflow into the nasal cavity during the recording. Participants were required to keep their eyes closed during the entire session and had their head gently leaned against a headrest. A constant 60–70 dB binaural white noise was delivered during the entire experiment through a set of headphones in order to mask the switching clicks of the stimulator device.

Olfactory stimulation. A relatively selective olfactory stimulant (Hummel et al., 1991; Kobal et al., 1989), hydrogen sulfide (H_2S, odor of rotten eggs), was delivered with the same concentration (4 ppm) using a pseudo-randomized interstimulus interval (23 s±1.7; stimulus duration 200 ms). During a single session a total of 80 stimuli per nostril (Boesveldt et al., 2007) were delivered. Total duration of the session was approximately 60 min. In order to ascertain that subjects would not fall asleep, the continuously displayed EEG was carefully observed for eventual signs of sleep in which case subjects were named. In addition, the stimulation was split into blocks of 40 stimuli with around 5 min brake between blocks. Across blocks, stimulus presentation was alternated between nostrils (monorhinic stimulation) and randomized across subjects. Odor stimuli were applied by means of a computer-controlled air-dilution olfactometer (OM2s, Burghart Instruments, Wedel, Germany), which delivered rectangular-shaped chemical stimuli with a controlled stimulus onset. The odorant was presented within a constant flow of humidified and thermo stabilized air stream (80% relative humidity, total flow 8 L/min, 36.5 °C; Hummel and Kobal, 2001; Kobal, 1981; Kobal and Plattig, 1978) in order to avoid mechanical stimulation of the mucosa. The outlet of the stimulator was placed in the naris with its opening just beyond the nasal valve (2–4 mm from the naris).

EEG acquisition

Olfactory ERPs were recorded from 64 Ag/AgCl sintered FE-electrodes mounted on an electrode cap (Easycap GmbH, Herrsching, Germany) in standard 10–10 position using a portable

EEG system (Brain Products GmbH, Gilching, Germany). The vertex electrode Cz served as common reference. Signals were continuously recorded at a sampling frequency of 1 kHz with hardware band-pass filters set to 0.01–250 Hz. Electrode impedances were kept below 10 kΩ, using a high chloride abrasive electrolyte gel.

Data analysis

The analysis was performed using the free academic software Cartool by Denis Brunet; http://brainmapping.unige.ch/cartool.htm).

EEG Pre-processing. Signals were offline filtered with a bandwidth of 1–30 Hz. EEG was visually inspected and artefact-free epochs ranging from 200 ms pre-stimulus to 1500 ms post-stimulus onset were averaged for each nostril and each subject, separately. A pre-stimulus baseline correction was thereby applied. Individual averaged olfactory ERP responses were obtained for each subject and stimulation condition (right and left nostril). Group-averaged olfactory ERPs were calculated and were down-sampled to 250 Hz for subsequent topographically-based analysis.

Topographic ERP analysis. In order to determine the spatial distribution and the temporal sequence of olfactory processing, the ERP analysis was based on global measures of the scalp electric field and used well-established spatio-temporal analysis methods (Brandeis and Lehmann, 1986; Lehmann and Skrandies, 1984; Michel et al., 1999, 2001, 2004, 2009; Murray et al., 2006, 2009). This analysis consisted in the following steps.

Topographic pattern analysis. In the first step we identified the most dominant scalp potential maps present in the left and right olfactory ERPs on the basis of their topographic distribution over the scalp. To this end, a spatial k-means cluster analysis followed by a cross validation criterion was applied to the group mean data of both stimulation conditions separately (Pascual-Marqui et al., 1995). Cluster maps that correlated more than 90% were merged. Subsequently, a fitting procedure based on the spatial correlation of the cluster maps and the map at each single time point, was applied to determine the time period during which each of these maps were present (Michel et al., 1999). It is well established that ERP scalp topographies do not shift randomly, but remain in a stable configuration for a certain period, supposed to reflect the different processing steps in the ERP. These periods have also been termed functional microstates (Lehmann et al., 2009; Lehmann and Skrandies, 1980; Michel et al., 2009). Since different map topographies forcibly follow from changes in the underlying configuration of intracranial generators (Vaughan, 1982) the identification of distinct map topographies in the ERP allows to better identify the sequential information processing steps than the identification of peaks at certain electrode positions (Michel et al., 2004; Murray et al., 2008).

Distributed source estimations. The second level of analysis consisted on applying a distributed linear inverse solution to the data with the purpose of estimating the intracranial current distribution of the different time segments of the olfactory ERP responses. The source localization method used here is a variation of the minimum norm least-squares inverse called LAURA (Grave de Peralta Menendez et al., 2001; Michel et al., 2004). It incorporates the constraint that the strength of the electric source in the brain falls off with the inverse of the cubic distance by calculating the local autoregressive average with coefficients depending on the distance between solution points. The head model was based on the averaged MRI brain anatomy scans provided by the Montreal Neurological Institute (MNI). This head model was transformed to the best-fitting sphere using the SMAC algorithm described in (Spinelli et al., 2000) and a spherical three-shell forward model was used to calculate the lead field. The three-dimensional solution space was constrained to the gray matter of the cerebral cortex and limbic structures of the segmented MNI brain. 2738 solution points were equidistantly distributed within this solution space. In order to assure symmetrical distribution of the solution points in the two hemispheres, the solution points of the left hemisphere were mirrored along the anterior-posterior axis.

Statistical parametric mapping. After calculating the LAURA inverse solutions for each time point and each subject's ERP, the estimated activities were statistically compared between left and right nostril stimulation by calculating paired *t*-tests ($P<0.05$) for each solution point in time periods of interest (Michel et al., 2004). In addition, mean and standard deviation of source waveforms in regions of interest were calculated and compared between stimulation conditions. Since the solution points were symmetrically distributed in the two hemisphere, the location and strength of ipsi- and contralateral activation of left and right nostril stimulation could be statistically compared by flipping the LAURA solution of one stimulation condition along the anterior-posterior axis.

RESULTS

Epicranial olfactory ERP mapping

Fig. 2 shows the grand-mean OERP response averaged over 12 healthy controls for both left and right nostril stimulation. Fig. 2A reveals the conventional ERP traces of the parietal electrode (Pz) referenced to the mean of the two mastoid electrodes (M1/M2), showing the expected N1 (Peak: 408 and 420 ms for the right and the left stimulation respectively) and P2–P3 components (Peak: 844 and 796 ms for the right and the left stimulation respectively) as described in previous literature (Kobal, 1981; Pause et al., 1996). Fig. 2B exhibits the overlapped ERP traces of all 64 electrodes (in average reference montage).

The microstate cluster analysis applied to the grand mean data identified four different ERP maps during the period of these two components (Fig. 1D). Fitting the component template maps back to the data, attributed the following time windows to each of them: Left stimulation: 300–388 ms (map 1), 388–576 ms (map 2), 576–636 ms (map 3) and 636–860 ms (map 4); Right stimulation: 264–348 ms (map 1), 348–524 ms (map 2), 524–596 ms (map 3) and 596–824 ms (map 4) (Fig. 2C). The global variance that these four maps explained was 88.1% and 85.5% for left and right stimulation respectively. From the average ERP response, no stable segment could be identified before the first 250 ms (Left stimulation: $<$299 ms; Right Stimulation: $<$263 ms) nor after 850 ms post-stimulus onset (Left stimulation: $>$861 ms; Right stimulation: $>$825 ms). Nonetheless, earlier responses could be visually detected in some individual subject's recordings (e.g. at around 160 ms post-stimulus onset).

Source estimation

Based on the above analysis, source estimations were then calculated for each of the segment maps in each stimulation condition. Fig. 3 depicts the results of this analysis. For left and right sided nostril stimulation, the evoked activity started in the ipsilateral hemisphere (map 1). The activation included ipsilateral mesial–temporal and lateral–temporal areas for both stimulation sides. The me-

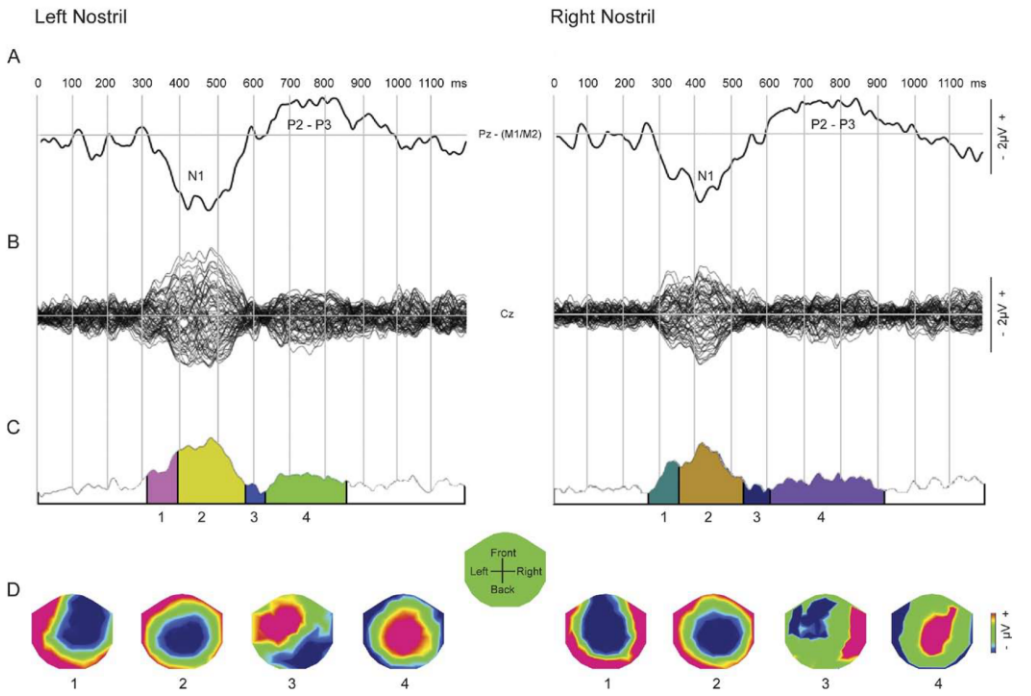

Fig. 2. Olfactory evoked potential mapping in response to right and left nostril stimulation. (A) Conventional analysis technique illustrating a single trace olfactory ERP response at a parietal electrode (Pz–M1/M2). Interval: 0 to 1200 ms post-stimulus. Average of 12 healthy controls. (B) Topographical approach showing butterfly plots (overlaid traces) of all 64 electrodes referenced to the average reference. Interval: 0 to 1200 ms post-stimulus. Average of 12 healthy controls. (C) The temporal extent of the five component maps identified by the cluster analysis as optimally summarizing the grand average map series appears as colored segments under the global field power trace. (D) The topography of the cortically segment maps is color-coded (red, positive voltage; blue, negative voltage). For interpretation of the references to color in this figure legend, the reader is referred to the Web version of this article.

sial–temporal areas incorporated the parahippocampal gyrus and the amygdala. The lateral–temporal areas enclosed the middle and superior–temporal gyrus as well as the inferior insular cortex. These areas were also predominantly activated during the second time period (map 2), but now expanded to append their contralateral counterpart, particularly the contralateral mesial structures. The same pattern was found for map 3, including bilateral mesial and lateral temporal structures. During the last time period (map 4) the middle and inferior frontal gyrus were activated bilaterally in addition to the mesial and lateral temporal areas.

Statistical parametric mapping

The statistical analysis of the inverse solution comparing left versus right nostril stimulation confirmed the initial ipsilateral activation of the temporal lobe. Significant activation differences were found in the solution points mainly including the insular cortex and the superior temporal gyrus (Fig. 4). The differences were found between 280 and 560 ms post-stimulus, corresponding to the first two maps. The source waveforms illustrate this finding: ipsilateral temporal areas are activated earlier and stronger than contralateral areas. The figure also suggests that right nostril stimulation activates contralateral temporal structures more than left sided stimulation. However, the statistical analysis did not confirm this observation: The comparison of the inverse solution of the left sided stimulation with the mirrored inverse solution of the right sided stimulation revealed no significant differences, neither ispi- nor contralaterally.

DISCUSSION

The major finding of this study is that source localization analysis of high-density olfactory ERPs identified a clear temporal succession of central nervous olfactory processing. Olfactory information is first processed in mesial and lateral temporal brain structures *ipsilaterally* to the stimulated nostril, before it reaches contralateral temporal and finally frontal areas.

The olfactory ERP waveforms in the present study stand in line with a large body of literature on chemosensory ERPs and confirm largely the already known and

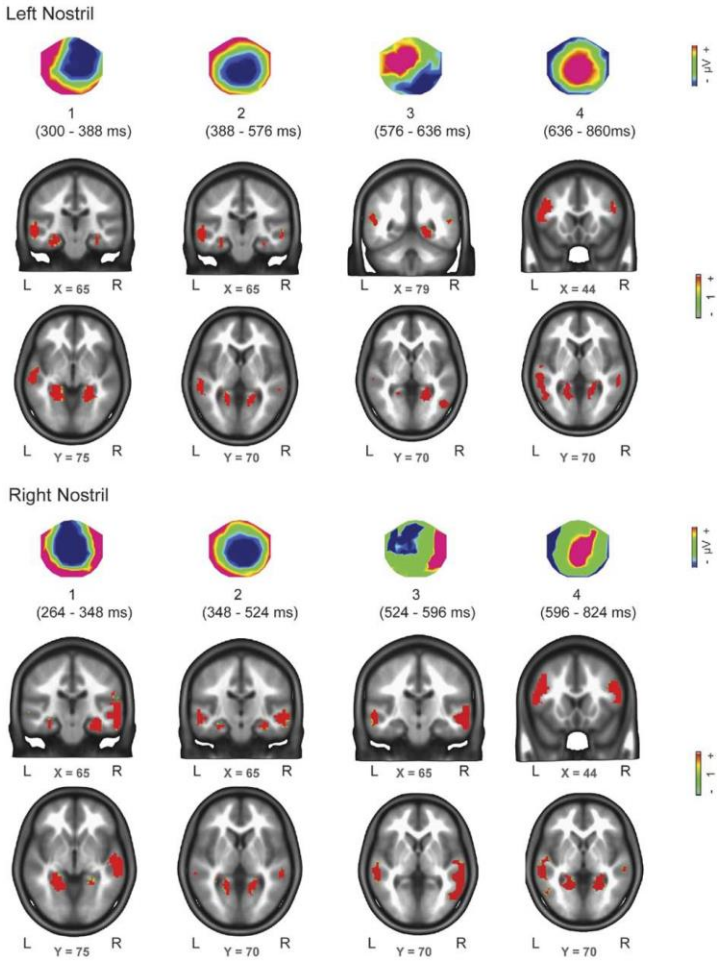

Fig. 3. Electrical source imaging results after olfactory stimulation. Current source distribution for the LAURA inverse solution in the eight maps which were identified by cluster analysis. Source estimations are rendered on the MNI template brain; red regions indicate areas of maximum activation. Note that the 3D activation pattern extended to adjacent slices and that only the slices with maximal activity are depicted here. The Talairach coordinates at the level of the slice is given for the corresponding axis. For interpretation of the references to color in this figure legend, the reader is referred to the Web version of this article.

well-described components of olfactory ERPS with similar amplitudes and latencies (for details see; Hummel and Kobal, 2001; Kobal and Hummel, 1988). However, in contrast to earlier ERP studies with conventional waveform analysis the topographic analysis presented here indicates that at least four prominent distinct processing steps underlie these ERP components. Since different map topographies by definition signify different distributions of neuronal generators in the brain, the four cluster maps that were identified for both stimulation conditions strongly indicate a sequential activation of different brain structures.

The source localization analysis applied to these different cluster maps identified mesial temporal, lateral temporal and frontal structures. Several fMRI and PET studies have previously identified these brain structures for being involved in central nervous olfactory processing (de Araujo et al., 2005; Gottfried and Dolan, 2003; Savic et al., 2001; Small et al., 2005; Sobel et al., 1998; Zatorre et al., 1992). However, in contrast to the other functional imaging techniques, the ERP source imaging method supplied novel information of *when in time* these areas were activated.

The data suggest that olfactory information is first processed ipsilaterally to the stimulated nostril, regardless

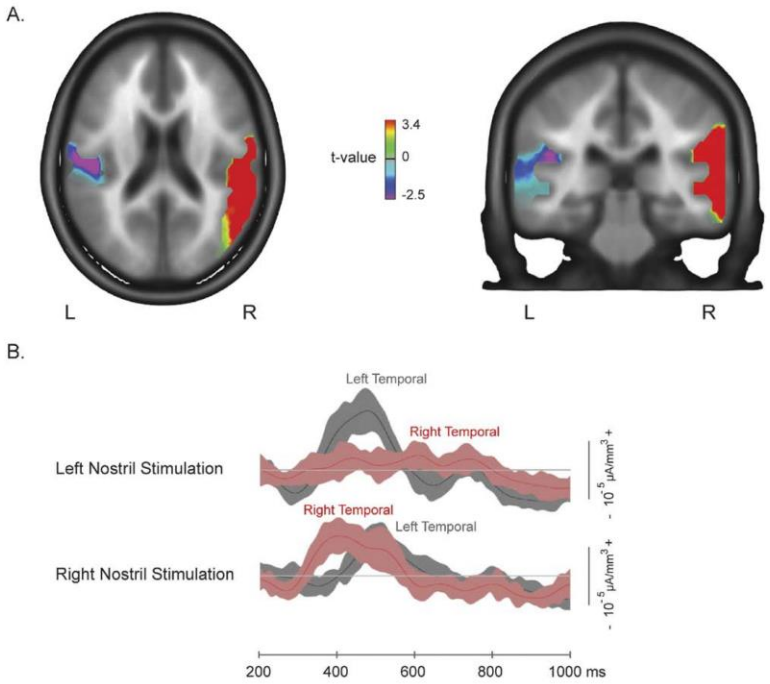

Fig. 4. Comparison between right and left nostril stimulation. (A) Paired *t*-test of right versus left stimulation ($P<0.05$) during the time period corresponding to 280–560 ms post-stimulus onset. Coronal and horizontal plane of the MNI brain show the different areas activated by both stimulation conditions, showing an ipsilateral predominance at the level of the temporal lobe. (B) Source waveforms of right and left temporal brain regions for the two stimulation conditions. For interpretation of the references to color in this figure legend, the reader is referred to the Web version of this article.

whether the stimulus is presented to the left or right nostril, and only later activates areas in both hemispheres. In fact, stages of processing appear to be identical, but mirrored for left- and right-sided stimulation. The ipsilateral structures comprise the amygdala and the parahippocampal gyrus (including the perirhinal and entorhinal cortices), as well as the lateral middle and superior temporal gyrus. Bilateral activations were found during later time periods in mesial and lateral temporal as well as in the middle and inferior frontal gyrus. The statistical analysis in the source space, comparing left versus right nostril stimulation clearly confirms this finding of ipsilateral stimulation onset by identifying significant differences in the temporal lobe, particularly around the insular cortex.

This result clearly extends previous work suggesting that odor information is first processed ipsilaterally to the stimulated nostril. On the other hand, the present results also qualify assumptions made on the basis of work in animals (Cross et al., 2006; McBride and Slotnick, 1997; Uva and de Curtis, 2005) and humans (Porter et al., 2005; Savic and Gulyas, 2000) which indicates that olfactory processing is not strictly ipsilateral to the stimulated nostril. The present study clearly argues for the idea that olfactory information is first processed ipsilaterally to the stimulated side, and then, during later stages of signal processing, both sides would contribute. This is also in line with human work done in patients with temporal lobe epilepsy, which clearly showed isolated ipsilateral olfactory deficits for complex tasks such as discrimination and identification and less for more peripheral dependent tasks such as thresholds (Dade et al., 2002; Hummel et al., 1995; Jones-Gotman et al., 1997; West and Doty, 1995).

The current data also further support findings in other modalities investigated with high resolution EEG source localization, that deep brain generators can be accurately localized (James et al., 2008, 2009). Here, deep mesial–temporal structures such as the amygdala, and the perirhinal and entorhinal cortices, known to be involved in odor perception, could be reliably detected by electric source imaging. Evidently, spatial resolution is limited and cannot reach the details of fMRI. More detailed information of which of these substructures is activated at what time period is hardly possible with EEG source imaging. This also concerns the distinction between the insula and the superior temporal gyrus that together appear as one blurred area in the statistical

analysis (Fig. 4). Nevertheless, in combination with known data from the literature, the areas that were identified here can easily be assigned to the central structures of the olfactory pathway.

Chemosensory ERPs have now widely been accepted to provide an excellent tool for temporal processing of the olfactory stimuli and found their way into clinical routine practice (Hummel and Kobal, 2001; Hummel and Welge-Luessen, 2006) as well as into basic human research areas (Welge-Lussen et al., 2009). In contrast to psychophysical olfactory testing, recordings of olfactory ERP unravel subtle changes of olfactory function that would not be detected by these earlier techniques (Kirchner et al., 2004; Peters et al., 2003). Furthermore, olfactory ERPs do, until now, represent the only objective measuring technique of olfactory function that has proven its clinical value and feasibility in routine patients' workup. The present study shows that by extending the number of electrodes and applying mapping and source imaging methods, ERPs can also provide information about the timing and location of the activated structures, and could thus provide means to determine not only whether, but also when and were olfactory processing might be disturbed in patients.

CONCLUSION

In conclusion, the present research shows that olfactory information can be traced with high temporal and good spatial resolution not only at neocortical sites but also at the level of deep brain structures. This approach opens new avenues for the analysis of olfactory information processing. As a first result the present data indicate that olfactory information is processed mostly ipsilaterally to the stimulated nostril in humans and that the information is not stationary but seems to go back and forth between the major relays in olfactory information processing.

Acknowledgments—This work was supported by a Fund of the Neuroscience Center of the University of Geneva to BNL, JSL and CMM. BNL was supported by a Grant of the Swiss National Fund for Scientific Research (SSMBS grant n° PASMA-119579/1). CMM was supported by the Swiss National Science Foundation (Grant No. 320030-111783. TH was supported by a grant from the Centre National de la Recherche Scientifique (European associated laboratory; EAL 549, CNRS-TUD). The Cartool software (http://brainmapping.unige.ch/Cartool.htm) has been programmed by Denis Brunet, from the Functional Brain Mapping Laboratory, Geneva, Switzerland, and is supported by the Center for Biomedical Imaging (CIBM) of Geneva and Lausanne.

REFERENCES

Attal Y, Bhattacharjee M, Yelnik J, Cottereau B, Lefevre J, Okada Y, Bardinet E, Chupin M, Baillet S (2007) Modeling and detecting deep brain activity with MEG and EEG. Conf Proc IEEE Eng Med Biol Soc 2007:4937–4940.

Axel R (1995) The molecular logic of smell. Sci Am 273:154–159.

Babiloni F, Babiloni C, Locche L, Cincotti F, Rossini PM, Carducci F (2000) High-resolution electro-encephalogram: source estimates of Laplacian-transformed somatosensory-evoked potentials using a realistic subject head model constructed from magnetic resonance images. Med Biol Eng Comput 38:512–519.

Baillet S, Mosher JC, Leahy RM (2001) Electromagnetic brain mapping. IEEE Signal Process Mag 18:14–30.

Boesveldt S, Haehner A, Berendse HW, Hummel T (2007) Signal-to-noise ratio of chemosensory event-related potentials. Clin Neurophysiol 118:690–695.

Brandeis D, Lehmann D (1986) Event-related potentials of the brain and cognitive processes: approaches and applications. Neuropsychologia 24:151–168.

Carmichael ST, Price JL (1994) Architectonic subdivision of the orbital and medial prefrontal cortex in the macaque monkey. J Comp Neurol 346:366–402.

Cross DJ, Flexman JA, Anzai Y, Morrow TJ, Maravilla KR, Minoshima S (2006) In vivo imaging of functional disruption, recovery and alteration in rat olfactory circuitry after lesion. Neuroimage 32:1265–1272.

Dade LA, Zatorre RJ, Jones-Gotman M (2002) Olfactory learning: convergent findings from lesion and brain imaging studies in humans. Brain 125:86–101.

de Araujo IE, Rolls ET, Velazco MI, Margot C, Cayeux I (2005) Cognitive modulation of olfactory processing. Neuron 46:671–679.

Gottfried JA (2006) Smell: central nervous processing. Adv Otorhinolaryngol 63:44–69.

Gottfried JA, Dolan RJ (2003) The nose smells what the eye sees: crossmodal visual facilitation of human olfactory perception. Neuron 39:375–386.

Grave de Peralta Menendez R, Gonzalez Andino S, Lantz G, Michel CM, Landis T (2001) Noninvasive localization of electromagnetic epileptic activity. I. Method descriptions and simulations. Brain Topogr 14:131–137.

Grave de Peralta Menendez R, Murray MM, Thut G, Landis T, Gonzalez Andino SL (2009) Noninvasive estimation of local field potentials: methods and applications. In: Brain signal analysis: advances in neuroelecric and neuromagnetic methods (Handy TC, ed), pp 55–78. London: MIT Press.

Haberly LB (1998) Olfactory cortex. In: The synaptic organization of the brain (Shepherd GM, ed), pp 377–416. New York: Oxford University Press.

He B, Wang Y, Pak S, Ling Y (1996) Cortical source imaging from scalp electroencephalograms. Med Biol Eng Comput 34:257–258.

Herz RS (2000) Scents of time. Sciences 40:34–39.

Holley A, Duchamp A, Revial MF, Juge A, Mac Leod P (1974) Qualitative and quantitative discrimination in the frog olfactory receptors: analysis from electrophysiological data. Ann N Y Acad Sci 237:102–114.

Hummel T, Kobal G (2001) Olfactory event-related potentials. In: Methods and frontiers in chemosensory research (Simon SA, Nicolelis MAL, eds), pp 429–464. Boca Raton, FL: CRC Press.

Hummel T, Pauli E, Schuler P, Kettenmann B, Stefan H, Kobal G (1995) Chemosensory event-related potentials in patients with temporal lobe epilepsy. Epilepsia 36:79–85.

Hummel T, Pietsch H, Kobal G (1991) Kallmann's syndrome and chemosensory evoked potentials. Eur Arch Otorhinolaryngol 248:311–312.

Hummel T, Welge-Luessen A (2006) Assessment of olfactory function. Adv Otorhinolaryngol 63:84–98.

James C, Morand S, Barcellona-Lehmann S, Michel CM, Schnider A (2009) Neural transition from short-to long-term memory and the medial temporal lobe: a human evoked-potential study. Hippocampus 19:371–378.

James CE, Britz J, Vuilleumier P, Hauert CA, Michel CM (2008) Early neuronal responses in right limbic structures mediate harmony incongruity processing in musical experts. Neuroimage 42:1597–1608.

Jones-Gotman M, Zatorre RJ (1993) Odor recognition memory in humans: role of right temporal and orbitofrontal regions. Brain Cogn 22:182–198.

Jones-Gotman M, Zatorre RJ, Cendes F, Olivier A, Andermann F, McMackin D, Staunton H, Siegel AM, Wieser HG (1997) Contribution of medial versus lateral temporal-lobe structures to human odour identification. Brain 120(Pt 10):1845–1856.

Kettenmann B, Hummel T, Kobal G (2001) Functional imaging of olfactory activation in the human brain. In: Methods and frontiers in chemosensory research (Simon SA, Nicolelis MAL, eds), pp 477–506. Baco Raton, FL: CRC Press.

Kettenmann B, Jousmaki V, Portin K, Salmelin R, Kobal G, Hari R (1996) Odorants activate the human superior temporal sulcus. Neurosci Lett 203:143–145.

Kirchner A, Landis BN, Haslbeck M, Stefan H, Renner B, Hummel T (2004) Chemosensory function in patients with vagal nerve stimulators. J Clin Neurophysiol 21:418–425.

Kobal G (1981) Elektrophysiologische Untersuchungen des menschlichen Geruchssinns. Stuttgart: Thieme Verlag.

Kobal G, Hummel C (1988) Cerebral chemosensory evoked potentials elicited by chemical stimulation of the human olfactory and respiratory nasal mucosa. Electroencephalogr Clin Neurophysiol 71:241–250.

Kobal G, Plattig KH (1978) Methodische Anmerkungen zur Gewinnung olfaktorischer EEG-Antworten des wachen Menschen (objektive Olfaktometrie). Z EEG-EMG 9:135–145.

Kobal G, Van Toller S, Hummel T (1989) Is there directional smelling? Experientia 45:130–132.

Kruger S, Haehner A, Thiem C, Hummel T (2008) Neuroleptic-induced parkinsonism is associated with olfactory dysfunction. J Neurol 255:1574–1579.

Lantz G, Grave de Peralta Menendez R, Gonzalez Andino S, Michel CM (2001) Noninvasive localization of electromagnetic epileptic activity. II. Demonstration of sublobar accuracy in patients with simultaneous surface and depth recordings. Brain Topogr 14:139–147.

Lehmann D, Pascual-Marqui R, Michel CM (2009) EEG microstates Scholarpedia 4:7632.

Lehmann D, Skrandies W (1980) Reference-free identification of components of checkerboard-evoked multichannel potential fields. Electroencephalogr Clin Neurophysiol 48:609–621.

Lehmann D, Skrandies W (1984) Spatial analysis of evoked potentials in man—a review. Prog Neurobiol 23:227–250.

McBride SA, Slotnick B (1997) The olfactory thalamocortical system and odor reversal learning examined using an asymmetrical lesion paradigm in rats. Behav Neurosci 111:1273–1284.

Michel CM, Brandeis D, Koenig T (2009) Electrical neuroimaging in the time domain. In: Electrical neuroimaging (Michel CM, Koenig T, Brandeis D, Gianotti LRR, Wackermann J, eds). Cambridge: Cambridge University Press.

Michel CM, Murray MM, Lantz G, Gonzalez S, Spinelli L, Grave de Peralta R (2004) EEG source imaging. Clin Neurophysiol 115: 2195–2222.

Michel CM, Seeck M, Landis T (1999) Spatiotemporal dynamics of human cognition. News Physiol Sci 14:206–214.

Michel CM, Thut G, Morand S, Khateb A, Pegna AJ, Grave de Peralta R, Gonzalez S, Seeck M, Landis T (2001) Electric source imaging of human brain functions. Brain Res Brain Res Rev 36:108–118.

Miyanari A, Kaneoke Y, Ihara A, Watanabe S, Osaki Y, Kubo T, Kato A, Yoshimine T, Sagara Y, Kakigi R (2006) Neuromagnetic changes of brain rhythm evoked by intravenous olfactory stimulation in humans. Brain Topogr 18:189–199.

Murray MM, Brunet D, Michel CM (2008) Topographic ERP analyses: a step-by-step tutorial review. Brain Topogr 20:249–264.

Murray MM, De Lucia M, Brunet D, Michel CM (2009) Principles of topographic analyses for electrical neuroimaging. In: Brain signal analysis: advances in neuroelectric and neuromagnetic methods (Handy TC, ed), pp 21–54. London: The MIT Press.

Murray MM, Imber ML, Javitt DC, Foxe JJ (2006) Boundary completion is automatic and dissociable from shape discrimination. J Neurosci 26:12043–12054.

Oldfield RC (1971) The assessment and analysis of handedness: the Edinburgh inventory. Neuropsychologia 9:97–113.

Pascual-Marqui RD, Michel CM, Lehmann D (1995) Segmentation of brain electrical activity into microstates: model estimation and validation. IEEE Trans Biomed Eng 42:658–665.

Pascual-Marqui RD, Sekihara K, Brandeis D, Michel CM (2009) Imaging the electrical neuronal generators of EEG/MEG. In: Electrical neuroimaging (Michel CM, Koenig T, Brandeis D, Gianotti LRR, Wackermann J, eds). Cambridge: Cambridge University Press.

Pause BM, Sojka B, Krauel K, Ferstl R (1996) The nature of the late positive complex within the olfactory event-related potential (OERP). Psychophysiology 33:376–384.

Peters JM, Hummel T, Kratzsch T, Lotsch J, Skarke C, Frolich L (2003) Olfactory function in mild cognitive impairment and Alzheimer's disease: an investigation using psychophysical and electrophysiological techniques. Am J Psychiatry 160:1995–2002.

Plailly J, Howard JD, Gitelman DR, Gottfried JA (2008) Attention to odor modulates thalamocortical connectivity in the human brain. J Neurosci 28:5257–5267.

Plailly J, Radnovich AJ, Sabri M, Royet JP, Kareken DA (2007) Involvement of the left anterior insula and frontopolar gyrus in odor discrimination. Hum Brain Mapp 28:363–372.

Porter J, Anand T, Johnson B, Khan RM, Sobel N (2005) Brain mechanisms for extracting spatial information from smell. Neuron 47:581–592.

Rolls ET (2008) Functions of the orbitofrontal and pregenual cingulate cortex in taste, olfaction, appetite and emotion. Acta Physiol Hung 95:131–164.

Rolls ET, Baylis LL (1994) Gustatory, olfactory, and visual convergence within the primate orbitofrontal cortex. J Neurosci 14:5437–5452.

Rolls ET, Grabenhorst F (2008) The orbitofrontal cortex and beyond: from affect to decision-making. Prog Neurobiol 86:216–244.

Royet JP, Hudry J, Zald DH, Godinot D, Gregoire MC, Lavenne F, Costes N, Holley A (2001) Functional neuroanatomy of different olfactory judgments. Neuroimage 13:506–519.

Salmelin R, Baillet S (2009) Electromagnetic brain imaging. Hum Brain Mapp 30:1753–1757.

Savic I, Berglund H, Gulyas B, Roland P (2001) Smelling of odorous sex hormone-like compounds causes sex-differentiated hypothalamic activations in humans. Neuron 31:661–668.

Savic I, Gulyas B (2000) PET shows that odors are processed both ipsilaterally and contralaterally to the stimulated nostril. Neuroreport 11:2861–2866.

Shipley MT, Geinisman Y (1984) Anatomical evidence for convergence of olfactory, gustatory, and visceral afferent pathways in mouse cerebral cortex. Brain Res Bull 12:221–226.

Small DM, Gerber JC, Mak YE, Hummel T (2005) Differential neural responses evoked by orthonasal versus retronasal odorant perception in humans. Neuron 47:593–605.

Sobel N, Prabhakaran V, Desmond JE, Glover GH, Goode RL, Sullivan EV, Gabrieli JD (1998) Sniffing and smelling: separate subsystems in the human olfactory cortex. Nature 392:282–286.

Spinelli L, Andino SG, Lantz G, Seeck M, Michel CM (2000) Electromagnetic inverse solutions in anatomically constrained spherical head models. Brain Topogr 13:115–125.

Uva L, de Curtis M (2005) Polysynaptic olfactory pathway to the ipsi- and contralateral entorhinal cortex mediated via the hippocampus. Neuroscience 130:249–258.

Vaughan HGJ (1982) The neural origins of human event-related potentials. Ann N Y Acad Sci 388:125–138.

Welge-Lussen A, Wattendorf E, Schwerdtfeger U, Fuhr P, Bilecen D, Hummel T, Westermann B (2009) Olfactory-induced brain activity in Parkinson's disease relates to the expression of event-related potentials: a functional magnetic resonance imaging study. Neuroscience 162:537–543.

West SE, Doty RL (1995) Influence of epilepsy and temporal lobe resection on olfactory function. Epilepsia 36:531–542.

Zatorre RJ, Jones-Gotman M, Evans AC, Meyer E (1992) Functional localization and lateralization of human olfactory cortex. Nature 360:339–340.

Zumsteg D, Friedman A, Wennberg RA, Wieser HG (2005) Source localization of mesial temporal interictal epileptiform discharges: correlation with intracranial foramen ovale electrode recordings. Clin Neurophysiol 116:2810–2818.

(Accepted 4 February 2010)
(Available online 12 February 2010)

Study V

Lascano AM, Brodbeck V, Lalive P, Chofflon M, Seeck M, Michel CM. Increasing the diagnostic value of evoked potentials in multiple sclerosis by quantitative topographic analysis of multichannel recordings. J Clin Neurophysiol 2009; 26: 316325. Doi: 10.1097/WNP.0b013e3181baac00.

- Impact Factor: 1.673
- Average citations per year: 0.75
- Sum of times cited (without self-citations): 9
- Copyright clearance: The manuscript may only appear in the electronic thesis if password protected

Increasing the Diagnostic Value of Evoked Potentials in Multiple Sclerosis by Quantitative Topographic Analysis of Multichannel Recordings

Agustina M. Lascano,† Verena Brodbeck,*† Patrice H. Lalive,† Michel Chofflon,† Margitta Seeck,† and Christoph M. Michel*†*

Summary: This study presents a method to record and analyze multichannel visual-evoked potential (VEP) and somatosensory-evoked potential (SEP) in an objective, automatic, and quantitative manner. The intention of this study was to assess their diagnostic value in multiple sclerosis (MS). A 256-channel VEP and SEP were recorded in 44 healthy subjects, 26 patients with MS, and 20 patients with other neurologic diseases. Topographic pattern recognition methods were applied and a normative database was established. *Z*-score statistics allowed identifying the number of subjects with significant abnormal values in each group. These values were compared with conventional single-channel waveform analysis. The diagnostic value of the new measures for MS reached a sensitivity of 72% and a specificity of 100% for the VEP, which was significantly higher than the conventional analysis. For the SEP, the specificity was also high (93%) but the sensitivity remained low as in the conventional analysis (30%). The quantitative topographic analysis of multichannel VEP revealed high-diagnostic sensitivity and specificity for MS. Moreover, the method reliably identified the most dominant VEP and SEP components in the healthy subject group. The results indicate that objective topographic analysis of multichannel recordings increase the value of VEP as surrogate marker for MS.

Key Words: Multiple sclerosis, EEG mapping, Visual-evoked potentials, Somatosensory-evoked potentials.

(*J Clin Neurophysiol* 2009;26: 316–325)

The role of evoked potentials (EPs) in the diagnosis of multiple sclerosis (MS) had diminished with the introduction of MRI, because the MRI is more sensitive in the identification of lesions than the EPs (Comi et al., 1993; Leocani and Comi, 2008; Polman et al., 2005). Such notwithstanding, the value of EPs rests in their ability to assess the functioning of the sensory pathway and in the quantification of the clinical dysfunction induced by a given lesion (Comi et al., 1999; Leocani et al., 2000; Restuccia, 2000). This is particularly important in the early stages of the disease where the correlation between MRI parameters and clinical symptoms is low and both the diagnosis and assessment of the prognostic course of MS is difficult (Emerson, 1998; Fuhr and Kappos, 2001; Gronseth and Ashman, 2000; Leocani et al., 2000). EPs can identify clinically silent lesions (Gronseth and Ashman, 2000) and are also able to predict the clinical course of the disease at an early stage (Fuhr and Kappos, 2001; Kallmann et al., 2006; Leocani et al., 2006; Mastaglia, 2006; Pohl et al., 2006; Weinstock-Guttman et al., 2003). Predicting the evolution of the disease at an early stage also helps to better tailor possible treatments and to monitor the effects of those treatments that aim to alter the progression of the disease or to ameliorate function (Emerson, 1998). Thus, any attempt to increase the sensitivity or specificity of EPs could be helpful to accelerate the diagnosis of definite MS and allow early treatment.

EP examinations are considered to have a low specificity and a high ambiguity regarding the interpretation of the recordings. Therefore, the general view is that the clinical indications for EP examinations for MS will not change, despite some promising results regarding the predictive value described earlier (Cruccu et al., 2008; Gronseth and Ashman, 2000; Mastaglia, 2006). However, the currently applied recording and analysis of EPs in clinical practice, as recommended by international federations (Cruccu et al., 2008; Mauguière et al., 1999), is at a great distance from what is nowadays used in modern EP research laboratories. In a standard clinical practice, EPs are measured from a few electrodes; the most dominant component peaks are identified manually and their morphology, latency, and amplitude are quantified (Cruccu et al., 2008). Conversely, research EP laboratories are routinely recording from multiple electrodes and are analyzing the scalp topography of the evoked electric field; often including the estimation of the neuronal sources in the brain that generated the different components (Bast et al., 2007; Desmedt et al., 1987; Kristeva-Feige et al., 1997; Michel et al., 2004*a*, *b*; Morand et al., 2000; Scherg et al., 1989; Spierer et al., 2008). This approach leads to a reference independent and global definition of these components and, thus, reduces the ambiguity in their identification.

This study focuses on the development of objective parameters, which allow to quantify multichannel-evoked potentials and to evaluate their diagnostic value in patients with MS. New automatic pattern recognition methods, which objectively quantify topography, latency, and strength of the different components, are evaluated in a control group, in patients with MS, and patients with other neurologic diseases (OND). The sensitivity and specificity values are also compared with the conventional EP analysis method in the same population.

SUBJECTS AND METHODS

Subjects

Healthy Subjects

A total of 44 healthy volunteers (25 women and 19 men; mean age, 29 years; age range, 18 to 52 years) were enrolled in this

From the *Functional Brain Mapping Laboratory, †Neurology Clinic, Departments of Clinical and Fundamental Neuroscience, University and University Hospital of Geneva, Switzerland.

This work was supported by the Center for Biomedical Imaging (CIBM), Geneva and Lausanne, Switzerland, and the Swiss National Science Foundation (320000-111783 to C.M.M.).

Address correspondence and reprint requests to C.M. Michel, Ph.D., Functional Brain Mapping Laboratory, Neurology Clinic, Departments of Clinical and Fundamental Neuroscience, University and University Hospital of Geneva, Switzerland; e-mail: Christoph.Michel@unige.ch.

ISSN: 0736-0258/09/2605-0316

study in which 41 were right-handed and three were left-handed according to the Edinburgh Handedness Inventory (Oldfield, 1971). All subjects had normal or corrected to normal vision, and none had any previous or current neurologic or psychiatric impairments. Before participation, the healthy subjects provided written informed consent to procedures that had been approved by the Ethics Committee of the University Hospital of Geneva, Switzerland, in agreement with the Declaration of Helsinki.

Twenty nine of the randomly selected subjects (16 women and 13 men; mean age, 30 years; age range, 18 to 52 years) served for the determination of normative values. The other 15 participants (9 women and 6 men; mean age, 27 years; age range, 20 to 45 years) formed the independent group of healthy subjects, meant to be used for comparison with the different clinical groups.

Patients

We studied two different groups of patients who were referred from the Department of Neurology. They were informed about the research nature of the examination and signed a consent form that was approved by the local Ethics Committee. One group of patients suffered from suspected or definitive MS, whereas the other presented OND and served as a clinical control group.

Multiple Sclerosis Group. Twenty-six patients were identified according to the revised McDonald criteria (Polman et al., 2005) (Table 1). Eleven patients had suspected MS, defined as clinically isolated syndrome (CIS) (Kappos et al., 2006), whereas the remaining 15 patients had definite MS with relapsing-remitting course (N = 6), primary progressive course (N = 4), or secondary progressive course (N = 5). At recruitment, a complete neurologic examination was performed and rated according to the expanded disability status scale (Kurtzke, 1983). Disease duration was determined by appropriate clinical history and examination. All patients underwent paraclinical studies: brain ± spinal cord MRI, cerebrospinal fluid analysis (including isoelectric focusing), and other examinations required to rule out an alternative diagnosis (Charil et al., 2006).

Group With OND. Twenty patients presenting diverse neurologic diseases were randomly recruited from the Neurology Unit (Table 2). Ten patients suffered from epilepsy, one patient presented other inflammatory neurologic disease, two patients presented clinical manifestations of peripheral neuropathy, two were diagnosed with an acute lacunar infarct, and five patients presented a combined or pure sensorimotor hemisyndrome of undetermined origin. Suspicion of MS was ruled out at the moment of the examination.

Stimulation Protocol

A standardized protocol for the recording of visual-evoked potential (VEP) and somatosensory-evoked potential (SEP) was developed based on the recommendations provided by the American Clinical Neurophysiology Society (*ACN*, 2006*a*, *b*). Experiments were conducted in a darkened room. During the recording, subjects were seated comfortably with their head against the headrest of the chair.

Somatosensory-Evoked Potentials

Electrical stimulation of the median nerve was administered with an electric square wave pulse (0.1 milliseconds duration) at the wrist. The anode was placed over the median nerve at the wrist, and the cathode was placed 2.5 cm proximal to the anode. A circumferential band ground electrode was placed on the forearm. Stimulus intensity was adjusted within the range of 2 to 8 mA to elicit a consistent but tolerated thumb twitch. According to the recommendations furnished by the American Clinical Neurophysiology Society (2006*a*, *b*), the stimuli were delivered at a repetition rate of 3.7 Hz. A total of 2000 stimuli were applied in two separate blocks on each arm (block duration: 4 minutes 45 seconds).

Visual-Evoked Potentials

Full-field pattern-reversal stimuli were delivered to each eye separately. Black and white checkerboard patterns with 55-inch check size were used (stimulus field, 18.5inch). Pattern reversal frequency was 2.4 Hz. A total of 400 stimuli per eye were applied, partitioned in two blocks (block duration: 1 minute 55 seconds). Monocular stimulation was achieved by covering one eye with a cotton pad fixed with medical tape. The stimuli were presented on a computer monitor (19.6-inch screen, 70-Hz screen refresh rate) placed 120 cm away from the subject. The distance was measured from the center of the screen up to the lateral canthus of the subject's right eye.

EEG Acquisition and Averaging

The EEG was collected from 256 silver chloride-plated carbon-fiber electrodes using a HydroCel Geodesic Sensor Net (Electrical Geodesics, Inc., Eugene, OR). The electrodes were interconnected by thin rubber bands and each contained a small sponge that touched the patient's scalp surface directly (Tucker, 1993). The nets were soaked in saline water before placement. The whole net was applied at once and no skin abrasion was required. The net was adjusted so that Fpz, Cz, Oz, and the preauricular points were correctly placed according to the international 10/10 system. The geodesic tension structure of the net assured that the electrodes were

TABLE 1. Demographic and Clinical Characteristics of the Multiple Sclerosis and Clinically Isolated Syndrome Sample

Clinical Course	CIS	RRMS	SPMS	PPMS	Total
n	11	6	5	4	26
Age (mean ± SD) (yrs)	29.2 ± 7.7	35.2 ± 7.6	52.4 ± 5.7	60.3 ± 17.5	39.8 ± 15.2
Gender (M/F)	3/8	1/5	3/2	3/1	10/16
Dominant hand (R/L)	10/1	6/0	4/1	3/1	23/3
Disease duration (mean ± SD) (yrs)	0.05 ± 0	1.9 ± 2.1	12 ± 4.3	4.6 ± 3.8	3.5 ± 5
EDSS Score (mean ± SD)	1.5 ± 0.8	2.0 ± 1.2	6.2 ± 1.2	4.6 ± 1.9	3.1 ± 2.1
Visual symptoms (P/A)	7/4	3/3	2/3	3/1	15/11
Somatosensory symptoms (P/A)	6/5	2/4	3/2	3/1	14/12
Multisymptomatic presentation (P/A)	7/4	3/3	5/0	4/0	19/7

CIS, clinically isolated syndrome; RRMS, relapsing remitting multiple sclerosis; SPMS, secondary progressive multiple sclerosis; PPMS, primary progressive multiple sclerosis; M/F, male/female; R/L, right/left; EDSS, expanded disability status scale; P/A, present/absent.

TABLE 2. Demographic and Clinical Features of Patients Presenting Other Neurological Diseases

		Other Neurological Disease (n = 20)
Age (mean ± SD) (yrs)	32.7 ± 9.6	
Gender (M/F)	7/13	
Dominant hand (R/L)	17/3	
Disease	**Group**	**Subgroup**
	Epilepsy (n = 10)	Symptomatic, nonlesional* (n = 3)
		Symptomatic, lesional* (n = 7)
	OIND (n = 1)	Inflammatory transverse myelitis (n = 1)
	Peripheral neuropathy (n = 2)	Mononeuropathy (n = 1)
		Polyneuropathy (n = 1)
	Stroke (n = 2)	Acute lacunar stroke‡ (n = 2)
	Undetermined (n = 5)	Pure sensitive syndrome (n = 2)
		Pure motor syndrome (n = 1)
		Combined sensorymotor syndrome (n = 2)

*ILAE classification of epilepsy syndromes.
‡Oxforshire community stroke project classification.
M/F, male/female; R/L, right/left; OIND, other inflammatory neurological disease.

evenly distributed across the head and at approximately the same location across subjects. Electrode-skin impedances were kept below 20 kΩ. EEG was continuously recorded at a sampling rate of 1 kHz and band-pass filtered between 0.1 and 100 Hz. The vertex (Cz) electrode was used as a reference electrode and the data were referenced off-line to the average reference after spherical spline interpolation of any damaged or artifact-contaminated electrodes (Perrin et al., 1989).

Data analysis was carried out using the free academic software Cartool (D. Brunet, Geneva University Hospital and Medical School, Center for Biomedical Imaging, Geneva, Switzerland; http://brainmapping.unige.ch/cartool.htm). Epochs were selected ranging from 50 milliseconds before to 200 milliseconds after electrical somatosensory stimulation and 100 milliseconds before to 400 milliseconds after visual stimulation. These epochs were band-pass filtered according to the type of stimulation (10 Hz high pass for somatosensory stimulation and 1 to 30 Hz for visual stimulation) and prestimulus baseline corrected. Epochs with occulomotor and other artifacts were determined by voltage thresholds and were excluded. The electrodes on the cheek area were kept out in this study and a standard electrode array of 204 channels was used for all subjects.

Topographic EP Analysis

Definition of the EP Components

We relied on an objective technique that defined EP components on the basis of their potential distribution over the scalp (Brandeis and Lehmann, 1986; Lehmann and Skrandies, 1980, 1984; Michel et al., 1999, 2001; Skrandies, 1993). The approach was reference free and did not rely on a few preselected electrodes in predefined time windows. It considered all electrodes and all time points together and searched for the most dominant scalp potential maps that were evoked by the stimuli. The method used a k-means cluster analysis to define the different distinct map topographies (Gianotti et al., 2008; Michel et al., 2004*a*, *b*; Pascual-Marqui et al., 1995), followed by a cross-validation criterion to determine the optimal number of maps (Murray et al., 2008; Pascual-Marqui et al., 1995).

Fitting these maps back to the data revealed the time segments during which each map was best representing the data (Pegna et al., 1997). It has been shown, in numerous studies, that these time segments coincided with the different well-described EP components, i.e., that each EP component is defined by a period with a stable and distinct map topography that merely varies in strength, a so-called functional microstate (for reviews see Brandeis and Lehmann, 1986; Lehmann and Skrandies, 1984; Michel et al., 1999, 2001; Murray et al., 2008).

The cluster analysis was applied to the strength-normalized EPs averaged over the 29 healthy subjects that served for the normative database. This analysis resulted in a limited number of template maps, for each stimulation condition, which were dominating during certain time windows and representing the voltage distribution of the different components. These template maps were considered as prototype maps and were the basis for the subsequent pattern analysis that determined a series of parameters, for each VEP and SEP component, in the normative group and in the different test groups.

Pattern Recognition Procedure

The template map of each component was fitted into each individual EP in the time windows determined from the grand mean data, and the following eight objective parameters were determined to describe strength, topography, and latency of the components:

Strength. (1) Maximum global field power (GFP) of the window; (2) mean GFP of the window; (3) GFP at time point of best spatial correlation between the template map and an individual's data. The GFP is the standard deviation of the average reference potential map and, thus, a measure of global strength of the electric field (Lehmann and Skrandies, 1980). Although the three strength measures are correlated, they differ in their sensitivity to steepness and duration of the component.

Topography. (4) Maximal spatial correlation of the template map within the window; (5) global explained variance of the template map for the whole EP. These two values indicate the goodness of fit of the map and its presence in general.

Latency. (6) Time point of maximum GFP in the window; (7) time point of the centroid (point of gravity) of the GFP in the window; and (8) time point of maximal spatial correlation with the template map. Because latency measures were restricted to the predetermined window, the three latency measures differently weighted strength and topography of the potential along this window.

Conventional Waveform Analysis

To verify that the conventional analysis of our recordings provides comparable results with those described in the literature, single-channel waveform analysis was performed on the same data. Only the most "solid" measures of the cortical EP components were considered (Comi et al., 1999). For the VEP, the electrode corresponding to midoccipital (MO) referenced to midfrontal (MF) was selected and the P100 component was manually marked. For the SEP, the electrode corresponding to C3′ and C4′ referenced to Fz was selected and the N20 component was marked. Normally, for standard clinical SEP recordings, the inclusion of a peripheral and a cervical channel is required to allow, by evaluating the interpeak latencies, detecting spinal or brainstem lesions. Because the 256-electrode net did not include these noncephalic electrodes, we did not include them in the conventional analysis. Consequently, only the cortical SEP component N20 was evaluated. The following conventional EP parameters were defined: (1) latency (absolute latency, interocular or interhemisphere difference), (2) amplitude (absolute amplitude, interocular or interhemisphere ratio), and (3) morphology (presence of component, normality of waveform morphology).

Group Analysis

To replace the disparate physical dimensions of the parameters by the common dimension of probability, all data were transformed to *Z*-standard scores according to the formula $Z = (Y - Y_m)/\sigma$, where Y indicates the individual parameter, Y_m the mean of this parameter over the 29 participants of the norm group, and σ the standard deviation of the norm group. A conservative probability of $P < 0.001$ ($Z > 3.1$) was set to minimize false positives due to the multiple tests.

Then, for each of the four groups (MS, CIS, OND, and healthy subjects), the percentage of subjects with a significant Z value in at least one of the parameters was determined for each of the components. Evidently, only change in one direction was considered as pathologic, i.e., lower strength, lower fit, or longer latencies.

The same analysis was performed with the conventional EP parameters, i.e., the values were Z-transformed and the percentage of subjects per group with at least one significant Z score ($P < 0.001$) was determined.

Sensitivity and Specificity Analysis

The following analysis step consisted in the determination of the sensitivity and specificity of those EP components that were defined in the previous step to best distinguish patients with MS from the other subjects. For these components, the number of subjects with significant deviations form the z-standard scores ($P < 0.001$) for at least one parameter, were determined for the patients with MS/CIS together (N = 24 were evaluated with SEP and N = 25 with VEP) and compared with the clinical control group, i.e., the patients with OND (N = 15 were evaluated with SEP and N = 10 with VEP). The results of left and right stimulation were thereby combined. Two by two tables were established for each component, and sensitivity and specificity values were calculated according to the following formulae:

$$\text{Sensitivity} = a/(a + c)$$

$$\text{Specificity} = d/(b + d)$$

where a is the abnormal Z scores in an MS patient, b the abnormal Z scores in a OND patient, c normal Z scores in an MS patient, and d is the normal Z scores in an OND patient.

These values were calculated for the topographical analysis based on the multichannel recordings and for the conventional analysis based on a single electrode.

RESULTS

Definition of the EP Components

Somatosensory-Evoked Potentials

Figure 1 shows the grand-mean SEP (average of 29 control subjects) for left and right median nerve stimulation. Figure 1A shows the EP traces of the contralateral (to the stimulation) centroparietal electrodes (C3′ and C4′, respectively) referenced to the frontal electrode Fz, i.e., the traces that were used for the conventional trace analysis. They showed the expected sharp N20 component. Figure 1B shows the overlapped traces of all 204 electrodes (butterfly plot), recalculated against the average reference. At least four clearly separable events, indicating different components, can be readily identified in these butterfly plots within the first 70 milliseconds. The k-means cluster analysis of these grand mean data identified these components by four different map topographies. Fitting them to the data attributed the following time windows to each of these components. Left SEP: map 1, 9 to 19 milliseconds; map 2, 19 to 23 milliseconds; map 3, 23 to 36 milliseconds; map 4, 36 to 59 milliseconds; right SEP: map 1, 9 to 19 milliseconds; map 2, 19 to 23 milliseconds; map 3, 23 to 39 milliseconds; map 4, 39 to 63 milliseconds. These different time periods are marked under the GFP trace that is plotted in Fig. 1C. It shows that most periods included only one GFP peak, except of map 3 that included two separate peaks, but they were topographically not distinct enough to be separated by the cluster analysis. The component maps (Fig. 1D) of left and right stimulation were nearly mirror images of each other with respect to the anterior-posterior axis. The second map encompassed the N20 component typically identified in conventional SEP analysis.

Visual-Evoked Potentials

Figure 2 shows the results of the left and right eye VEP of 25 healthy subjects (four of the initial 29 subjects had to be discarded because of the presence of occulomotor artifacts). Figure 2A shows the EP trace of the occipital electrode (MO) referenced to a frontal electrode (MF) that was used for the conventional trace analysis. It shows the typical negative-positive–negative-positive sequence of peaks at around 75, 100, 160, and 240 milliseconds known as N75 (or C1), P100 (or P1), N160 (or N1), and P240. The butterfly plot (Fig. 2B) also clearly displays these four components. The k-means cluster analysis easily revealed four maps for both left and right eye stimulations. Each one includes a distinct GFP peak, as illustrated in Fig. 2C. Note that the first map, which not yet represented a clear component with a dominant peak, showed a frontal maximum lateralized to the side of the stimulated eye. It is most probably generated by activations in the retina and is, thus, not considered in the subsequent analysis. The considered components spanned the following time windows: left VEP—map 1, 38 to 67 milliseconds; map 2, 67 to 89 milliseconds; map 3, 89 to 132 milliseconds; map 4, 132 to 205 milliseconds; map 5, 205 to 301 milliseconds; right VEP—map 1, 38 to 68 milliseconds; map 2, 68 to 89 milliseconds; map 3, 89 to 133 milliseconds; map 4, 133 to 198 milliseconds; map 5, 198 to 320 milliseconds.

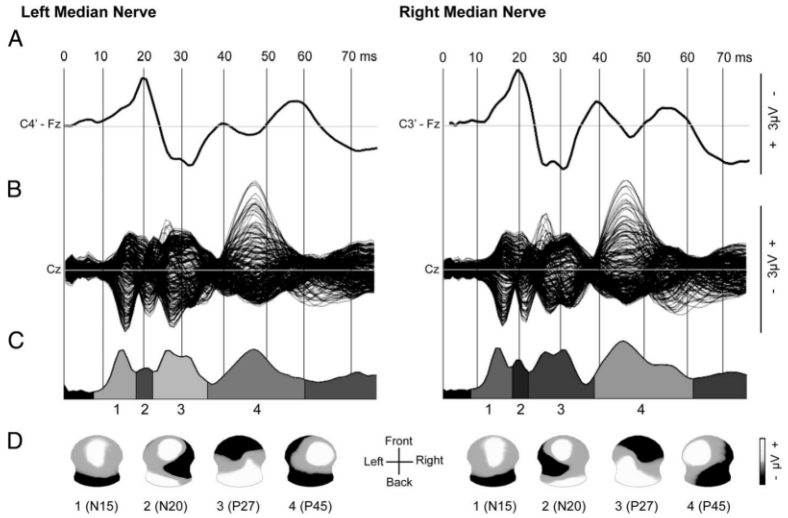

FIGURE 1. Somatosensory-evoked potential (SEP) mapping in response to median nerve stimulation. Average of 29 healthy subjects. **A**, Conventional analysis technique illustrating a single-trace SEP response at a contralateral centroparietal electrode (C3′-Fz and C4′-Fz). Interval: 0 to 70 milliseconds poststimulus. **B**, Topographical approach showing butterfly plots (overlaid traces) of all 204 electrodes referenced to the average reference. Interval: 0 to 70 milliseconds poststimulus. **C**, The temporal extent of the 4 component maps identified by the cluster analysis as optimally summarizing the grand average map series appears as gray-coded segments on the global field power trace. **D**, The topography of the subcortically (map 1) and the cortically originated component maps (map 2 to 4) are plotted (white, positive voltage; black, negative voltage).

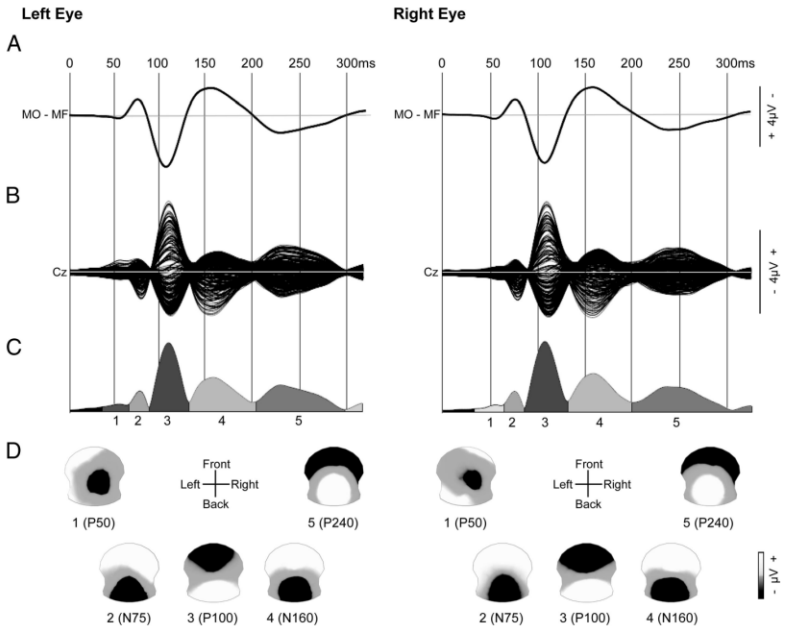

FIGURE 2. Visual-evoked potential (VEP) mapping after right and left eye stimulation using full-field pattern-reversal checkerboard. Average of 25 healthy subjects. **A**, Conventional method showing an individual trace of the averaged VEP response at an MO electrode (MO-MF). Time interval: 0 to 300 milliseconds poststimulus. **B**, Topographical technique illustrating superimposed grand average waveforms (204 electrodes). Time interval: 0 to 300 milliseconds poststimulus. **C**, Five maps were found by the k-means cluster analysis, representing the different components. The period during which they were present is gray coded under the GFP curve. **D**, The scalp potential maps of these components are plotted (white, positive voltage; black, negative voltage).

Group Analysis

For each component, eight different parameters were defined by fitting the component maps determined by the cluster analysis of the grand mean data to the individual data.

Figure 3 shows the results of the *Z*-score statistics for the different groups. It displays the percentage of subjects in each group who had *z* values that were significantly different from the norm at $P < 0.001$ in at least one of the parameters of the EP component. Left and right stimulations were combined in this analysis. As can be readily seen, the P100 component of the VEP was significantly abnormal in most of the patients with MS (86%). Also 55% of the patients with CIS presented abnormal P100. Conversely, none of the patients with OND or the healthy subjects had abnormal P100 components. With the conventional analysis of the VEP P100 component, only 64% of the patients with definite MS and 45% of the patients with CIS were detected. In addition, 10% of the patients with OND were considered as abnormal (Fig. 3, labeled as P100c). The topographic analysis also revealed relatively high-detection rates for the N160 component with 78% of the patients with MS and 45% with CIS. However, 10% of the OND also showed abnormal N160 components.

Concerning the SEP, the *Z*-score statistics was less convincing. Only the P27 component was abnormal in 43% of the patients with MS and 11% with CIS. For the other components (including the N20), the detection of patients with MS was modest and equal to the number of patients with OND considered abnormal. The conventional analysis of the SEP N20 component seemingly identified more patients with MS and CIS than the topographical analysis of this component (36% and 22%). However, it even considered 40% patients with OND as abnormal, thus showing very low specificity (Fig. 3, labeled N20c).

In the light of the VEP findings, we focused on the characteristics of those patients with MS who were detected as abnormal by using the topographical analysis approach (n = 18). Table 3 details the information of those patients in terms of clinical visual symptoms, MRI visible optic nerve lesions, and results obtained using conventional P100 VEP analysis. On the one hand, all of the patients who presented optic nerve lesions in the MRI (N = 7) belonged to the 18 patients with abnormal topographic VEP, but only five of these seven patients were identified using the conventional method. Furthermore, of these seven patients, one of them did not manifest any visual complaint (i.e., clinically silent lesion); this

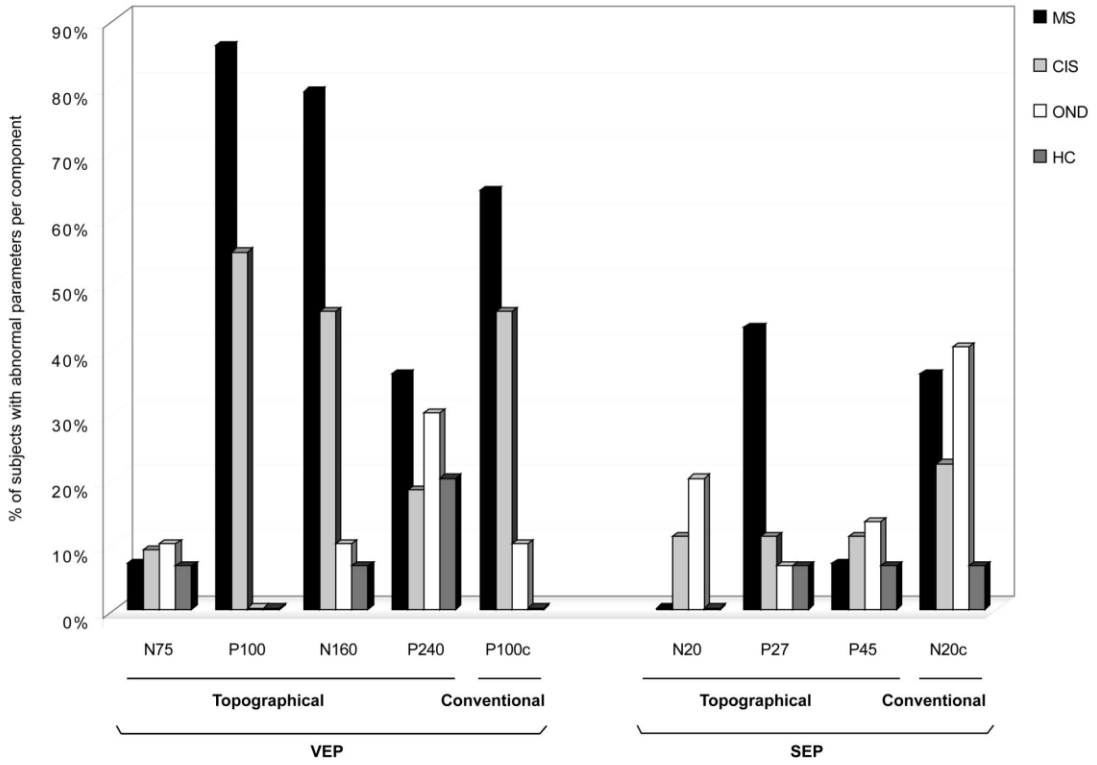

FIGURE 3. Result of the *Z*-score statistics of the individual subjects in each of the four groups. The bar chart indicates the percentage of subjects presenting at least one, of the eight, significantly abnormal parameter in a given component ($P < 0.001$). Results attained from both stimulation conditions (VEP on the left side and SEP on the right side of the bar chart) and both types of analysis (topographical and conventional) are displayed. Among all the components displayed, VEP P100 topographical analysis seems to depict the largest number of patients with MS and CIS and the smallest amount of OND and healthy subjects when compared with the other EP components. MS, multiple sclerosis; CIS, clinically isolated syndrome; OND, other neurologic disease; HC, healthy controls; SEP, somatosensory-evoked potentials; VEP, visual-evoked potentials.

TABLE 3. Clinical Data and MRI Result of the MS Patients Presenting an Abnormal P100 Component as Detected by Topographic VEP Analysis

No. Patient	Sex (M/F)	Age (yrs)	Visual Symptoms	MRI Optic Nerve Lesion	VEP P100 Conventional
CIS					
1	F	26	+	+	+
2	M	32	+	+	+
3	F	33	+	+	+
4	F	22	+	−	+
5	F	23	+	−	−
6	F	34	−	−	−
RRMS					
7	F	29	+	+	+
8	F	39	−	+	−
9	M	30	+	+	−
10	F	49	+	+	+
SPMS					
11	M	45	−	−	+
12	M	50	+	−	+
13	F	56	−	−	−
14	F	51	+	−	+
15	M	60	−	−	+
PPMS					
16	F	72	−	−	+
17	M	74	+	−	+
18	M	36	+	−	+

CIS, clinically isolated syndrome; RRMS, relapsing remitting multiple sclerosis; SPMS, secondary progressive multiple sclerosis; PPMS, primary progressive multiple sclerosis; MRI, magnetic resonance imaging; VEP, visual-evoked potentials; M/F, male/female; +, presence/test positivity; −, absence/test negativity.

particular patient was spotted out using topographical but not conventional analysis. Conversely, six of the 18 patients presented visual symptoms but no MRI optic nerve lesion. All six were detected by the topographic analysis, whereas one was missed by the conventional analysis. Finally, five of the 18 patients detected as presenting an abnormal VEP topography had neither MRI optic nerve lesions nor visual symptoms at the moment of the examination. Three patients of this particular group were also depicted by the conventional analysis.

Sensitivity and Specificity

The sensitivity and specificity of the objective topographical analysis were evaluated by comparing all patients with MS (definite MS and CIS) with those with OND. These values were again compared with the conventional analysis of the VEP P100 and SEP N20 based on one single recording channel. Only the most significant components from the previous analysis were considered for this comparison, i.e., the visual P100 and N160 and the somatosensory P27. The results are given in Table 4. For the visual P100, this analysis revealed a sensitivity of 72% and a specificity of 100%. Fisher's exact test was significant with $P < 0.0001$. The conventional analysis of the VEP revealed clearly lower values with a sensitivity of 56% and a specificity of 90%. Fisher's exact test revealed $P < 0.02$ only. The specificity of the topographic analysis was also high for the N160 component (90%) but the sensitivity was lower (64%). Concerning the SEP, the topographic analysis of the P27 component revealed a relatively low sensitivity of 30% only, but with a high specificity of 93%. The conventional analysis of the SEP N20 component disclosed a comparably low sensitivity (30%), but in addition a lower specificity (60%).

DISCUSSION

This study has been performed with two principle aims. First, the study intended to develop an objective method to determine components of multichannel-evoked potentials on the basis of the spatial configuration of the EP maps and, therefore, quantify latency, strength, and topography of these components. The performance of this method, in terms of identification of dominant EP components and stability of the quantitative parameters, was tested in a normative data set.

Second, we wanted to evaluate the diagnostic value of this new EP recording and analysis method in multiple sclerosis by determining sensitivity and specificity of the objective EP parameters.

Topographic Component Recognition

The k-means cluster analysis of the grand mean data of the healthy subjects revealed four component maps for the SEP and five maps for the VEP. Concerning the SEP, the first component, peaking at 15 milliseconds, showed an occipital negative potential with a very steep gradient, slightly lateralized ipsilateral to the stimulation side. Generators in the dorsal column nuclei of the medial lemniscus system before decussating in the brainstem are most probably underlying this component map, usually labeled as N15 (Cruccu et al., 2008; Desmedt and Cheron, 1980; Moller et al., 1986). However, because of the low sampling rate of our recording system, this component could also reflect the N13 component from midcervical cord. Nevertheless, the result indicates that the electrode array that extends to low positions in the neck is capable of reliably recording the far-field potential. The second component corresponds to the well-known N20 with a parietal negative potential contralateral to the stimulation side. Generators in the primary somatosensory area underlie this component (Allison and Hume, 1981; Allison et al., 1989; Waberski et al., 1999). The two subsequent maps show nearly mirrored configurations for right and left stimulations. Generators of these components are mainly located in the contralateral somatosensory cortex (Allison et al., 1991; Balzamo et al., 2004), but direct

TABLE 4. Analysis of Effectiveness of Diagnostic Criterion

	Topographical Analysis				Conventional Analysis	
	VEP P100	SEP N20	VEP N160	SEP P27	VEP P100	SEP N20
Fisher's exact test two-tailed (*P*)	0.000	0.279	0.007	0.114	0.022	0.728
Sensitivity (%)	72	4	64	30.4	56	30.4
Specificity (%)	100	80	90	93.3	90	60

Results obtained after observed two-way contingency table (multiple sclerosis and patients with clinically isolated syndrome vs. other neurological disease) while applying topographical- and conventional-evoked potential analysis.

VEP, visual-evoked potentials; SEP, somatosensory-evoked potentials.

thalamic projections to precentral areas as well as pre- and postcentral cortical connections lead to widespread simultaneous activation of primary and secondary sensorimotor areas (Rossini et al., 1996).

Concerning the VEP, the first map, appearing in the time window between 38 and 68 milliseconds, showed a frontal positivity lateralized to the side of the stimulated eye. It most probably corresponds to the P50 component of the pattern electroretinogram that is assumed to be generated by ganglion cell activation in the retina (Holder et al., 2007). Again, the extended electrode array that included several electrodes close to the eye permits a reliable recording of this noncortical activity. The subsequent components are well described in the literature and correspond to activities in the primary and secondary visual cortex (Jeffreys and Axford, 1972; Di Russo et al., 2002).

Group Analysis

The second analysis step consisted in a pattern recognition procedure that determined when and to which degree these typical component maps were present in the EPs of the individual patients within the given time windows. It is important to note that this procedure relies on pattern recognition and template matching rather than on morphology and latency characterization of peaks at certain electrodes.

We determined the percentage of abnormal subjects in each of the four patient groups for each component with the aim to identify those components that best discriminated patients with suspected and definite MS from the two control groups. This was clearly the case for the visual P100 component of the VEP. It was abnormal in most of the patients with MS and more than half of the patients with CIS, but in none of the patients with OND and healthy subjects. Also, the visual N160 component was relatively sensitive, but here 10% of the patients with OND were also considered as abnormal, reducing its specificity. For the SEP, the results were less striking. The P27 component identified 43% of the patients with MS, but only 11% of the patients with CIS. The other components were abnormal in a few cases only.

Sensitivity and Specificity for Diagnosis of MS

In the last analysis step, we calculated the sensitivity and specificity of these components by comparing the MS/CIS group with the group of patients with OND and compared the topographical analysis with the conventional analysis of latency and amplitude of the P100 component for the VEP and the N20 component for the SEP. This analysis revealed a superiority of the topographical analysis of the VEP when compared with the conventional analysis. The topographical analysis achieved a sensitivity of 72% and a specificity of 100%, whereas the conventional analysis had a sensitivity of 56% and a specificity of 90%. These specificity and sensitivity values of the conventional analysis correspond to the values described in the literature (Gronseth and Ashman, 2000; Leocani and Comi, 2000). Recent studies indicated some increase in sensitivity when multimodal EPs are used (Fuhr et al., 2001; Kallmann et al., 2006) but with the expense of specificity. In our patient cohort, the SEP examination did not increase the sensitivity of the topographic VEP analysis any further. Interestingly, in the conventional analysis, the sum of both VEP and SEP examinations managed to identify two more patients with MS; thus confirming the increase in sensitivity, but specificity values decreased tremendously. Still, the conventional analysis of VEP and SEP together identified fewer patients than the topographic analysis of the VEP P100 alone.

In general, the SEP examinations showed low sensitivity for both the topographic and the conventional analysis. This result is in line with previous MS studies (Friedli and Fuhr, 1990). Several reasons might account for this finding; on the one hand, SEP examinations usually include recordings from cervical and Erb's point, allowing the detection of brainstem and spinal cord lesions (Cruccu et al., 2008). Our study was concentrated on the analysis and observation of cortical components only. Conversely, several physiologic factors, which are known to influence the SEP components, were not taken into consideration i.e., age, height, or sex (Tanosaki et al., 1999). Such variables might have increased the variance of the SEP parameters in both the topographic and conventional analyses. An additional confounding factor for the SEP could be due to the lack of control for eventual sensory peripheral neuropathy. Unfortunately, this information was not systematically available in all patients.

Our data demonstrate that the sensitivity and specificity of the VEP were substantially improved in patients with MS when using the objective topographic analysis measures. Abnormalities were detected in 86% of the patients with definite MS and 55% of them with CIS. Additional clinical information of these patients showed that those who presented MRI lesion on the optic nerve were correctly detected with the topographic analysis, whereas two of them were not depicted by using the conventional analysis technique. Interestingly, one of those two patients in whom the conventional analysis failed to detect did not present visual symptoms. The ability to detect clinically silent lesions with the EPs has always been considered an important contribution of the electrophysiologic methods (Gronseth and Ashman, 2000). The topographic analysis presented here apparently enhances this capability even further. Furthermore, another interesting group is conformed by the patients who presented clinical symptoms but no MRI lesions in the optic nerve ($n = 6$). The capability of EPs to confirm clinical symptoms before MRI lesions become apparent is another strong point that speaks in favor of electrophysiologic methods, at least with regard to optic nerve lesions (Comi et al., 1999; Leocani and Comi, 2008; Miller et al., 1987; Youl et al., 1991). Finally, those patients who were considered as abnormal in the VEP measurement but who had neither clinical symptoms nor optic nerve MRI lesions constitute the last group of interest. Although these cases could be false-positive findings, one might also speculate that the topographical analysis of the VEP detects very early symptoms, even before they become apparent for the patient and before routine clinical MRI shows an objectively defined lesion. Although such early diagnostic capabilities have been advocated for the evoked potentials in longitudinal studies (Kallmann et al., 2006), follow-up examinations are needed to confirm that the patients detected in our study will ultimately develop visual symptoms and eventually MRI lesions.

In addition to the increased sensitivity of the objective topographic VEP analysis, the new technique also shows higher specificity than the conventional analysis technique. In our collective patient, the lower specificity of the conventional analysis was due to fact that one of the patients with OND suffering from symptomatic epilepsy was falsely considered as abnormal. This patient did not present any clinical sign or symptom or brain MRI compatible with optic neuritis. Further, a clinical follow-up of up to 3 years could reasonably rule out the diagnosis of optic neuritis or MS.

The advantage of the proposed method is the objective analysis based on topographic pattern recognition. It avoids the subjective determination of components by the experimenter and thus avoids inter- and intrarater variability (Emerson, 1998). The values defined by the pattern recognition method are not on an ordinal scale but are metric and allow objective statistical testing.

Our study did not look at the predictive value and only, indirectly, at early detection by including a CIS group for which the outcome is not yet known. However, as for every new method, a first step in evaluating the utility is to show that it reliably detects a given pathology with high sensitivity and specificity once the diagnosis is clear. This is what this study was able to show. Because these first results also look promising with respect to the patients with CIS, longitudinal prospective studies with patients who are at risk for developing MS, and considering both cortical and medullar lesions, are now planned.

ACKNOWLEDGMENTS

The authors thank Mrs. Claudie Fossati and Dr. Laurent Spinelli for their technical assistance during the recordings. The Cartool software (http://brainmapping.unige.ch/Cartool.php) is developed by Denis Brunet, from the Functional Brain Mapping Laboratory, Geneva and is supported by the Lemanic Center for Biomedical Imaging (CIBM).

REFERENCES

Allison T, Hume AL. A comparative analysis of short-latency somatosensory evoked potentials in man, monkey, cat, and rat. *Exp Neurol*. 1981;72:592–611.

Allison T, McCarthy G, Wood CC, et al. Human cortical potentials evoked by stimulation of the median nerve. I. Cytoarchitectonic areas generating short-latency activity. *J Neurophysiol*. 1989;62:694–710.

Allison T, McCarthy G, Wood CC, et al. Potentials evoked in human and monkey cerebral cortex by stimulation of the median nerve. A review of scalp and intracranial recordings. *Brain*. 1991;114:2465–2503.

Balzamo E, Marquis P, Chauvel P, et al. Short-latency components of evoked potentials to median nerve stimulation recorded by intracerebral electrodes in the human pre- and postcentral areas. *Clin Neurophysiol*. 2004;115:1616–1623.

Bast T, Wright T, Boor R, et al. Combined EEG and MEG analysis of early somatosensory evoked activity in children and adolescents with focal epilepsies. *Clin Neurophysiol*. 2007;118:1721–1735.

Brandeis D, Lehmann D. Event-related potentials of the brain and cognitive processes: approaches and applications. *Neuropsychologia*. 1986;24:151–168.

Charil A, Yousry TA, Rovaris M, et al. MRI and the diagnosis of multiple sclerosis: expanding the concept of "no better explanation." *Lancet Neurol*. 2006;5:841–852.

Comi G, Filippi M, Martinelli V, et al. Brain stem magnetic resonance imaging and evoked potential studies of symptomatic multiple sclerosis patients. *Eur Neurol*. 1993;33:232–237.

Comi G, Leocani L, Medaglini S, et al. Measuring evoked responses in multiple sclerosis. *Mult Scler*. 1999;5:263–267.

Cruccu G, Aminoff MJ, Curio G, et al. Recommendations for the clinical use of somatosensory-evoked potentials. *Clin Neurophysiol*. 2008;119:1705–1719.

Desmedt JE, Cheron G. Central somatosensory conduction in man: neural generators and interpeak latencies of the far-field components recorded from neck and right or left scalp and earlobes. *Electroencephalogr Clin Neurophysiol*. 1980;50:382–403.

Desmedt JE, Nguyen TH, Bourguet M. Bit-mapped colour imaging of human evoked potentials with reference to the N20, P22, P27 and N30 somatosensory responses. *Electroencephalogr Clin Neurophysiol*. 1987;68:1–19.

Di Russo F, Martinez A, Sereno MI, et al. Cortical sources of the early components of the visual evoked potential. *Hum Brain Mapp*. 2002;15:95–111.

Emerson RG. Evoked potentials in clinical trials for multiple sclerosis. *J Clin Neurophysiol*. 1998;15:109–116.

Friedli WG, Fuhr P. Electrocutaneous reflexes and multimodality evoked potentials in multiple sclerosis. *J Neurol Neurosurg Psychiatry*. 1990;53:391–397.

Fuhr P, Borggrefe-Chappuis A, Schindler C, et al. Visual and motor evoked potentials in the course of multiple sclerosis. *Brain*. 2001;124:2162–2168.

Fuhr P, Kappos L. Evoked potentials for evaluation of multiple sclerosis. *Clin Neurophysiol*. 2001;112:2185–2189.

Gianotti LR, Faber PL, Schuler M, et al. First valence, then arousal: the temporal dynamics of brain electric activity evoked by emotional stimuli. *Brain Topogr*. 2008;20:143–156.

Gronseth GS, Ashman EJ. Practice parameter: the usefulness of evoked potentials in identifying clinically silent lesions in patients with suspected multiple sclerosis (an evidence-based review): Report of the Quality Standards Subcommittee of the American Academy of Neurology. *Neurology*. 2000;54:1720–1725.

Holder GE, Brigell MG, Hawlina M, et al. ISCEV standard for clinical pattern electroretinography–2007 update. *Documenta Ophthalmologica*. 2007;114:111–116.

Jeffreys DA, Axford JG. Source locations of pattern-specific components of human visual evoked potentials. I. Component of striate cortical origin. *Exp Brain Res*. 1972;16:1–21.

Kallmann BA, Fackelmann S, Toyka KV, et al. Early abnormalities of evoked potentials and future disability in patients with multiple sclerosis. *Mult Scler*. 2006;12:58–65.

Kappos L, Polman CH, Freedman MS, et al. Treatment with interferon beta-1b delays conversion to clinically definite and McDonald MS in patients with clinically isolated syndromes. *Neurology*. 2006;67:1242–1249.

Kristeva-Feige R, Grimm C, Huppertz HJ, et al. Reproducibility and validity of electric source localisation with high-resolution electroencephalography. *Electroencephalogr Clin Neurophysiol*. 1997;103:652–660.

Kurtzke JF. Rating neurologic impairment in multiple sclerosis: an expanded disability status scale (EDSS). *Neurology*. 1983;33:1444–1452.

Lehmann D, Skrandies W. Reference-free identification of components of checkerboard-evoked multichannel potential fields. *Electroencephalogr Clin Neurophysiol*. 1980;48:609–621.

Lehmann D, Skrandies W. Spatial analysis of evoked potentials in man—a review. *Prog Neurobiol*. 1984;23:227–250.

Leocani L, Comi G. Neurophysiological investigations in multiple sclerosis. *Curr Opin Neurol*. 2000;13:255–261.

Leocani L, Comi G. Neurophysiological markers. *Neurol Sci*. 2008;29:218–221.

Leocani L, Medaglini S, Comi G. Evoked potentials in monitoring multiple sclerosis. *Neurol Sci*. 2000;21:889–891.

Leocani L, Rovaris M, Boneschi FM, et al. Multimodal evoked potentials to assess the evolution of multiple sclerosis: a longitudinal study. *J Neurol Neurosurg Psychiatry*. 2006;77:1030–1035.

Mastaglia FL. Can abnormal evoked potentials predict future clinical disability in patients with multiple sclerosis? *Nat Clin Pract Neurol*. 2006;2:304–305.

Mauguière F, Allison T, Babiloni C, et al. Somatosensory evoked potentials. The International Federation of Clinical Neurophysiology. *Electroencephalogr Clin Neurophysiol*. 1999;52:79–90.

Michel CM, Murray MM, Lantz G, et al. EEG source imaging. *Clin Neurophysiol*. 2004*a*;115:2195–2222.

Michel CM, Seeck M, Landis T. Spatiotemporal dynamics of human cognition. *News Physiol Sci*. 1999;14:206–214.

Michel CM, Seeck M, Murray MM. The speed of visual cognition. *Suppl Clin Neurophysiol*. 2004*b*;57:617–627.

Michel CM, Thut G, Morand S, et al. Electric source imaging of human brain functions. *Brain Res Brain Res Rev*. 2001;36:108–118.

Miller DH, McDonald WI, Blumhardt LD, et al. Magnetic resonance imaging in isolated noncompressive spinal cord syndromes. *Ann Neurol*. 1987;22:714–723.

Moller AR, Jannetta PJ, Burgess JE. Neural generators of the somatosensory evoked potentials: recording from the cuneate nucleus in man and monkeys. *Electroencephalogr Clin Neurophysiol*. 1986;65:241–248.

Morand S, Thut G, Grave de Peralta R, et al. Electrophysiological evidence for fast visual processing through the human koniocellular pathway when stimuli move. *Cereb Cortex*. 2000;10:817–825.

Murray MM, Brunet D, Michel CM. Topographic ERP analyses: a step-by-step tutorial review. *Brain Topogr*. 2008;20:249–264.

Oldfield RC. The assessment and analysis of handedness: the Edinburgh inventory. *Neuropsychologia*. 1971;9:97–113.

Pascual-Marqui RD, Michel CM, Lehmann D. Segmentation of brain electrical activity into microstates: model estimation and validation. *IEEE Trans Biomed Eng*. 1995;42:658–665.

Pegna AJ, Khateb A, Spinelli L, et al. Unravelling the cerebral dynamics of mental imagery. *Hum Brain Mapp*. 1997;5:410–421.

Perrin F, Pernier J, Bertrand O, et al. Spherical splines for scalp potential and current density mapping. *Electroencephalogr Clin Neurophysiol*. 1989;72:184–189.

Pohl D, Rostasy K, Treiber-Held S, et al. Pediatric multiple sclerosis: detection of clinically silent lesions by multimodal evoked potentials. *J Pediatr*. 2006;149:125–127.

Polman CH, Reingold SC, Edan G, et al. Diagnostic criteria for multiple sclerosis: 2005 revisions to the "McDonald Criteria." *Ann Neurol*. 2005;58:840–846.

Restuccia D. Anatomic origin of P13 and P14 scalp far-field potentials. *J Clin Neurophysiol*. 2000;17:246–257.

Rossini PM, Deuschl G, Pizzella V, et al. Topography and sources of electromagnetic cerebral responses to electrical and air-puff stimulation of the hand. *Electroencephalogr Clin Neurophysiol*. 1996;100:229–239.

Scherg M, Vajsar J, Picton TW. A source analysis of the late human auditory evoked potential. *J Cogn Neurosci*. 1989;1:336–355.

ACN Society. Guideline 9B: guidelines on visual evoked potentials. *J Clin Neurophysiol*. 2006*a*;23:138–156.

ACN Society. Guideline 9D: guidelines on short-latency somatosensory evoked potentials. *J Clin Neurophysiol*. 2006*b*.;23:168–179.

Skrandies W. EEG/EP: new techniques. *Brain Topogr*. 1993;5:347–350.
Spierer L, Murray MM, Tardif E, et al. The path to success in auditory spatial discrimination: electrical neuroimaging responses within the supratemporal plane predict performance outcome. *Neuroimage*. 2008;41:493–503.
Tanosaki M, Ozaki I, Shimamura H, et al. Effects of aging on central conduction in somatosensory evoked potentials: evaluation of onset versus peak methods. *Clin Neurophysiol*. 1999;110:2094–2103.
Tucker DM. Spatial sampling of head electrical fields: the geodesic sensor net. *Electroencephalogr Clin Neurophysiol*. 1993;87:154–163.
Waberski TD, Buchner H, Perkuhn M, et al. N30 and the effect of explorative finger movements: a model of the contribution of the motor cortex to early somatosensory potentials. *Clin Neurophysiol*. 1999;110:1589–1600.
Weinstock-Guttman B, Baier M, Stockton R, et al. Pattern reversal visual evoked potentials as a measure of visual pathway pathology in multiple sclerosis. *Mult Scler*. 2003;9:529–534.
Youl BD, Turano G, Miller DH, et al. The pathophysiology of acute optic neuritis. An association of gadolinium leakage with clinical and electrophysiological deficits. *Brain*. 1991;114:2437–2450.

Conclusion

Source imaging (ESI) is a model-based and non-invasive imaging technique that combines temporal and spatial components of EEG/EP. It provides new insights in understanding brain function (study III and IV) and adds valuable information in terms of diagnostic yield (study V), prognosis, and localization precision (study I and II). Hopefully the five studies presented in this dissertation helped to answer the following questions:

Is ESI useful in presurgical assessment for epilepsy surgery?

Study I and II show that ESI is a non-invasive method which precisely localizes the sources of the interictal EEG signal recorded with scalp electrodes in patients with focal epilepsy. The accuracy of ESI was higher when high-density EEG (i.e. > 128 electrodes) and an individual head model was employed. Although localization precision of ESI was somewhat better in patients with temporal lobe epilepsy, no statistically significant difference was found compared to patients with extratemporal lobe epilepsy.

While comparing with other techniques, EEG source localization using high-density array showed the highest sensibility and specificity rate (84% and 87%, respectively), while compared to structural MRI (76% and 53%), PET (69% and 44%) and SPECT (58% and 47%). The second study showed that the combination of structural MRI and ESI best correlated with favourable postsurgical outcome in terms of seizure freedom. The positive predictive value for good outcome was 92% and negative predictive value was extremely high (100%). If only one of the exams was positive, the proportion of seizure-free patients dropped to 63% and nuclear imaging techniques were not able to add further information. Since the different techniques provide complementary information, a multimodal approach is required in presurgical epilepsy evaluation.

The question remains as to whether the results provided by ESI change the management plan of the patients. Ictal and interictal ESI provided relevant information in the surgical decision-making process in 14-34% of drug-resistant focal epileptic patients in two prospective studies[123, 124]. In a Danish cohort, 13/28 (69%) of patients in whom ESI led to a change in clinical management, intracranial EEG recordings confirmed location at a sub-lobar level[124].

Intracranial EEG recording is still considered as the “gold standard” in terms of localization precision. ESI can achieve anatomical concordance at a sub-lobar level with

a median distance of 15 millimetres from the source maximum to the nearest electrode revealing pathological activity[101]. To summarize, ESI could have an important role in defining surgical strategy (i.e. lesion resection and intracranial electrode implantation site) and should be part of the multimodal workup in the presurgical evaluation of epilepsy surgery.

Is ESI valuable in mapping functional brain regions to create a presurgical plan?

Surgical treatment of lesions lying in close vicinity to functional eloquent areas of the brain remains a challenge. Basic knowledge in anatomy is not enough to establish the extension of lesion resection. Brain mapping is not generalizable and should be performed on an individual patient-level.

Several techniques are used to identify the brain lesion (i.e. tumour, epileptogenic foci, etc.) and allow sparing of the eloquent cortex to avoid permanent handicap. DCES using subdural electrodes is considered the gold standard for mapping brain function. However, this method is invasive, time-consuming and requires patients' ability to understand and complete a given task, which can be particularly delicate in children. In this case, alternative non-invasive techniques for mapping brain function should be privileged.

A recent meta-analysis of 34 studies (n= 353 patients) confirmed that MEG and functional MRI (fMRI) provide information on language lateralisation and localization of the central sulcus using a motor stimulation paradigm in paediatric epilepsy surgery candidates[14]. At present, fMRI is the most frequently used non-invasive imaging technique for surgical planning. Nonetheless, fMRI may not be appropriate in patients who are claustrophobic or with vascular malformations (AVM). Electromagnetic based studies (MEG, EEG) should be considered as an alternative in these cases.

Study III compares localization precision of source imaging based on high-density SEP and DCES in six candidates for epilepsy surgery (n=4 were < 13 years old). A median distance of only 13 mm was observed between SEP and DCES, showing a good correlation between both techniques. Moreover, high-density SEP was compared to fMRI in 4/6 patients and in 18 healthy volunteers showing high anatomical concordance except in the dorsal-ventral orientation, which is probably explained by differences related to each technique. Finally, fMRI and high-density EP showed comparable

distances with DCES, indicating they have similar capacities to localize the somatosensory cortex.

Compared with DCES, electric source imaging SEP has the advantages of non-invasiveness and ability of mapping the entire brain. This method can be considered as part of the presurgical workup since it can provide functional information non-invasively, especially in those patients in which fMRI is contraindicated or difficult to perform (i.e. limited cooperation, alterations in the vascular coupling). An alternative solution is to combine both techniques and quantify the concordance between fMRI and EEG results. When applying source imaging in clinical settings, optimizing its benefits, and mitigating its limitations necessitates an understanding of the fundamentals of the technique.

Is ESI able to map the human olfactory cortex?

The human olfactory system represents one of the oldest sensory modalities in phylogenetics terms. The most unique aspect of human olfaction, compared to other sensory systems, is the lack of thalamic relay and its predominant ipsilateral cortical projections. Olfactory human system includes the olfactory nucleus, the olfactory tubercle, the frontal and temporal piriform cortices, the amygdala, and the entorhinal cortex[125].

Prior studies have used fMRI and nuclear medicine imaging procedures to examine human olfactory networks[108, 126]. However, imaging techniques do not provide information on the temporal aspect of olfactory processing. Electrophysiological methods, namely CSERP embedded with the ongoing EEG, are more suitable for this purpose.

ESI can be used to understand the neural generators of CSERP. Study IV provides an insight into the spatiotemporal pattern of activity of olfactory processing by applying hydrogen sulfide as stimuli. CSERP map topography showed initial activation of the medial temporal lobe (parahippocampal gyrus and amygdala) and lateral temporal lobe ipsilateral to the stimulated nostril. Subsequently, activation spread to the same areas on the contralateral side and, finally, to the bilateral inferior frontal gyrus. To conclude, source imaging CSERP provides simultaneous spatial and temporal information on olfactory central processing in healthy volunteers. Further studies should be performed

to study the clinical interest of source imaging CSERP in patients with olfactory complaints and in early detection of neurodegenerative disorders.

Does ESI applied to visual and somatosensory evoked potentials provide more reliable information than conventional waveform analysis?

Traditional analysis of EP relies on visual inspection of the generated waveforms. Absence of quantitative analysis lends itself to a problem of subjective interpretation of EP results. Study V proposes an objective measure of EP components based on their potential distribution over the scalp[87]. Visual and somatosensory stimulation was applied in a group of 26 patients with MS. Results were compared to: i) those obtained after traditional EP analysis to assess sensitivity and ii) a matched control group of healthy volunteers and patients with other neurological diseases to test for specificity.

Amongst the different EP components and assessment types, topographic recognition of VEP P100 component rendered the highest sensitivity and specificity rate (72% and 100% respectively) versus conventional waveform analysis (56% and 90%, respectively). Quantitative analysis of somatosensory multichannel EP parameters showed more accurate results than traditional analysis. Our findings agrees with previous studies which have shown the clinical value of VEP over other modalities[127, 128].

To sum up, topographic analysis of VEP is a reliable and sensitive method of objectively quantifying pathological results in MS. Results need to be validated in larger cohorts, correlated with different clinical/paraclinical parameters and in combination with other EP modalities (sum score), in order to improve disease and treatment monitoring in MS.

In a nutshell, EEG/EP source imaging is functional brain imaging technology with a high temporal and spatial resolution. This technique is extremely attractive because of its low-cost and non-invasiveness. It is, therefore, suitable for children and non-cooperative subjects. Nonetheless, its use in clinical routine remains limited and traditional EEG/EP analysis prevails. To achieve a change in paradigm, clinicians should abandon ambiguous waveform description and switch over to a comprehensive analysis of the electric field.

Current challenges and future perspectives

The advent of new technologies has changed the landscape of neuroscience which became more explorative and fuelled the field of brain connectivity, brain stimulation, neurorobotics, and neuroinformatics. Unfortunately, clinical neurophysiology failed to keep up with the progress made since many of those technological innovations were not applied in routine neurological practice. A main issue of concern is that clinical use of many neurophysiological methods is not being updated and, thus, lack modern standards and guidelines of use.

Simplification of high-density EEG analysis

After years of research in the epilepsy field, ESI has finally found a place as part of the presurgical evaluation work-up of patients with focal epilepsy. Since 2017, the International Federation of Clinical Neurophysiology recommends the use of ESI whenever standard EEG recordings provide ambiguous or inconclusive results[84]. However, one main limitation of high-density EEG recordings is that it requires computer skills and knowledge of the different steps involved in electric source reconstruction.

One way to solve this conundrum is to simplify the EEG analysis process and limit data managing. A recent publication showed that visual high-density EEG inspection (i.e. select maximal amplitude spike and determine their location) and ESI provided concordant results in 2/3 of the patients[129].

Other ways of rendering ESI more attractive for routine use in the clinical setting is to improve software user experience. It is of utmost importance to avoid overwhelming users with data entry and data processing by automating the entire selection and source localization process from high-density EEG recordings[104]. This proposal can also be applied to high-density EP studies.

Validation from a larger data set

Even though ESI allows accurate localization of the epileptogenic zone, a recent systematic review concluded that there is insufficient clinical evidence on its diagnostic added value[130]. Study I and II need to be validated in a larger data set.

Previous studies did not address the role of ESI on the clinical decision-making process. Value of combined ESI and MEG source imaging (technique referred to as EMSI) was assessed prospectively and blinded to clinical data in a set 85 patients with normal MRI or discordant data before intracranial EEG recordings[6]. Blinded decision based on EMSI results changed the management plan in 29/85 (34%) patients. However, a limitation of this study is that implantation of intracranial electrodes was not blinded to EMSI results. There is a need for prospective studies in which preliminary decision is made blinded to the ESI data and, subsequently, the final decision is based upon this result.

Biomarker in neurological disorders

The terms biomarker refers to a set of clinical and paraclinical signs which can be measured reliably and reproducibly. Reliability of any EP can be improved by standardizing recording procedures across laboratories. The creation of international guidelines for the recording, interpretation and analysis of all EP modalities is required. This is the case for CSERP and laser-induced pain-related EP (LEP).

As detailed in the previous sections, the future of EP lies in its capacity to monitor treatment and prognosticate disease progression. In this dissertation we used MS as a model to assess CNS status by means of a neurophysiological approach. Although there is no such thing as a disease-specific biomarker in MS, EP can be combined with different modalities (i.e. sum score) or together with other paraclinical exams to increase diagnostic/prognostic yield. Efficiency and added value of EP in MS clinical trials should be further tested.

Objective pain assessment in multiple sclerosis

Pain in MS has been reported by Charcot in the end of the 19th century: spanning from trigeminal neuralgia to tonic spasms, Lhermitte sign, radicular and thalamic pain (for a review see Seixas et al., 2014)[131]. Despite the fact that its prevalence rises to 25-60% (depending on the cohort)[132], MS specialists usually neglect this complaint since it is poorly understood. However, pain affects MS patients' quality of life and, thus, requires our utmost consideration.

While pain in MS is common, in many cases the exact mechanism is unknown. A distinction can be made between nociceptive (e.g. back pain) and neuropathic pain (e.g.

ongoing pain extremity), since the latter is supposed to result as a consequence of demyelination, inflammation and axonal damage[133]. In addition, neuropathic pain responds to antiepileptic medication and antidepressants as opposed to nociceptive pain. Targeting optimal pain-related treatment will avoid medication overuse and will improve pain relief.

Clinical assessment of neuropathic pain usually relies merely on psychometric tests. Nowadays, there are very few objective methods readily available that can measure or locate neuropathic pain with precision. LEP allow studying the spinothalamic pathway and could be helpful in determining lesion pain site (e.g.: cortical, medullar, etc.) [134, 135]. Laser-generated radiant heat pulses (Nd:YAG) excite free nerve endings in the superficial skin layers and selectively activate A-delta and /or C nociceptors.

A recent study showed that 90% of 10 patients presenting with neuropathic pain had abnormal LEPs (vs. 16% with nociceptive pain) and only 30% presented with pathological SEP results[136]. This finding points to a high sensitivity and specificity and, thus, highlights the importance of LEPs in MS pain assessment and treatment management.

Current research project aims at studying the underlying nociceptive mechanisms in MS, by means of LEP. Very few studies have addressed this topic [136, 137]. The main aim is to validate LEP as a tool [138, 139], which allows determining whether pain is from neuropathic or nociceptive origin in an MS population. LEP's results will be correlated with epidemiological features (e.g. age, disease type, disease duration, lesion location: medullar vs cortical) parameters of disease activity (e.g. relapse rate, handicap score, MRI lesions), biological signs of neurodegeneration (serum neurofilaments) and pain assessment questionnaires (DN4 for neuropathic pain and visual ratings). A fatigue and a depression scale (Hamilton Depression Rating Scale) will also be included. This project has a practical impact, since abnormal findings will lead to treatment decisions and guide pharmacological approaches for addressing pain in MS[140].

References

1. Tassinari CA. An electroencephalographer recalls the history of the Federation on the 70th anniversary of its journal, Clinical Neurophysiology. Clin Neurophysiol 2019;130:2258-2263.
2. Berger H. Über das Elektroenkephalogramm des Menschen. 1st Report. Arch Psychiatr 1929;Nervenkr., 87:527-570.
3. Lantz G, Grave de Peralta R, Spinelli L, Seeck M, Michel CM. Epileptic source localization with high density EEG: how many electrodes are needed? Clin Neurophysiol 2003;114:63-69.
4. Michel CM, Murray MM, Lantz G, Gonzalez S, Spinelli L, Grave de Peralta R. EEG source imaging. Clin Neurophysiol 2004;115:2195-2222.
5. Baumgartner C, Koren JP, Britto-Arias M, Zoche L, Pirker S. Presurgical epilepsy evaluation and epilepsy surgery. F1000Res 2019;8.
6. Duez L, Tankisi H, Hansen PO, et al. Electromagnetic source imaging in presurgical workup of patients with epilepsy: A prospective study. Neurology 2019;92:e576-e586.
7. Sharma P, Seeck M, Beniczky S. Accuracy of Interictal and Ictal Electric and Magnetic Source Imaging: A Systematic Review and Meta-Analysis. Front Neurol 2019;10:1250.
8. Brodbeck V, Lascano AM, Spinelli L, Seeck M, Michel CM. Accuracy of EEG source imaging of epileptic spikes in patients with large brain lesions. Clin Neurophysiol 2009;120:679-685.
9. Brodbeck V, Spinelli L, Lascano AM, et al. Electrical source imaging for presurgical focus localization in epilepsy patients with normal MRI. Epilepsia 2010;51:583-591.
10. Baldini S, Coito A, Korff CM, et al. Localizing non-epileptiform abnormal brain function in children using high density EEG: Electric Source Imaging of focal slowing. Epilepsy Res 2020;159:106245.
11. Sperli F, Spinelli L, Seeck M, Kurian M, Michel CM, Lantz G. EEG source imaging in pediatric epilepsy surgery: a new perspective in presurgical workup. Epilepsia 2006;47:981-990.

12. Rosenow F, Luders H. Presurgical evaluation of epilepsy. Brain 2001;124:1683-1700.

13. Towle VL, Khorasani L, Uftring S, et al. Noninvasive identification of human central sulcus: a comparison of gyral morphology, functional MRI, dipole localization, and direct cortical mapping. Neuroimage 2003;19:684-697.

14. Collinge S, Prendergast G, Mayers ST, et al. Pre-surgical mapping of eloquent cortex for paediatric epilepsy surgery candidates: Evidence from a review of advanced functional neuroimaging. Seizure 2017;52:136-146.

15. Papanicolaou AC, Rezaie R, Narayana S, et al. On the relative merits of invasive and non-invasive pre-surgical brain mapping: New tools in ablative epilepsy surgery. Epilepsy Res 2018;142:153-155.

16. Niedermeyer E. EEG and clinical neurophysiology at Johns Hopkins medical institutions: roots and development. J Clin Neurophysiol 1993;10:83-88.

17. Murakami S, Okada Y. Contributions of principal neocortical neurons to magnetoencephalography and electroencephalography signals. J Physiol 2006;575:925-936.

18. Keil A, Debener S, Gratton G, et al. Committee report: publication guidelines and recommendations for studies using electroencephalography and magnetoencephalography. Psychophysiology 2014;51:1-21.

19. Guideline thirteen: guidelines for standard electrode position nomenclature. American Electroencephalographic Society. J Clin Neurophysiol 1994;11:111-113.

20. Nuwer MR, Comi G, Emerson R, et al. IFCN standards for digital recording of clinical EEG. The International Federation of Clinical Neurophysiology. Electroencephalogr Clin Neurophysiol Suppl 1999;52:11-14.

21. Acharya JN, Hani AJ, Cheek J, Thirumala P, Tsuchida TN. American Clinical Neurophysiology Society Guideline 2: Guidelines for Standard Electrode Position Nomenclature. Neurodiagn J 2016;56:245-252.

22. American Clinical Neurophysiology S. Guideline 9A: guidelines on evoked potentials. Am J Electroneurodiagnostic Technol 2006;46:240-253.

23. American Clinical Neurophysiology S. Guideline 9D: guidelines on short-latency somatosensory evoked potentials. Am J Electroneurodiagnostic Technol 2006;46:287-300.

24. American Clinical Neurophysiology S. Guideline 9C: guidelines on short-latency auditory evoked potentials. Am J Electroneurodiagnostic Technol 2006;46:275-286.
25. American Clinical Neurophysiology S. Guideline 9B: guidelines on visual evoked potentials. Am J Electroneurodiagnostic Technol 2006;46:254-274.
26. Legatt AD, Emerson RG, Epstein CM, et al. ACNS Guideline: Transcranial Electrical Stimulation Motor Evoked Potential Monitoring. J Clin Neurophysiol 2016;33:42-50.
27. Lascano AM, Lalive PH, Hardmeier M, Fuhr P, Seeck M. Clinical evoked potentials in neurology: a review of techniques and indications. J Neurol Neurosurg Psychiatry 2017;88:688-696.
28. Weinstein GW, Odom JV, Cavender S. Visually evoked potentials and electroretinography in neurologic evaluation. Neurol Clin 1991;9:225-242.
29. Pihl-Jensen G, Schmidt MF, Frederiksen JL. Multifocal visual evoked potentials in optic neuritis and multiple sclerosis: A review. Clin Neurophysiol 2017;128:1234-1245.
30. Heidari M, Radcliff AB, McLellan GJ, et al. Evoked potentials as a biomarker of remyelination. Proc Natl Acad Sci U S A 2019.
31. Thompson AJ, Banwell BL, Barkhof F, et al. Diagnosis of multiple sclerosis: 2017 revisions of the McDonald criteria. Lancet Neurol 2018;17:162-173.
32. Wingerchuk DM, Banwell B, Bennett JL, et al. International consensus diagnostic criteria for neuromyelitis optica spectrum disorders. Neurology 2015;85:177-189.
33. Filippini G, Comi GC, Cosi V, et al. Sensitivities and predictive values of paraclinical tests for diagnosing multiple sclerosis. J Neurol 1994;241:132-137.
34. Calabrese M, Gasperini C, Tortorella C, et al. "Better explanations" in multiple sclerosis diagnostic workup: A 3-year longitudinal study. Neurology 2019;92:e2527-e2537.
35. Iodice R, Carotenuto A, Dubbioso R, Cerillo I, Santoro L, Manganelli F. Multimodal evoked potentials follow up in multiple sclerosis patients under fingolimod therapy. J Neurol Sci 2016;365:143-146.
36. Schlaeger R, Schindler C, Grize L, et al. Combined visual and motor evoked potentials predict multiple sclerosis disability after 20 years. Mult Scler 2014;20:1348-1354.

37. Cadavid D, Balcer L, Galetta S, et al. Safety and efficacy of opicinumab in acute optic neuritis (RENEW): a randomised, placebo-controlled, phase 2 trial. Lancet Neurol 2017;16:189-199.
38. Green AJ, Gelfand JM, Cree BA, et al. Clemastine fumarate as a remyelinating therapy for multiple sclerosis (ReBUILD): a randomised, controlled, double-blind, crossover trial. Lancet 2017;390:2481-2489.
39. Albert C, Mikolajczak J, Liekfeld A, et al. Fingolimod after a first unilateral episode of acute optic neuritis (MOVING) - preliminary results from a randomized, rater-blind, active-controlled, phase 2 trial. BMC Neurol 2020;20:75.
40. Ringelstein M, Harmel J, Zimmermann H, et al. Longitudinal optic neuritis-unrelated visual evoked potential changes in NMO spectrum disorders. Neurology 2020;94:e407-e418.
41. Kim NH, Kim HJ, Park CY, Jeong KS, Cho JY. Optical Coherence Tomography versus Visual Evoked Potentials for Detecting Visual Pathway Abnormalities in Patients with Neuromyelitis Optica Spectrum Disorder. J Clin Neurol 2018;14:200-205.
42. Holder GE. Electrophysiological assessment of optic nerve disease. Eye (Lond) 2004;18:1133-1143.
43. Parisi V, Miglior S, Manni G, Centofanti M, Bucci MG. Clinical ability of pattern electroretinograms and visual evoked potentials in detecting visual dysfunction in ocular hypertension and glaucoma. Ophthalmology 2006;113:216-228.
44. Chen CS, Lee AW, Karagiannis A, Crompton JL, Selva D. Practical clinical approaches to functional visual loss. J Clin Neurosci 2007;14:1-7.
45. Gandevia SC, Burke D, McKeon B. The projection of muscle afferents from the hand to cerebral cortex in man. Brain 1984;107 (Pt 1):1-13.
46. Kuwabara S, Mizobuchi K, Toma S, Nakajima Y, Ogawara K, Hattori T. "Tactile" sensory nerve potentials elicited by air-puff stimulation: a microneurographic study. Neurology 2000;54:762-765.
47. Mizobuchi K, Kuwabara S, Toma S, Nakajima Y, Ogawara K, Hattori T. Single unit responses of human cutaneous mechanoreceptors to air-puff stimulation. Clin Neurophysiol 2000;111:1577-1581.
48. Garcia-Larrea L, Hagiwara K. Electrophysiology in diagnosis and management of neuropathic pain. Rev Neurol (Paris) 2019;175:26-37.

49. Baker JB, Larson SJ, Sances A, White PT. Evoked potentials as an aid to the diagnosis of multiple sclerosis. Neurology 1968;18:286.

50. Polman CH, Reingold SC, Edan G, et al. Diagnostic criteria for multiple sclerosis: 2005 revisions to the "McDonald Criteria". Ann Neurol 2005;58:840-846.

51. Drislane FW. Use of evoked potentials in the diagnosis and follow-up of multiple sclerosis. Clin Neurosci 1994;2:196-201.

52. Polman CH, Reingold SC, Banwell B, et al. Diagnostic criteria for multiple sclerosis: 2010 revisions to the McDonald criteria. Ann Neurol 2011;69:292-302.

53. Schlaeger R, Hardmeier M, D'Souza M, et al. Monitoring multiple sclerosis by multimodal evoked potentials: Numerically versus ordinally scaled scoring systems. Clin Neurophysiol 2016;127:1864-1871.

54. Kallmann BA, Fackelmann S, Toyka KV, Rieckmann P, Reiners K. Early abnormalities of evoked potentials and future disability in patients with multiple sclerosis. Mult Scler 2006;12:58-65.

55. Giffroy X, Maes N, Albert A, Maquet P, Crielaard JM, Dive D. Multimodal evoked potentials for functional quantification and prognosis in multiple sclerosis. BMC Neurol 2016;16:83.

56. Invernizzi P, Bertolasi L, Bianchi MR, Turatti M, Gajofatto A, Benedetti MD. Prognostic value of multimodal evoked potentials in multiple sclerosis: the EP score. J Neurol 2011;258:1933-1939.

57. London F, El Sankari S, van Pesch V. Early disturbances in multimodal evoked potentials as a prognostic factor for long-term disability in relapsing-remitting multiple sclerosis patients. Clin Neurophysiol 2017;128:561-569.

58. Rothstein TL. The role of evoked potentials in anoxic-ischemic coma and severe brain trauma. J Clin Neurophysiol 2000;17:486-497.

59. Wijdicks EF, Hijdra A, Young GB, Bassetti CL, Wiebe S, Quality Standards Subcommittee of the American Academy of N. Practice parameter: prediction of outcome in comatose survivors after cardiopulmonary resuscitation (an evidence-based review): report of the Quality Standards Subcommittee of the American Academy of Neurology. Neurology 2006;67:203-210.

60. Gobert F, Dailler F, Fischer C, Andre-Obadia N, Luaute J. Proving cortical death after vascular coma: Evoked potentials, EEG and neuroimaging. Clin Neurophysiol 2018;129:1105-1116.
61. Koenig MA, Kaplan PW. Clinical neurophysiology in acute coma and disorders of consciousness. Semin Neurol 2013;33:121-132.
62. Kondziella D, Bender A, Diserens K, et al. European Academy of Neurology guideline on the diagnosis of coma and other disorders of consciousness. Eur J Neurol 2020.
63. MacDonald DB, Dong C, Quatrale R, et al. Recommendations of the International Society of Intraoperative Neurophysiology for intraoperative somatosensory evoked potentials. Clin Neurophysiol 2019;130:161-179.
64. Nunes RR, Bersot CDA, Garritano JG. Intraoperative neurophysiological monitoring in neuroanesthesia. Curr Opin Anaesthesiol 2018;31:532-538.
65. Whitcroft KL, Hummel T. Olfactory Dysfunction in COVID-19: Diagnosis and Management. JAMA 2020.
66. Doty RL. Olfactory dysfunction and its measurement in the clinic. World J Otorhinolaryngol Head Neck Surg 2015;1:28-33.
67. Stuck BA, Frey S, Freiburg C, Hormann K, Zahnert T, Hummel T. Chemosensory event-related potentials in relation to side of stimulation, age, sex, and stimulus concentration. Clin Neurophysiol 2006;117:1367-1375.
68. Rombaux P, Collet S, Eloy P, Ledeghen S, Bertrand B. Smell disorders in ENT clinic. B-ENT 2005;Suppl 1:97-107; quiz 108-109.
69. Xydakis MS, Dehgani-Mobaraki P, Holbrook EH, et al. Smell and taste dysfunction in patients with COVID-19. Lancet Infect Dis 2020.
70. Schrauwen EJ, Herfst S, Leijten LM, et al. The multibasic cleavage site in H5N1 virus is critical for systemic spread along the olfactory and hematogenous routes in ferrets. J Virol 2012;86:3975-3984.
71. Rombaux P, Huart C, Collet S, Eloy P, Negoias S, Hummel T. Presence of olfactory event-related potentials predicts recovery in patients with olfactory loss following upper respiratory tract infection. Laryngoscope 2010;120:2115-2118.
72. Moberg PJ, Doty RL, Mahr RN, et al. Olfactory identification in elderly schizophrenia and Alzheimer's disease. Neurobiol Aging 1997;18:163-167.

73. Wetter S, Murphy C. Individuals with Down's syndrome demonstrate abnormal olfactory event-related potentials. Clin Neurophysiol 1999;110:1563-1569.

74. Barz S, Hummel T, Pauli E, Majer M, Lang CJ, Kobal G. Chemosensory event-related potentials in response to trigeminal and olfactory stimulation in idiopathic Parkinson's disease. Neurology 1997;49:1424-1431.

75. Hawkes CH, Shephard BC, Kobal G. Assessment of olfaction in multiple sclerosis: evidence of dysfunction by olfactory evoked response and identification tests. J Neurol Neurosurg Psychiatry 1997;63:145-151.

76. Hummel T, Pauli E, Schuler P, Kettenmann B, Stefan H, Kobal G. Chemosensory event-related potentials in patients with temporal lobe epilepsy. Epilepsia 1995;36:79-85.

77. Kim SG, Richter W, Ugurbil K. Limitations of temporal resolution in functional MRI. Magn Reson Med 1997;37:631-636.

78. Schomer DL, Lopes da Silva FH. Niedermeyer's Electroencephalography: basic principles, clinical applications and related fields.: Oxford University Press, 2017.

79. Cohen D, Cuffin BN. EEG versus MEG localization accuracy: theory and experiment. Brain Topogr 1991;4:95-103.

80. Murzin V, Fuchs A, Kelso JA. Anatomically constrained minimum variance beamforming applied to EEG. Exp Brain Res 2011;214:515-528.

81. Hamalainen MS. Magnetoencephalography: a tool for functional brain imaging. Brain Topogr 1992;5:95-102.

82. Baumgartner C. Controversies in clinical neurophysiology. MEG is superior to EEG in the localization of interictal epileptiform activity: Con. Clin Neurophysiol 2004;115:1010-1020.

83. Cohen D, Cuffin BN, Yunokuchi K, et al. MEG versus EEG localization test using implanted sources in the human brain. Ann Neurol 1990;28:811-817.

84. Seeck M, Koessler L, Bast T, et al. The standardized EEG electrode array of the IFCN. Clin Neurophysiol 2017;128:2070-2077.

85. Brodbeck V, Spinelli L, Lascano AM, et al. Electroencephalographic source imaging: a prospective study of 152 operated epileptic patients. Brain 2011;134:2887-2897.

86. Michel CM, Lantz G, Spinelli L, De Peralta RG, Landis T, Seeck M. 128-channel EEG source imaging in epilepsy: clinical yield and localization precision. J Clin Neurophysiol 2004;21:71-83.
87. Brunet D, Murray MM, Michel CM. Spatiotemporal analysis of multichannel EEG: CARTOOL. Comput Intell Neurosci 2011;2011:813870.
88. Wang Z, Chen C, Li W, et al. A Multichannel EEG Acquisition System With Novel Ag NWs/PDMS Flexible Dry Electrodes. Conf Proc IEEE Eng Med Biol Soc 2018;2018:1299-1302.
89. Duffy FH. Topographic mapping of brain electrical activity: Butterworth-Heinemann, 2013.
90. Lehmann D, Skrandies W. Spatial analysis of evoked potentials in man--a review. Prog Neurobiol 1984;23:227-250.
91. Malmivuo J PR. Bioelectromagnetism: Principles and Applications of Bioelectric and Biomagnetic Fields. . New York, NY: Oxford University Press 1995.
92. Michel CM HB. EEG mapping and source imaging. In: Schomer DL, Silva, FHLd, editors. Niedermeyer's Electroencephalography. . New York, NY: Oxford University Press 2018:1135–1156.
93. H H. Ueber einige Gesetze der Vertheilung elektrischer Ströme in körperlichen Leitern mit Anwendung auf die thierisch-elektrischen Versuche. Ann Phys Chem 1953;89:211-233; 353-377.
94. He B, Musha T, Okamoto Y, Homma S, Nakajima Y, Sato T. Electric dipole tracing in the brain by means of the boundary element method and its accuracy. IEEE Trans Biomed Eng 1987;34:406-414.
95. Pascual-Marqui RD. Standardized low-resolution brain electromagnetic tomography (sLORETA): technical details. Methods Find Exp Clin Pharmacol 2002;24 Suppl D:5-12.
96. Michel CM, Brunet D. EEG Source Imaging: A Practical Review of the Analysis Steps. Front Neurol 2019;10:325.
97. Kwan P, Brodie MJ. Early identification of refractory epilepsy. N Engl J Med 2000;342:314-319.
98. Miller JW, Hakimian S. Surgical treatment of epilepsy. Continuum (Minneap Minn) 2013;19:730-742.

99. Luders HO, Burgess R, Noachtar S. Expanding the international classification of seizures to provide localization information. Neurology 1993;43:1650-1655.

100. Bien CG, Szinay M, Wagner J, Clusmann H, Becker AJ, Urbach H. Characteristics and surgical outcomes of patients with refractory magnetic resonance imaging-negative epilepsies. Arch Neurol 2009;66:1491-1499.

101. Megevand P, Spinelli L, Genetti M, et al. Electric source imaging of interictal activity accurately localises the seizure onset zone. J Neurol Neurosurg Psychiatry 2014;85:38-43.

102. Bautista RE, Cobbs MA, Spencer DD, Spencer SS. Prediction of surgical outcome by interictal epileptiform abnormalities during intracranial EEG monitoring in patients with extrahippocampal seizures. Epilepsia 1999;40:880-890.

103. Mouthaan BE, Rados M, Barsi P, et al. Current use of imaging and electromagnetic source localization procedures in epilepsy surgery centers across Europe. Epilepsia 2016;57:770-776.

104. Baroumand AG, van Mierlo P, Strobbe G, et al. Automated EEG source imaging: A retrospective, blinded clinical validation study. Clin Neurophysiol 2018;129:2403-2410.

105. Conde S, Creac'h C, Brun X, Moreau R, Convers P, Peyron R. Pneumatic evoked potential. Sensory or auditive potential? Neurophysiol Clin 2013;43:189-195.

106. Carmichael ST, Clugnet MC, Price JL. Central olfactory connections in the macaque monkey. J Comp Neurol 1994;346:403-434.

107. Haberly LB. Parallel-distributed processing in olfactory cortex: new insights from morphological and physiological analysis of neuronal circuitry. Chem Senses 2001;26:551-576.

108. Zatorre RJ, Jones-Gotman M, Evans AC, Meyer E. Functional localization and lateralization of human olfactory cortex. Nature 1992;360:339-340.

109. Tabert MH, Steffener J, Albers MW, et al. Validation and optimization of statistical approaches for modeling odorant-induced fMRI signal changes in olfactory-related brain areas. Neuroimage 2007;34:1375-1390.

110. Hummel T, Haehner A, Hummel C, Croy I, Iannilli E. Lateralized differences in olfactory bulb volume relate to lateralized differences in olfactory function. Neuroscience 2013;237:51-55.

111. Doty RL. Olfactory dysfunction in neurodegenerative diseases: is there a common pathological substrate? Lancet Neurol 2017;16:478-488.
112. Braak H, Braak E. Morphological criteria for the recognition of Alzheimer's disease and the distribution pattern of cortical changes related to this disorder. Neurobiol Aging 1994;15:355-356; discussion 379-380.
113. Suzuki Y, Yamamoto S, Umegaki H, et al. Smell identification test as an indicator for cognitive impairment in Alzheimer's disease. Int J Geriatr Psychiatry 2004;19:727-733.
114. Murphy C, Solomon ES, Haase L, Wang M, Morgan CD. Olfaction in aging and Alzheimer's disease: event-related potentials to a cross-modal odor-recognition memory task discriminate ApoE epsilon4+ and ApoE epsilon 4- individuals. Ann N Y Acad Sci 2009;1170:647-657.
115. Wetter S, Murphy C. Apolipoprotein E epsilon4 positive individuals demonstrate delayed olfactory event-related potentials. Neurobiol Aging 2001;22:439-447.
116. McCaffrey RJ, Duff K, Solomon GS. Olfactory dysfunction discriminates probable Alzheimer's dementia from major depression: a cross-validation and extension. J Neuropsychiatry Clin Neurosci 2000;12:29-33.
117. Fullard ME, Tran B, Xie SX, et al. Olfactory impairment predicts cognitive decline in early Parkinson's disease. Parkinsonism Relat Disord 2016;25:45-51.
118. Muller A, Mungersdorf M, Reichmann H, Strehle G, Hummel T. Olfactory function in Parkinsonian syndromes. J Clin Neurosci 2002;9:521-524.
119. Mahlknecht P, Iranzo A, Hogl B, et al. Olfactory dysfunction predicts early transition to a Lewy body disease in idiopathic RBD. Neurology 2015;84:654-658.
120. Kebir S, Hattingen E, Niessen M, et al. Olfactory function as an independent prognostic factor in glioblastoma. Neurology 2020;94:e529-e537.
121. Rotstein DL, Healy BC, Malik MT, Chitnis T, Weiner HL. Evaluation of no evidence of disease activity in a 7-year longitudinal multiple sclerosis cohort. JAMA Neurol 2015;72:152-158.
122. Gschwind M, Hardmeier M, Van De Ville D, et al. Fluctuations of spontaneous EEG topographies predict disease state in relapsing-remitting multiple sclerosis. Neuroimage Clin 2016;12:466-477.

123. Boon P, D'Have M, Vanrumste B, et al. Ictal source localization in presurgical patients with refractory epilepsy. J Clin Neurophysiol 2002;19:461-468.
124. Foged MT, Martens T, Pinborg LH, et al. Diagnostic added value of electrical source imaging in presurgical evaluation of patients with epilepsy: A prospective study. Clin Neurophysiol 2020;131:324-329.
125. Doty RL. Handbook of Olfaction and Gustation: John Wiley & Sons, 2015.
126. Karunanayaka P, Eslinger PJ, Wang JL, et al. Networks involved in olfaction and their dynamics using independent component analysis and unified structural equation modeling. Hum Brain Mapp 2014;35:2055-2072.
127. Fuhr P, Borggrefe-Chappuis A, Schindler C, Kappos L. Visual and motor evoked potentials in the course of multiple sclerosis. Brain 2001;124:2162-2168.
128. Hardmeier M, Leocani L, Fuhr P. A new role for evoked potentials in MS? Repurposing evoked potentials as biomarkers for clinical trials in MS. Mult Scler 2017;23:1309-1319.
129. Toscano G, Carboni M, Rubega M, et al. Visual analysis of high density EEG: As good as electrical source imaging? Clin Neurophysiol Pract 2020;5:16-22.
130. Tatum WO, Rubboli G, Kaplan PW, et al. Clinical utility of EEG in diagnosing and monitoring epilepsy in adults. Clin Neurophysiol 2018;129:1056-1082.
131. Seixas D, Foley P, Palace J, Lima D, Ramos I, Tracey I. Pain in multiple sclerosis: a systematic review of neuroimaging studies. NeuroImage: Clinical 2014;5:322-331.
132. O'connor AB, Schwid SR, Herrmann DN, Markman JD, Dworkin RH. Pain associated with multiple sclerosis: systematic review and proposed classification. Pain 2008;137:96-111.
133. Truini A, Barbanti P, Pozzilli C, Cruccu G. A mechanism-based classification of pain in multiple sclerosis. J Neurol 2013;260:351-367.
134. Kakigi R, Inui K, Tran DT, et al. Human brain processing and central mechanisms of pain as observed by electro-and magneto-encephalography. Journal-Chinese Medical Association 2004;67:377-386.
135. Valeriani M, Pazzaglia C, Cruccu G, Truini A. Clinical usefulness of laser evoked potentials. Neurophysiologie Clinique/Clinical Neurophysiology 2012;42:345-353.

136. Truini A, Galeotti F, La Cesa S, et al. Mechanisms of pain in multiple sclerosis: a combined clinical and neurophysiological study. Pain 2012;153:2048-2054.
137. Spiegel J, Hansen C, Baumgartner U, Hopf HC, Treede RD. Sensitivity of laser-evoked potentials versus somatosensory evoked potentials in patients with multiple sclerosis. Clin Neurophysiol 2003;114:992-1002.
138. Garcia• Larrea L, Convers P, Magnin M, et al. Laser evoked potential abnormalities in central pain patients: the influence of spontaneous and provoked pain. Brain 2002;125:2766-2781.
139. Cruccu G, Garcia-Larrea L. Clinical utility of laser-evoked potentials. Advances in evoked potentials Clinical Neurophysiology Supplement 2004;57:1223-1234.
140. Solaro C, Uccelli MM. Management of pain in multiple sclerosis: a pharmacological approach. Nat Rev Neurol 2011;7:519-527.

REVIEW

Clinical evoked potentials in neurology: a review of techniques and indications

Agustina M Lascano,[1] Patrice H Lalive,[1] Martin Hardmeier,[2] Peter Fuhr,[2] Margitta Seeck[1]

[1]Department of Clinical Neurosciences, Division of Neurology, Faculty of Medicine, Geneva University Hospitals, Geneva, Switzerland
[2]Department of Neurology, University Hospital Basel, Basel, Switzerland

Correspondence to
Dr Agustina M Lascano, Division of Neurology, Geneva University Hospitals, Rue Gabrielle-Perret-Gentil 4, Geneva CH-1211, Switzerland; Agustina.Lascano@hcuge.ch

Received 29 August 2016
Revised 27 January 2017
Accepted 01 February 2017

ABSTRACT

Evoked potentials (EPs) are a powerful and cost-effective tool for evaluating the integrity and function of the central nervous system. Although imaging techniques, such as MRI, have recently become increasingly important in the diagnosis of neurological diseases, over the past 30 years, many neurologists have continued to employ EPs in specific clinical applications. This review presents an overview of the recent evolution of 'classical' clinical applications of EPs in terms of early diagnosis and disease monitoring and is an extension of a previous review published in this journal in 2005 by Walsh and collaborators. We also provide an update on emerging EPs based on gustatory, olfactory and pain stimulation that may be used as clinically relevant markers of neurodegenerative disorders such as Parkinson's disease, Alzheimer's disease and cortical or peripheral impaired pain perception. EPs based on multichannel electroencephalography recordings, known as high-density EPs, help to better differentiate between healthy subjects and patients and, moreover, they provide valuable spatial information regarding the site of the lesion. EPs are reliable disease-progression biomarkers of several neurological diseases, such as multiple sclerosis and other demyelinating disorders. Overall, EPs are excellent neurophysiological tools that will expand standard clinical practice in modern neurology.

INTRODUCTION

Clinical evoked potentials (EPs) allow non-invasive functional examination of the sensorimotor pathways. The advent of MRI in the mid-1980s has replaced the use of neurophysiological tools in a clinical setting in terms of anatomic accuracy and detection of underlying pathologies. In contrast to EPs, MRI is currently considered a key player in the diagnosis of multiple sclerosis (MS).[1 2] However, electrophysiological techniques allow non-invasive exploration and provide quantitative information on the functional status of selected functional systems with a temporal resolution in the range of milliseconds; in addition, they can be repeated as often as necessary with relatively low cost. EP studies allow the detection of subclinical lesions,[3] and the prediction of long-term disability[4] and/or conversion to symptomatic disease phases.[5] Further attempts to increase the diagnostic and prognostic accuracy by using multimodal EP (mmEP) scoring systems[6] and high-density electroencephalogram (HD EEG:>64 electrodes) analysis with topographical mapping and dipole modelling have been proposed.[7]

This review is a continuation and extension of the excellent work by Walsh and collaborators[8] on standard EP clinical uses, which was published more than 10 years ago. The aim of the current review is to describe EPs' current clinical uses and to address novel applications, based on literature published after the year 2005, with a particular focus on scalp EEG. Intraoperative EP monitoring, cognitive event-related potentials and intracranial EP recordings will not be discussed in this review due to space limitations.

VISUAL EVOKED POTENTIALS

Visual EPs (VEPs) allow functional exploration of the visual pathway from the retina to the occipital cortex. Standard clinical evaluations include monocular full-field pattern reversal, with alternating black and white checkerboards, given its low intrasubject and intersubject variability (figure 1A). Unpatterned stimulus, namely strobe flash visual testing, is less reliable and is, thus, limited to patients who are unable to fixate on a visual target. Half-field distribution is more sensitive for detecting retrochiasmatic lesions than full-field stimulation. Table 1 summarises the clinical applications, other than in demyelinating disorders.

Multiple sclerosis

Detection of visual dysfunction

Optic neuritis is a common clinical presentation that affects 20%–30% of patients with MS at some point in their disease. Expert consensus of the MAGNIMS network proposed the inclusion of optic nerve lesions in the imaging criteria for the spatial dissemination of the revised McDonald's criteria.[1] Clinical evidence of optic neuritis confirmed by ophthalmological evaluation, MRI, optical coherence tomography (OCT) measure of retinal nerve fibre layer (RNFL) thinning[9] or VEPs hastens diagnosis (figure 2B). A cross-sectional study including 65 patients with MS, clinically isolated syndrome (CIS) and neuromyelitis optical spectrum disorder demonstrated that VEPs were superior to OCT for detecting mild and moderate forms of optic neuritis (68% and 27%, respectively) as well as changes in the presumably unaffected eye (86% and 14%, respectively).[3] The reason why VEP incongruities are observed in the asymptomatic eye remains debated. Three main hypotheses have been discussed in the literature: (1) VEPs are able to detect subclinical abnormalities of the optic nerve due to previous injury or (2) due to retrograde

To cite: Lascano AM, Lalive PH, Hardmeier M, *et al. J Neurol Neurosurg Psychiatry* Published Online First: [*please include* Day Month Year]. doi:10.1136/jnnp-2016-314791

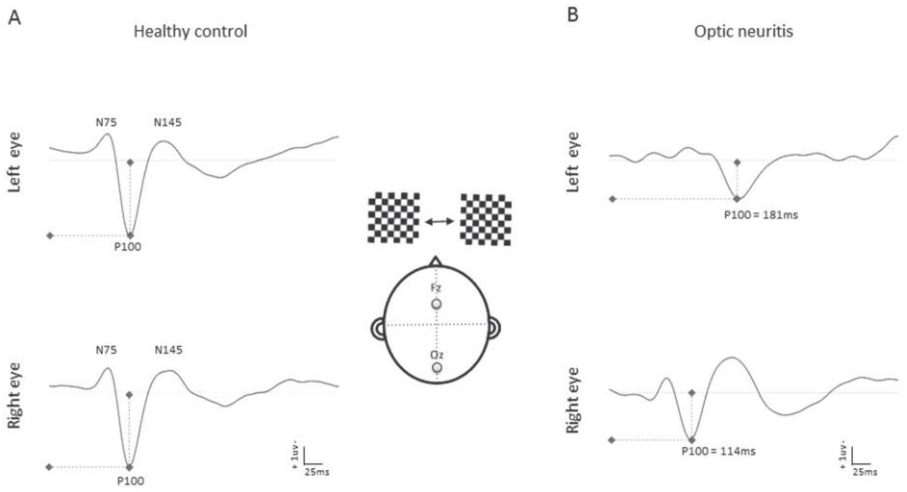

Figure 1 Visual evoked potentials (VEPs) on an patient with multiple sclerosis presenting with optic neuritis. VEPs are recorded from a scalp electrode placed on the mid-occipital (Oz) region referenced to a mid-frontal (Fz) channel. (A) The normal response results in a sequence of three main negative (N)–positive (P)–negative (N) components that peak at approximately 75–100–145 ms, with a topographical distribution in the occipital and midline region. All components originate in the striate cortex (area 17). VEPs are interpreted in terms of latency, amplitude and intereye differences of the P100 component, which is the most stable component obtained after pattern-reversal stimulation. (B) Abnormal P100 in a 26-year-old female patient diagnosed with left acute optic neuritis and sensory disturbances as initial symptoms.

axonal degeneration[9] or (3) its latency delay results from a visual compensation in the attempt to coordinate information arriving to the occipital cortex.[10]

Increased diagnostic sensitivity of VEPs in MS can be achieved by using multifocal VEPs (mfVEPs), which record different regions of the visual field simultaneously with an eccentricity angle of approximately 20°, assessing the central and the peripheral segment of the optic nerve. This method is more effective at detecting retrochiasmal and subclinical lesions, but the results are more difficult to analyse and interpret than standard VEPs.[11] Both standard VEPs and mfVEPs complement OCT in examining the integrity of the prechiasmatic and retrochiasmatic segment of the optic nerve.[12]

New ways of analysing EPs with topographical pattern recognition methods by using of HD EEG recordings compared with standard analysis have provided higher reliability, sensitivity and specificity rates.[13] HD EEG, together with mathematical modelling, helps to elucidate the electric generators of EP components and, thereby, advances our understanding of the underlying mechanisms of central integration processes. Despite its high spatial and temporal resolution, HD EEG has not yet found its place in current clinical practice.

Monitoring disease progression

VEPs have proven their worth as a diagnostic tool that is capable of evaluating asymptomatic demyelination and axonal loss and as a potential predictor of axonal damage when measured at disease onset. Prolongation of P100 latency, assessed by mfVEPs, predicted RNFL thickness loss as early as 3 and as late as 12 months after the first episode of acute unilateral optic neuritis in a group of relapsing-remitting MS, CIS and isolated optic neuritis.[11] VEPs also correlate with early microstructural white matter changes in the frontoparietal cortex, corpus callosum and optic nerve as detected by fractional anisotropy.[14] This is of utmost importance because 'normal-appearing' white matter damage occurs already in the early stages of the disease and most likely contributes to subsequent grey matter lesions and clinical disability.[15] Moreover, follow-up of disease progression using MRI has its own economical and biological constraints in contrast to more accessible and less costly tools, such as OCT and VEPs.

Despite the high correlation between VEP abnormalities and early OCT and MRI changes, the role of EPs as a potential biomarker in MS progression needs to be established. Two recent prospective studies have shown that early mmEP changes are associated with clinical outcome in relapsing-remitting[16] and progressive forms of the disease.[17] Early VEP and motor EP (MEP) abnormalities predicted the development of long-term clinical disability as much as 20 years later.[16] Interestingly, no clear correlation between T2 or gadolinium enhanced lesions or Expanded Disability Status Score (EDSS) at baseline was identified.

Treatment efficacy

Over the years, several innovative agents that promote remyelination and neuroprotection were studied using VEP because it can be used to assess optic nerve status.[18] An open-label phase IIa study, involving autologous mesenchymal stem cells for secondary progressive MS treatment, reported an increase in the optic nerve thickness assessed by OCT, VEP latency reduction and EDSS improvement at 6 months.[19] Few studies have involved primary progressive patients with MS given the limited treatment options and the partial benefits obtained with currently available drugs. However, a recent randomised, double-blind phase III study (ORATORIO) showed an impact on EDSS of ocrelizumab compared with placebo. Based on the findings overall, VEPs should be considered in drug trials as a marker of disease progression and remyelination, as demonstrated in the anti-LINGO1 monoclonal antibody-related studies,[20] focused on myelin repair.

Table 1 Current and future applications of evoked potentials in neurological and psychiatric diseases

	Current use	Reported applications	Potential use
VEP	▶ Optic nerve disease: (1) inflammatory (MS, CIS, NMOSD, neurosarcoidosis, Tolosa-Hunt syndrome), (2) tumour (glioma, meningioma, neuroblastoma, etc), (3) trauma, (4) toxic (ethambutol, isoniazid, amiodarone, sildenafil, linezolid, vigabatrin), (5) ischaemic, (6) hereditary (eg, Leber's optic neuropathy, ALD), (7) metabolic (diabetes, hypothyroidism) ▶ Retrochiasmatic and chiasmatic involvement unexplained by MRI lesions	▶ Refractive errors, glaucoma and retinopathy ▶ Non-organic visual loss ▶ Visual function in infants and children ▶ Hereditary ataxias	▶ Treatment monitoring and disease progression in MS ▶ Predict RIS and CIS conversion to MS ▶ Differentiation between AQP4+ and AQP4– NMOSD
SEP	▶ Coma prognostication ▶ Pathway integrity in patients with MS and having symptoms of uncertain significance ▶ Spinal cord lesion detection and localization ▶ Preoperative monitoring (eg, surgical scoliosis treatment)	▶ Cortical myoclonus (giant SEPs) ▶ Lance-Adams syndrome ▶ Hereditary ataxias ▶ Presurgical mapping of the eloquent cortex (in specialised centres)	▶ Treatment monitoring and disease progression in MS (in combination with other EP) ▶ BCI for rehabilitation purposes
LEP	▶ Small fibre sensory neuropathy ▶ Organic versus non-organic pain	▶ Complex regional pain syndrome ▶ Syringomyelia ▶ Headache (trigeminal)	▶ Pain assessment in cognitive impairment, coma or lack of cooperation ▶ Dopatherapy dose adjustment in PD ▶ Neuropathic pain after thalamic or operculo-insular stroke
MEP	▶ Pyramidal tract abnormalities in MND ▶ Spinal cord injury ▶ Presurgical functional mapping ▶ Prognostication of Bell's palsy ▶ Differentiate myelopathy from MND ▶ Non-organic paralysis	▶ Motor recovery in stroke ▶ Epilepsy	▶ Treatment monitoring and disease progression in MS (in combination with other EPs) ▶ BCI for rehabilitation purposes
BAEP	▶ Preoperative assessment (eg, cerebral vascular, Chiari malformation, cerebellopontine angle tumour) ▶ Coma prognostication (in combination with other EPs) ▶ Detect speech delay in auditory processing disorders; testing hearing in infants and children	▶ MS	▶ Differentiation between NMOSD and MS
VEMP	▶ Differentiate neuro-otologic diseases (eg: vestibular schwannoma, meningioma, Menière's disease etc) ▶ Assess vestibular symptoms in MS	▶ Differentiation between idiopathic and Parkinson-plus syndromes such as olivo-pontocerebellar atrophy and PSP ▶ Stroke and lateral medullar infarction	▶ Predict RIS and CIS to MS conversion ▶ Screening and postoperative follow-up of vestibular schwannoma ▶ Monitoring damage of the otolithic end organ input after cochlear implant ▶ Detect antibody-negative ocular forms of MG
CSERP	▶ Olfactory and taste disorders in malingering (medicolegal issues)	▶ Post-trauma and postinfectious olfactory loss ▶ Temporal lobe epilepsy (focus localization)	▶ Treatment response in MDD ▶ Detection of presymptomatic neurodegenerative disorders ▶ Differential diagnosis of PD with other Parkinson-plus syndromes (especially PSP) ▶ Psychotic features in schizotypic personality

AD, Alzheimer's disease; ALD, X-linked adrenoleukodystrophy; AQP4, auto-antibodies to aquaporine-4; BAEP, brainstem auditory evoked potential; BCI, brain–computer interface; CIS, clinically isolated syndrome; CSERP, chemosensory event-related potential; EP, evoked potential; LEP, laser evoked potentials; MCI, mild cognitive impairment; MDD, major depression disorder; MEP, motor evoked potential; MG, myasthenia gravis; MND, motor neuron disease; MS, multiple sclerosis; NMOSD, neuromyelitis optica spectrum disorder; PD, Parkinson's disease; PSP, progressive supranuclear palsy; RIS, radiologically isolated syndrome; SEP, somatosensory evoked potential; VEP, visual evoked potential; VEMP, vestibular evoked myogenic potential.

Clinically isolated syndrome

More than half of the patients convert from CIS to MS during the first year. Characteristic findings on brain MRI, the presence of oligoclonal bands and high IgG index in cerebrospinal fluid imply a higher risk of MS conversion. Independent of MRI findings, the presence of three abnormal EP modalities (SEPs, VEPs and BAEPs) predicted the conversion of CIS to MS in a 5-year follow-up period in 8% of the patients.[21] As opposed to mmEPs, single EP modality testing was not correlated with MS conversion or disability and is, thus, not recommended in CIS prognosis.

Neuromyelitis optica spectrum disorder

In contrast to MS, this disorder is associated with autoantibodies to aquaporine-4 (70%) and with more severe visual impairment.[22] Still, neither VEP correlation study comparing both antibody-positive and antibody-negative groups nor disease duration has been performed. This disorder has a different pathophysiological mechanism that differs from that of MS, and it is also characterised by a distinctive neurophysiological pattern; that is, a rather preserved VEP P100 latency, although with smaller amplitude, that is accompanied by a severely pathological OCT.[23] The combined application of VEPs and OCT might help in the differentiation of MS from antibody-negative neuromyelitis optica spectrum disorder.

SOMATOSENSORY EVOKED POTENTIALS

Somatosensory EPs (SEPs) are used to evaluate the somatosensory pathway at the peripheral, spinal, cortical and subcortical level and have proven their benefit in assessing disorders of the central nervous system rather than peripheral nerve lesions given that nerve conduction studies are more suited for peripheral nerve injuries (see Cruccu *et al*).[24] However, SEPs can be used to assess combined central and peripheral disorders (table 1; figure 2).

Multiple sclerosis

While each modality evaluates a specific system/pathway, the combination of the different EP modalities (ie, mmEPs) provides

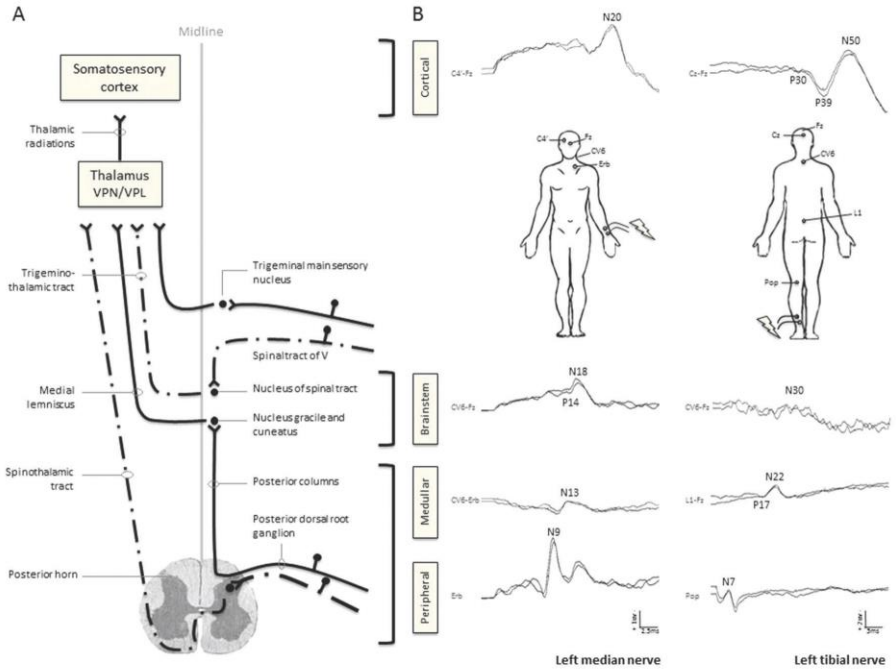

Figure 2 Somatosensory evoked potentials (SEPs). (A) Representation of the medial lemniscal pathway (solid line), which transmits well-localised touch, pressure and joint position as well as the spinothalamic tract (dotted line), which conveys information on pain and temperature (Adapted with permission from Campbell WW, *DeJong's the neurological examination*, 6th edn, Lippincott Williams & Wilkins, Philadelphia, PA, 2005, p.431.). In a nutshell, laser evoked potentials (LEPs) are composed of three main transient components: N1 (120–180 ms), the N2–P2 complex (180–350 ms) and P4 (350–450 ms). Additional 'ultra-late' LEP components were described between 650 and 1500 ms possibly resulting from nociceptive C fibres afferent volleys. (B) Early left median and tibial nerve SEP response in a healthy control after bipolar transcutaneous electric stimulation. Peripheral (Erb's point and popliteal fossa), medullar (C6 and L1) and cortical (contralateral centroparietal for the upper limb and Cz for the lower limb) contacts, referenced to a cephalic (Fz) or extracephalic electrode, are placed to obtain subcortical far-field and cortical responses. Exact anatomical localization of each SEP component is not fully known due to the mixed sensory and motor nerve stimulation. Nerve action potentials are recorded from the brachial plexus trunk (N9) and the popliteal fossa (Pop) (N7). The spinal cord potential is obtained at the level of C6 (N13) followed by the afferent volley from the cervicomedullar junction (P14) after the median nerve and at L1 (N22) after tibial nerve stimulation. Cortical components, N20 for the upper limb and P39 for the lower limb, are somatotopically distributed (area 3b). Later, cortical components are less stable and modulated by cognitive load. V, trigeminal nerve; VPL, ventral posterior lateral nucleus of the thalamus; VPN, ventral posterior medial nucleus of the thalamus.

a more global assessment of the central functional status and can be correlated with other paraclinical or clinical parameters. In two studies, both SEPs and MEPs were shown to have the highest sensitivity and specificity in predicting MS-related disability.[4] This correlation was even higher than that obtained with MRI and EDSS.[25] Various scoring systems have been applied to increase sensitivity; these have ranged from qualitative assessment of each individual EP result in terms of latency and amplitude to quantitative evaluations based on the sum of z-transformed results of single EP measurements. Regardless of which scoring system is used, mmEP assessment showed a significant cross-sectional and longitudinal correlation with clinical outcome at year 3.[6] Multimodal and not individual assessment of EPs should be considered in MS prognostication.

Disorders of consciousness after traumatic and ischaemic brain injury

Identifying patients who can benefit from maximal intensive care is crucial. Accurate prognosis depends on both local and national guidelines and includes neurological examination, neurophysiological tools (like EEG and SEPs), serum markers and imaging techniques (for a review see Rossetti *et al*[26]). Clinical and paraclinical assessment of patients with disorders of consciousness should be performed within the first 24–72 hours of brain injury. In contrast to EEG and neurological examination, short-latency SEPs are less influenced by sedation. The combination of an abnormal EEG recording (ie, low-voltage, isoelectric and burst-suppression) at 24 hours, the absence of brainstem reflexes at 48 hours and the bilateral absence of the short-latency N20 component at 72 hours, with or without hypothermia, is correlated with poor prognosis with a 100% specificity and with a 41%–58% sensitivity in postanoxic comatose patients.[27] The early absence of the N20 component is not considered a reliable marker of coma prognostication since SEP abnormalities can be caused by oedema instead of irreversible cortical damage (for a review see Koenig and Kaplan, 2015).[28] Thus, the presence of N20 shows limited ability to predict favourable outcome in contrast to a reactive EEG pattern recorded at >12 hours, which has an 80% positive predictive value.[26 27] Serial short-latency and middle-latency SEPs improve the diagnostic accuracy. Bilateral

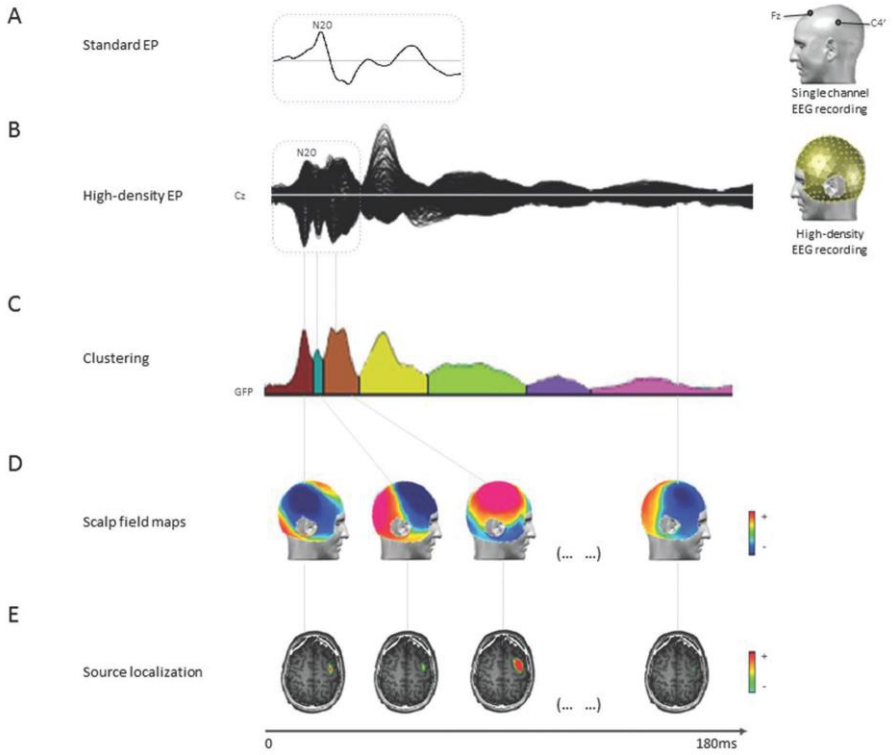

Figure 3 High-density somatosensory evoked potentials (SEPs). In contrast to standard evoked potential (EP) responses (A), high-density EPs are recorded from a large array of electrodes, up to 256 channels (B) superimposed in a butterfly plot. Spatiotemporal distribution of the scalp electric field (D) was identified using cluster analysis (C) and fitted back to the individual data. Three-dimensional localization of intracranial generators was obtained in the realistic brain (E). GFP, global field power; EEG, electroencephalogram. (Adapted from Lascano AM, Clinical evoked potential mapping [thèse de doctorat]. Geneva, Switzerland, Université de Genève et Lausanne, 2009.)

absence of the N20 component of short-latency SEPs (20.8%–43.2% sensitivity and 77.1%–100% specificity) and the N60 component of middle-latency SEPs (37.3%–61.3% sensitivity and 77.1%–100% specificity) were highly correlated with unfavourable clinical outcome at 6 months after stroke (modified Rankin scale 4–6).[29]

Non-invasive presurgical brain mapping of the eloquent cortex

In preoperative planning for epilepsy surgery or malignant tissue resection, non-invasive investigation of sensory and language processing is particularly important for obtaining accurate localization, on the millimetre scale, of the so-called 'eloquent cortex', which can be adjacent to the abnormal brain tissue. Despite its invasiveness, direct cortical stimulation is referred to as the 'gold-standard' for eloquent cortex localization and functional MRI is considered its non-invasive counterpart. A recent study highlighted the excellent localising value of SEPs recorded with HD EEG compared with functional MRI and intracranial EPs.[7] The use of HD EEG in localising the vital cortex in presurgical planning was inspired by the success of EEG source imaging in detecting plausible generators of epileptic activity (figure 3). SEPs can be applied whenever direct cortical stimulation is not feasible or in case MRI is contraindicated or limited by patient cooperation.

PAIN-RELATED LASER EVOKED POTENTIALS (LEPS)

Neuropathic pain is a prevalent clinical symptom; it affects around 8% of the general population[30] and constitutes a global health priority due to its high socioeconomic burden. Given that pain is an individual perception, it is therefore difficult to obtain objective measurements. Pain-related EPs using laser (LEP) stimulation allows for objective functional assessment of Aδ small myelinated and unmyelinated C fibres in a large number of neurological disorders of central or peripheral origin (figure 2).

Small fibre sensory neuropathy

Diagnosis of small fibre sensory neuropathy relies on the visual analogue scale, the pain-related reflexes, the quantitative sensory testing (QST) and the density of intraepidermal nerve fibres in punch biopsies of the skin. The latter is defined as the gold standard (see review by Garcia-Larrea, 2012).[31] A recent study showed abnormal LEPs in a subgroup of 29 patients with painful peripheral neuropathy associated to hepatitis C virus, in contrast to normal sensory action potentials and intra-epidermal nerve fibre density.[32] A comparative study including punch skin biopsies, QST and LEPs showed that the latter presented the highest specificity (83%) and sensitivity (91%) in detecting asymptomatic diabetic neuropathy in the distal leg in a cohort of 23 patients with a disease duration of >10 years.[33] Taking these observations

into account, a three-step diagnostic approach is recommended: (1) QST and nerve conduction studies and, if negative, followed by (2) LEPs and finally by (3) punch skin biopsy.

Parkinson's disease

In 15% of patients with Parkinson's disease, neuropathic pain (mainly musculoskeletal and dystonic) was the initial clinical manifestation, preceding motor symptoms.[34] Pain correlates with disease duration and clinical evolution in 40%–75% of the patients. Schestatsky and collaborators applied LEPs in 18 patients with and without pain prior to L-DOPA administration and found higher LEP amplitudes in patients with neuropathic pain.[35] Surprisingly, patients reported pain improvement after L-dopa intake, which correlated with an amplitude decrease, suggesting a contribution of dopamine to the pain experience.

Other pain syndromes

Neuropathic pain generally occurs several weeks (>1 month) after a stroke and its prevalence can be as high as 43%.[36] The identification of patients who are at risk of developing poststroke pain is important to insure rapid treatment, especially for those who are unable to communicate. LEP abnormalities were associated with abnormal heat/pain ratings and anterior pulvinar nucleus lesions in 27/31 patients, rendering a positive predictive value of 87% for thalamic poststroke pain.[37] Interestingly, SEPs can be normal in these patients. Extra-thalamic lesions leading to pain and abnormal LEP results include the opercular-insular and posterior perisylvian regions.[38]

In contrast, non-organic pain disorders are characterised by the integrity of the nociceptive pathway and therefore show no LEP attenuation compared with the organic pain group, including patients with brain and spinal lesions, with stimulation on the symptomatic site.[31] Thus, LEPs help to differentiate between organic and functional pain syndromes.

MOTOR EVOKED POTENTIALS

Transcranial magnetic stimulation (TMS) is a non-invasive method suited for investigating the functional integrity of the corticospinal tract using a wire coil generating a magnetic pulse and leading to multiple descending waves in the pyramidal tract and subsequently, to a contraction of a specific muscle or group of muscles. Motor-EPs (MEPs) are recorded using surface electrodes and their results are reported in terms of absolute latency and peak-to-peak amplitudes. Additional information is obtained by assessing the following: (a) the central conduction time estimated by subtracting the latency of the peripheral conduction time and the latency of the TMS response and (b) the cortical silent period defined as the time of electromyographic suppression after voluntary muscle contraction and suprathreshold TMS pulse (for more details see).[39]

Multiple sclerosis

The yield of MEPs for MS follow-up and prognosis is promising: correlation between central conduction time and motor disability has been documented.[40] Moreover, MEP amplitude assessment was able to predict disability at 6 months in a cohort of 15 patients treated with interferon-β1a, confirming its value in disease prognostication.[41] Increasing the sensitivity and prognostic accuracy by using mmEP has been discussed above.

Poststroke recovery

Stroke is often associated with significant residual physical disability. In case of motor deficit, upper limb motor recovery after 6 months is estimated at 70% of the maximum possible provided that corticomotor tract is preserved.[42] MEPs performed within the first 2 weeks after stroke predicted motor recovery at 26 weeks in a cohort of 93 patients. Thus, MEPs can help to promptly identify patients who are more likely to benefit from a motor rehabilitation programme. Functional reorganisation of the affected and unaffected motor cortices plays a role in clinical recovery. Both cortical and subcortical strokes entail a transient increase in the excitability of the unaffected motor cortex, which can be considered a precursor of brain plasticity. However, persistence of cortical excitability in the non-lesional motor cortex beyond 1 month was correlated with poor prognosis in 13 patients with subcortical ischaemic stroke.[43]

Motor neuron disease

Amyotrophic lateral sclerosis is a rather heterogeneous disease with upper and lower motor neuron involvement whose origin remains unknown. Objective evidence of central nervous system dysfunction is essential for the diagnosis of amyotrophic lateral sclerosis. In this sense, TMS is a suitable tool that is used to demonstrate the early signs of hyperexcitability due to deficits in the inhibitory GABAergic system, translated as a shorter cortical silent period duration, increased intracortical facilitation and reduced short-interval intracortical inhibition (SICI). Abnormal short-interval intracortical inhibition, assessed by threshold-tracking TMS, has shown high sensitivity (73%) and specificity (81%) in patients with lower motor neuron features and with equivocal upper motor signs versus amyotrophic lateral sclerosis phenocopies.[44] Early demonstration of cortical dysfunction can hasten the diagnosis by 16 months when combined with clinical and standard neurophysiological tests. In an elegant recent study, it was shown that reduced short-interval intracortical inhibition is an independent factor of poor prognosis in patients with <2-year disease duration.[45]

Epilepsy

Polyphasic responses have also been described in myoclonus dystonia and in genetic generalised epilepsies. Actually, polyphasic oscillations were observed in both patients with epilepsy and their asymptomatic relatives, which supports a common genetic background.[46] In addition, patients responding to topiramate stopped presenting TMS-induced hyperexcitability.[47] TMS could be a valuable tool for establishing pharmaco-resistance and the likelihood of a response to a particular antiepileptic drug, although further studies on an individual level and other drugs needs to be performed.

BRAINSTEM AUDITORY EVOKED POTENTIALS

This technique is used to evaluate the integrity of the auditory pathway up to the midbrain (table 1). It can also be used to evaluate hearing status in non-cooperative subjects and in paediatric patients. Brainstem auditory EPs (BAEPs) elicit between five and seven positive waveforms designated by roman numbers (I–VII) occurring within the first 10 ms, known as short latency components, which allow determining the integrity between the peripheral portion of the VIII cranial nerve and the inferior colliculi. Peaks VI and VIII are less well defined and are observed in only half of the population, probably generated in higher brainstem structures.[48] Latencies of waves I, III and V, interpeak latencies of I–III, III–V and I–V and amplitude ratios are commonly studied.

Brainstem demyelinating lesions

BAEPs are used to detect brainstem lesions in MS mainly in combination with other EP modalities.[25] Their diagnostic yield

as a stand-alone technique is lower than that of VEPs, SEPs and MEPs,[25] and they exhibit a poor correlation with MRI. Notwithstanding, a more recent study on 18 patients with neuromyelitis optica showed that none presented with abnormal BAEPs, in contrast to the MS group, even though MEPs and VEPs were pathological.[49] These findings suggest a potential crucial role of BAEPs in distinguishing between different neuroinflammatory diseases with similar clinical manifestations.

Critical care patients

Two recent reviews of coma prognostication highlighted the potential value of long-latency components (>100 ms) obtained with deviant auditory stimuli embedded in a stream of standard stimuli (so-called mismatch negativity) as a positive predictive factor of awakening from coma.[26 28] Worsening on auditory decoding during the first 2 days, using an automated EEG analysis based on voltage topography, was a poor prognostic factor. In this sense, mismatch negativity could be used to establish residual cognitive processing in coma prognosis at an individual level and at an early stage.

VESTIBULAR EVOKED MYOGENIC POTENTIALS

Vestibular evoked myogenic potentials (VEMPs) assess brainstem integrity by studying the vestibulospinal pathway (cervical or cVEMPs), the vestibulo-ocular reflex (ocular or oVEMPs) and, more recently, the vestibulomasseteric reflex (mVEMP), with different recording sites (cVEMPs from the sternocleidmastoid muscle; oVEMPs from the inferior oblique or the inferior rectus muscle; mVEMPs from the masseter muscle).[50–52]

Neuro-otologic disorders

VEMPs are used to differentiate neuro-otologic diseases with similar clinical presentations. For example, Menière's disease and vestibular migraine can both present with acute vestibular symptoms of moderate-to-severe intensity. However, only oVEMPs were significantly abnormal in patients with migraine compared with those suffering from Menière's disease.[53] Superior canal dehiscence can present with apparent conductive hearing loss without vestibular symptoms, thus, mimicking otosclerosis. The former shows an increased cVEMP response, whereas the latter is characterised by absent or attenuated cVEMPs (70%–80% sensitivity).[51] Finally, cVEMPs are normal and oVEMPs are decreased or absent in vestibular neuritis affecting the superior but not the inferior division of the nerve.[51]

Disorders of the central nervous system

Vestibular symptoms in patients without brainstem lesions on MRI are extremely difficult to explore and VEMPs can provide localising value. For example, in a study including 62 patients with MS: 9/20 presented with clinical complaints suggestive of brainstem dysfunction but without compatible MRI lesions. 4/9 patients (44%) showed abnormal cVEMPs and oVEMPs results.[54] A more recent MS study showed that the combination of cVEMPs, mVEMPs, trigeminocollic reflex and vestibulocollic reflex, detected brainstem involvement with the same precision as mmEPs (86.9% vs 82.7%) and, moreover, even better than MRI (71.7%) and clinical examination (37.7%).[55] The yield on diagnosis or prediction appears to be low in other neurological diseases like migraine with brainstem aura, supranuclear palsy, Parkinson's and Alzheimer's disease.[50] However, Natale and collaborators showed a significant correlation between the amount of abnormal VEMPs (ie, all three modalities) with Parkinson's disease non-motor symptoms such as postural instability and REM sleep behaviour disorders, often difficult to diagnose otherwise and indicates the involvement of both the upper and lower brainstem.[56]

In addition, oVEMPs are a promising marker of extraocular muscle fatigability (ie, unilateral or bilateral decrement >15.2%) in ocular forms of myasthenia gravis with a sensitivity of 92% in contrast to acetylcholine receptor antibodies (54%), repetitive nerve stimulation (43%) or edrophonium test (78%),[57] although not as sensitive as single-fibre EMG.[58] This is particularly important in antibody-negative patients.

CHEMOSENSORY EVENT-RELATED POTENTIALS

The term "chemosensory" is used to describe specific substances that involve selective stimulation of either the olfactory (figure 4), trigeminal or gustatory system. Odour and taste compounds are delivered using a tubing system that is inserted into the nostril (olfactometer; for a description see Doty *et al*, 2015)[59] or the lateral aspects of the anterior tongue (gustometer; for a technical explanation see Hummel *et al*, 2010).[60] Currently, there is no recommendation for the clinical uses of chemosensory event-related potentials (CSERPs) (table 1), recording parameters and analysis. While most olfactory studies are based on psychophysical measurements of odour identification, there is relatively little research on CSERPs.

Neurodegenerative and psychiatric diseases

Impaired olfactory detection is observed at an early presymptomatic stage in neurodegenerative diseases such as Alzheimer's disease and Parkinson's disease. The preclinical stage of Alzheimer's disease is known as mild cognitive impairment, and its prompt diagnosis might have prognostic and therapeutic implications.[61] CSERPs demonstrated significant delays in clinically normal E4 allele carriers of the apolipoprotein gene, that is, at high risk of developing Alzheimer's disease, in contrast to non-carriers.[59] A recent study showed an association between abnormal odour ratings, amyloid burden (PiB-PET) and entorhinal cortex thinning, known to be risk factors for neurodegeneration.[62] Detection of hyposmia based on CSERPs could help to determine patients who benefit from neuroprotective drugs at an early stage of the disease.

Olfactory dysfunction is present in approximately 90% patients with idiopathic Parkinson's disease but is not observed in genetic forms. Several CSERP studies found latency delays after olfactory but not after trigeminal stimulation.[59] Atypical parkinsonism presents with a preserved or mildly abnormal olfactory function. Thus, CSERPs could be used to detect early idiopathic Parkinson's disease and to differentiate between other neurodegenerative disorders, such as supranuclear palsy and corticobasal degeneration.[59]

Major depressive disorder and symptom severity present with a strong volume reduction of the olfactory bulb, which is not modified by treatment.[59] Because the size of the CSERP response depends on the integrity of the olfactory bulb, CSERPs could be used to differentiate major depressive syndromes from other depressive syndromes because patients with major depressive disorder are more likely to present with abnormal CSERP responses.

CONCLUSION

The current use of EPs in clinical practice is mainly limited to monitoring in the intensive care unit, for diagnostic purposes in some neurological disorders such as MS or spinal cord lesions and, to a lesser degree, in preoperative monitoring. MRI replaced

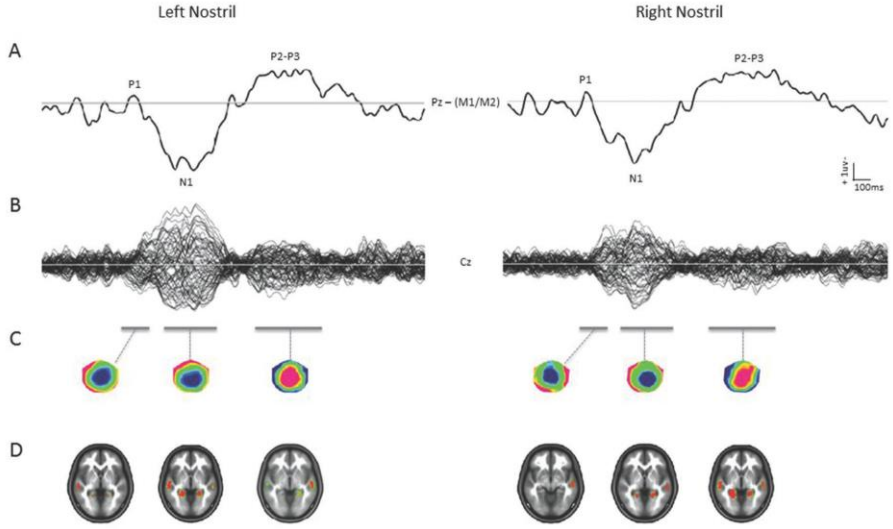

Figure 4 Chemosensory event-related potentials (CSERPs) mapping. CSERP are usually recorded from Pz, Fz and Cz referenced to the linked mastoid electrodes (M1/M2) or earlobes (A1/A2). (A) Single trace evoked potetial (EP) response recorded at a parietal electrode, showing an unstable initial component (P1) followed by N1 and P2–P3 complex observed between 300 and 1000 ms after unpleasant odour stimulation (hydrogen sulfide). (B) High-density EP topographical analysis of 12 healthy controls portrayed as a butterfly plot of 64 superimposed electrodes. (C), (D) Scalp topographies of the three main components and their probable corresponding intracranial generators with an initial ipsilateral activation of the anterior temporal lobe, followed by bilateral activation of mesial posterior temporal structures. (Adapted with permission from Lascano AM, *et al*, Spatio-temporal dynamics of olfactory processing in the human brain: an event-related source imaging study, *Neuroscience* 2010;167:700–8.)

EPs as a diagnostic tool since it provides images of lesion localisation with an excellent anatomical resolution. In a number of immunologically mediated syndromes, the detection of antibodies is mandatory for diagnosis. In that sense, the diagnostic utility of EPs decreased, but they are still excellent tools for monitoring changes over time: they are cheap and easy to obtain repeatedly. New clinical applications are aimed at the preclinical detection of neurodegenerative diseases, the prognostication of disorders of consciousness, the objective assessment of pain perception and the non-invasive mapping of eloquent brain regions in neurosurgery. Future research should target at predicting or monitoring the ultimate evolution of neurological diseases, such as MS or dementia, to identify early possible responders and to avoid cost-intensive but ineffective therapies. EPs might help to define and quantify the integrity of motor and sensory systems whose correct functioning is otherwise difficult to assess. If EPs are acquired with a high number of electrodes and novel analysis algorithms, there is an infinite number of ways of extracting prognostic and spatially significant information, which cannot be provided by MRI.

Acknowledgements This work was supported by the University of Geneva, Switzerland (Subdside Tremplin to AML), the Swiss National Science Foundation (grant nos 33CM30-140332 and 163 398 to MS, no 310 030–153 164 to PHL and no 33CM30-140338 to PF) and the Swiss Multiple Sclerosis Society (PHL).

Competing interests None declared.

Provenance and peer review All authors have directly participated in the conception, planning and execution of the manuscript. AML has written the manuscript and together with MS, they have elaborated the design. MS has been the main supervisor of this manuscript. PHL has extensively contributed to the section on demyelinating diseases. PF and MH have provided their knowledge on multifocal EP and MEP. The work has been revised in detail by all five authors.

Provenance and peer review Not commissioned; externally peer reviewed.

References

1 Filippi M, Rocca MA, Ciccarelli O, *et al*; MAGNIMS Study Group. MRI criteria for the diagnosis of multiple sclerosis: MAGNIMS consensus guidelines. *Lancet Neurol* 2016;15:292–303.
2 Polman CH, Reingold SC, Banwell B, *et al*. Diagnostic criteria for multiple sclerosis: 2010 revisions to the McDonald criteria. *Ann Neurol* 2011;69:292–302.
3 Naismith RT, Tutlam NT, Xu J, *et al*. Optical coherence tomography is less sensitive than visual evoked potentials in optic neuritis. *Neurology* 2009;73:46–52.
4 Kiylioglu N, Parlaz AU, Akyildiz UO, *et al*. Evoked potentials and disability in multiple sclerosis: A different perspective to a neglected method. *Clin Neurol Neurosurg* 2015;133:11–17.
5 Johnson JK, Chow ML. Hearing and music in dementia. *Handb Clin Neurol* 2015;129:667–87.
6 Schlaeger R, Hardmeier M, D'Souza M, *et al*. Monitoring multiple sclerosis by multimodal evoked potentials: Numerically versus ordinally scaled scoring systems. *Clin Neurophysiol* 2016;127:1864–71.
7 Lascano AM, Grouiller F, Genetti M, *et al*. Surgically relevant localization of the central sulcus with high-density somatosensory-evoked potentials compared with functional magnetic resonance imaging. *Neurosurgery* 2014;74:517–26.
8 Walsh P, Kane N, Butler S. The clinical role of evoked potentials. *J Neurol Neurosurg Psychiatry* 2005;76(Suppl 2):ii16–22.
9 Martinez-Lapiscina EH, Arnow S, Wilson JA, *et al*; IMSVISUAL consortium. Retinal thickness measured with optical coherence tomography and risk of disability worsening in multiple sclerosis: a cohort study. *Lancet Neurol* 2016;15:574–84.
10 Raz N, Chokron S, Ben-Hur T, *et al*. Temporal reorganization to overcome monocular demyelination. *Neurology* 2013;81:702–9.
11 Alshowaeir D, Yannikas C, Garrick R, *et al*. Multifocal VEP assessment of optic neuritis evolution. *Clin Neurophysiol* 2015;126:1617–23.
12 Balcer LJ, Miller DH, Reingold SC, *et al*. Vision and vision-related outcome measures in multiple sclerosis. *Brain* 2015;138:11–27.
13 Hardmeier M, Hatz F, Naegelin Y, *et al*. Improved characterization of visual evoked potentials in multiple sclerosis by topographic analysis. *Brain Topogr* 2014;27:318–27.

14 Lobsien D, Ettrich B, Sotiriou K, *et al*. Whole-brain diffusion tensor imaging in correlation to visual-evoked potentials in multiple sclerosis: a tract-based spatial statistics analysis. *AJNR Am J Neuroradiol* 2014;35:2076–81.
15 Steenwijk MD, Daams M, Pouwels PJ, *et al*. Unraveling the relationship between regional gray matter atrophy and pathology in connected white matter tracts in long-standing multiple sclerosis. *Hum Brain Mapp* 2015;36:1796–807.
16 Schlaeger R, Schindler C, Grize L, *et al*. Combined visual and motor evoked potentials predict multiple sclerosis disability after 20 years. *Mult Scler* 2014;20:1348–54.
17 Schlaeger R, D'Souza M, Schindler C, *et al*. Electrophysiological markers and predictors of the disease course in primary progressive multiple sclerosis. *Mult Scler* 2014;20:51–6.
18 Mallik S, Samson RS, Wheeler-Kingshott CA, *et al*. Imaging outcomes for trials of remyelination in multiple sclerosis. *J Neurol Neurosurg Psychiatry* 2014;85:1396–404.
19 Connick P, Kolappan M, Crawley C, *et al*. Autologous mesenchymal stem cells for the treatment of secondary progressive multiple sclerosis: an open-label phase 2a proof-of-concept study. *Lancet Neurol* 2012;11:150–6.
20 Cadavid DB, Galetta S, Aktas O, *et al*. Efficacy analysis of the anti-LINGO-1 monoclonal antibody BIIB033 in acute optic neuritis: the RENEW trial. *Neurology* 2015;84:202.
21 Pelayo R, Montalban X, Minoves T, *et al*. Do multimodal evoked potentials add information to MRI in clinically isolated syndromes? *Mult Scler* 2010;16:55–61.
22 Watanabe A, Matsushita T, Doi H, *et al*. Multimodality-evoked potential study of anti-aquaporin-4 antibody-positive and -negative multiple sclerosis patients. *J Neurol Sci* 2009;281:34–40.
23 Neto SP, Alvarenga RM, Vasconcelos CC, *et al*. Evaluation of pattern-reversal visual evoked potential in patients with neuromyelitis optica. *Mult Scler* 2013;19:173–8.
24 Cruccu G, Aminoff MJ, Curio G, *et al*. Recommendations for the clinical use of somatosensory-evoked potentials. *Clin Neurophysiol* 2008;119:1705–19.
25 Invernizzi P, Bertolasi L, Bianchi MR, *et al*. Prognostic value of multimodal evoked potentials in multiple sclerosis: the EP score. *J Neurol* 2011;258:1933–9.
26 Rossetti AO, Rabinstein AA, Oddo M. Neurological prognostication of outcome in patients in coma after cardiac arrest. *Lancet Neurol* 2016;15:597–609.
27 Hofmeijer J, Beernink TM, Bosch FH, *et al*. Early EEG contributes to multimodal outcome prediction of postanoxic coma. *Neurology* 2015;85:137–43.
28 Koenig MA, Kaplan PW. Clinical Applications for EPs in the ICU. *J Clin Neurophysiol* 2015;32:472–80.
29 Zhang Y, Su YY, Ye H, *et al*. Predicting comatose patients with acute stroke outcome using middle-latency somatosensory evoked potentials. *Clin Neurophysiol* 2011;122:1645–9.
30 Attal N, Lanteri-Minet M, Laurent B, *et al*. The specific disease burden of neuropathic pain: results of a French nationwide survey. *Pain* 2011;152:2836–43.
31 Garcia-Larrea L, diagnostics O. Clinical neurophysiology. *Neurophysiol Clin* 2012;42:187–97.
32 Biasiotta A, Casato M, La Cesa S, *et al*. Clinical, neurophysiological, and skin biopsy findings in peripheral neuropathy associated with hepatitis C virus-related cryoglobulinemia. *J Neurol* 2014;261:725–31.
33 Ragé M, Van Acker N, Knaapen MW, *et al*. Asymptomatic small fiber neuropathy in diabetes mellitus: investigations with intraepidermal nerve fiber density, quantitative sensory testing and laser-evoked potentials. *J Neurol* 2011;258:1852–64.
34 O'Sullivan SS, Williams DR, Gallagher DA, *et al*. Nonmotor symptoms as presenting complaints in Parkinson's disease: a clinicopathological study. *Mov Disord* 2008;23:101–6.
35 Schestatsky P, Kumru H, Valls-Solé J, *et al*. Neurophysiologic study of central pain in patients with Parkinson disease. *Neurology* 2007;69:2162–9.
36 ; Paolucci S, Iosa M, Toni D, *et al*; Neuropathic pain special interest group of the Italian Neurological Society. Prevalence and time course of post-stroke pain: a multicenter prospective hospital-based study. *Pain Med* 2016;17:924–30.
37 Vartiainen N, Perchet C, Magnin M, *et al*. Thalamic pain: anatomical and physiological indices of prediction. *Brain* 2016;139:708–22.
38 Garcia-Larrea L, Peyron R. Pain matrices and neuropathic pain matrices: a review. *Pain* 2013;154 Suppl 1:S29–43.
39 Groppa S, Oliviero A, Eisen A, *et al*. A practical guide to diagnostic transcranial magnetic stimulation: report of an IFCN committee. *Clin Neurophysiol* 2012;123:858–82.
40 Schlaeger R, D'Souza M, Schindler C, *et al*. Prediction of long-term disability in multiple sclerosis. *Mult Scler* 2012;18:31–8.
41 Leocani L, Comi G. Clinical neurophysiology of multiple sclerosis. *Handb Clin Neurol* 2014;122:671–9.
42 Byblow WD, Stinear CM, Barber PA, *et al*. Proportional recovery after stroke depends on corticomotor integrity. *Ann Neurol* 2015;78:848–59.
43 Chieffo R, Inuggi A, Straffi L, *et al*. Mapping early changes of cortical motor output after subcortical stroke: a transcranial magnetic stimulation study. *Brain Stimul* 2013;6:322–9.
44 Menon P, Geevasinga N, Yiannikas C, *et al*. Sensitivity and specificity of threshold tracking transcranial magnetic stimulation for diagnosis of amyotrophic lateral sclerosis: a prospective study. *Lancet Neurol* 2015;14:478–84.
45 Shibuya K, Park SB, Geevasinga N, *et al*. Motor cortical function determines prognosis in sporadic ALS. *Neurology* 2016;87:513–20.
46 Kimiskidis VK, Valentin A, Kälviäinen R. Transcranial magnetic stimulation for the diagnosis and treatment of epilepsy. *Curr Opin Neurol* 2014;27:236–41.
47 Inghilleri M, Gilio F, Conte A, *et al*. Topiramate and cortical excitability in humans: a study with repetitive transcranial magnetic stimulation. *Exp Brain Res* 2006;174:667–72.
48 Hatem SM, Attal N, Ducreux D, *et al*. Clinical, functional and structural determinants of central pain in syringomyelia. *Brain* 2010;133:3409–22.
49 Ohnari K, Okada K, Takahashi T, *et al*. Evoked potentials are useful for diagnosis of neuromyelitis optica spectrum disorder. *J Neurol Sci* 2016;364:97–101.
50 Venhovens J, Meulstee J, Verhagen WI. Vestibular evoked myogenic potentials (VEMPs) in central neurological disorders. *Clin Neurophysiol* 2016;127:40–9.
51 Colebatch JG, Rosengren SM, Welgampola MS. Vestibular-evoked myogenic potentials. *Handb Clin Neurol* 2016;137:133–55.
52 Deriu F, Giaconi E, Rothwell JC, *et al*. Reflex responses of masseter muscles to sound. *Clin Neurophysiol* 2010;121:1690–9.
53 Inoue A, Egami N, Fujimoto C, *et al*. Vestibular evoked myogenic potentials in vestibular migraine: do they help differentiating from Menière's disease? *Ann Otol Rhinol Laryngol* 2016;125:931–7.
54 Gazioglu S, Boz C. Ocular and cervical vestibular evoked myogenic potentials in multiple sclerosis patients. *Clin Neurophysiol* 2012;123:1872–9.
55 Magnano I, Pes GM, Pilurzi G, *et al*. Exploring brainstem function in multiple sclerosis by combining brainstem reflexes, evoked potentials, clinical and MRI investigations. *Clin Neurophysiol* 2014;125:2286–96.
56 de Natale ER, Ginatempo F, Paulus KS, *et al*. Abnormalities of vestibular-evoked myogenic potentials in idiopathic Parkinson's disease are associated with clinical evidence of brainstem involvement. *Neurol Sci* 2015;36:995–1001.
57 Valko Y, Rosengren SM, Jung HH, *et al*. Ocular vestibular evoked myogenic potentials as a test for myasthenia gravis. *Neurology* 2016;86:660–8.
58 Gilhus NE, Verschuuren JJ. Myasthenia gravis: subgroup classification and therapeutic strategies. *Lancet Neurol* 2015;14:1023–36.
59 Doty RL. *Handbook of olfaction and gustation*. 3rd edn. Hoboken, NJ: John Wiley & Sons, 2015.
60 Hummel T, Genow A, Landis BN. Clinical assessment of human gustatory function using event related potentials. *J Neurol Neurosurg Psychiatry* 2010;81:459–64.
61 Roberts RO, Christianson TJ, Kremers WK, *et al*. Association between olfactory dysfunction and amnestic mild cognitive Impairment and Alzheimer disease dementia. *JAMA Neurol* 2016;73:93–101.
62 Growdon ME, Schultz AP, Dagley AS, *et al*. Odor identification and Alzheimer disease biomarkers in clinically normal elderly. *Neurology* 2015;84:2153–60.